JOURNAL OF APPLIED PHYSICS

JOURNAL
OF
APPLIED PHYSICS

Vol. 14, No. 6 JUNE, 1943

In This Issue

Page

New Murray Hill Laboratory of Bell Telephone Laboratories FRANKLIN L. HUNT 249

Frictional Phenomena. XIV. ANDREW GEMANT 258

Résumés of Recent Research 271

Contributed Original Research

On Torsion Combined with Compression P. W. BRIDGMAN 273

A Tension-Compression Device for Quantitative X-Ray Diffraction Evaluation of Strain in Metals and a Calibrated Series of Aluminum Alloys GEORGE L. CLARK, GEORGE PISH, AND RALPH SEABURY 284

Studies on the Structure of Thin Metallic Films by Means of the Electron Microscope ROBERT G. PICARD AND O. S. DUFFENDACK 291

A Note on the Mutual Impedance of Antennas CHARLES W. HARRISON, JR. 306

In Every Issue

Here and There 309

Calendar of Meetings 310

Recent Applications of Physics x

New Instrument Booklets x

Index to Advertisers xviii

BOARD OF EDITORS

ELMER HUTCHISSON, *Editor*

Associate Editors

FRANCIS BITTER
W. F. BUSSE
S. H. CALDWELL
ROBLEY D. EVANS
SELIG HECHT
W. J. LYONS
MORRIS MUSKAT
THOMAS H. OSGOOD
PAUL E. SABINE
FREDERICK SEITZ
J. R. TOWNSEND
B. E. WARREN
J. B. WHITEHEAD

Publication of the American Institute of Physics

ADMINISTRATIVE STAFF

HENRY A. BARTON, *Director*

MADELINE M. MITCHELL, *Publications Manager*

JOHN T. TATE, *Adviser on Publications*

GOVERNING BOARD

PAUL E. KLOPSTEG, *Chairman*

GEORGE B. PEGRAM, *Secretary*

T. D. COPE
R. B. DOW
L. A. DUBRIDGE
FLOYD A. FIRESTONE
HARVEY FLETCHER
R. C. GIBBS
K. S. GIBSON
ARTHUR C. HARDY
HERMANN MARK
A. G. WORTHING
JOHN T. TATE
N. W. TAYLOR
WALLACE WATERFALL

The JOURNAL OF APPLIED PHYSICS, published monthly at Prince and Lemon Sts., Lancaster, Pa., is devoted to physics in its role as the science basic to other natural sciences and to the arts and industries. Previous to 1937 this publication was known as PHYSICS. The JOURNAL OF APPLIED PHYSICS publishes editorials, news of physicists and reviews, as well as technical papers of applied physics.

Manuscripts should be submitted to Elmer Hutchisson, Editor, 172 Fulton Street, Eleventh Floor, New York, New York.

Subscriptions and orders for back numbers should be addressed to Prince and Lemon Streets, Lancaster, Pa. or to the American Institute of Physics, 175 Fifth Avenue, New York, N. Y.

Subscription Price

	U. S. AND CANADA	ELSEWHERE
To members of scientific societies	$5.00	$5.70
To all others	7.00	7.70

Back Number Prices

Complete set: Vol. 1, July, 1931–Vol. 13, 1942—**$80.50**
Yearly back number rate: **$7.70**
Single copies: **$0.70** each.

Changes of address and proofs should be addressed to the Publications Manager.

Advertising rates supplied on request. Orders, advertising copy and cuts should be sent to the American Institute of Physics.

Entered as second class matter January 22, 1937, at the Post Office at Lancaster, Pennsylvania, under the Act of March 3, 1879. Accepted for mailing at the special rate of postage provided for in the Act of February 28, 1925, authorized May 2, 1932.

Copyright 1943, by the American Institute of Physics.

Journal
of
Applied Physics

Volume 14, Number 6 June, 1943

New Murray Hill Laboratory of Bell Telephone Laboratories

By Franklin L. Hunt
Bell Telephone Laboratories, New York, New York

In open country along the Watchung Mountain range of New Jersey and about twenty-five miles from New York City is situated the new Murray Hill unit of Bell Telephone Laboratories. An extensive wooded reservation borders the site on one side and the nearest highway is several hundred yards away, thus assuring ideal conditions for the conduct of experimental investigations which would be adversely affected by city noise, dust, vibration, and electrical disturbances. The buildings were designed to meet the special needs of research scientists and engineers. Long preparation, including inspection trips to many other research laboratories in this country and abroad, was made to assure that all features were included which would increase operating efficiency and provide added comfort for the personnel.

Since 1907, Bell System research and development work has been carried on at 463 West Street, New York City, which until 1916 was one of the manufacturing buildings of the Western Electric Company. Allied work was also conducted in Boston and at the headquarters building of the American Telephone and Telegraph Company in New York City. In 1925 most of these activities were consolidated by incorporating Bell Telephone Laboratories to undertake the research and development work of the Bell System. This new organization took over the entire building at 463 West Street.

Rapid growth of the Bell System during the years which immediately followed increased the need for improved telephone facilities and made further demands on the research and development program. Bell Laboratories grew rapidly and the organization increased further by the consolidation with it in 1934 of the Development and Research Department of the American Telephone and Telegraph Company. The West Street building soon became inadequate and space was leased in several buildings in nearby parts of the city. New York City has many advantages as a location for telephone development work because the headquarters of both the American Telephone and Telegraph Company and its manufacturing organization, the Western Electric Company, are there but it lacks the quiet and freedom from disturbance which are important in many research projects. The desirability of having laboratory buildings in some quiet country location had therefore long been contemplated for housing at least part of the Bell System's research work.

THE BUILDINGS

The new laboratory property at Murray Hill includes over two hundred acres on gently sloping terrain. On this ground is built an H-shaped

FIG. 1. New Murray Hill Laboratory of Bell Telephone Laboratories situated in New Jersey in open country twenty-five miles from New York City. (Photograph by Eric Baker.)

structure of buff brick which provides approximately 215,000 square feet of net area (Fig. 1). There is also a separate acoustics building with a small auditorium, a boiler house, and a garage. The main building is in two parallel sections, 675 and 340 feet long. These are connected by a 144-foot transverse building in which the entrance is located. There are also five fifty-foot projecting wings on the two parallel buildings to provide additional space for offices. Each section of the building has three laboratory and office floors and also a cellar and an attic. The latter are used exclusively for pipe services, pumps, ventilating systems, auxiliary laboratory equipment, and storage. Although designed as a walk-up structure there are three elevators for moving material and equipment and for limited passenger use.

Restaurant, cafeteria, and lunch room facilities, with a combined seating capacity of over four hundred persons, and a kitchen completely furnished with the most up-to-date culinary equipment have been provided. These facilities are essential to the operation of the plant because other eating places are not available in the immediate vicinity. Built of Princeton stone and connected to one of the wings of the main building, the restaurant is entered through an attractive lounge and solarium, thence down a broad interior stairway to the tables on the main floor below (Figs. 2 and 3). From the restaurant one sees a broad expanse of lawn studded with newly planted trees and bordered with a thick growth of natural wood.

FIG. 2. An extension of the employees' lounge surrounds the stair well which leads to the restaurant below. (Photograph by Gottscho-Schleisner.)

FIG. 3. The restaurant is a one story building of Princeton stone. It is connected to one of the office wings by an attractive second story lounge. (Photograph by Gottscho-Schleisner.)

FIG. 4. Partitions throughout the buildings are made of sheet-steel panels which are readily removable to accommodate constantly changing space requirements.

PERSONNEL

The personnel of the new laboratory is now a little over nine hundred including the scientific and technical staff, clerical, shop, and maintenance groups. The technical groups there are the Physical Research Department which is concerned with fundamental researches in acoustics, speech and hearing, magnetics, electronics, and other fundamental physical properties of matter; the Chemical Laboratories' activities relating to general chemical and metallurgical research; the Station Apparatus Development Department which is responsible for the development of telephone sets, coin collectors, booths, microphones, and loud speakers; the Outside Plant Development Department whose work involves all of the equipment between the subscriber's telephone set and the central office, such as cables, wires and associated apparatus, poles, conduits, hardware, and the tools required to maintain this equipment; and part of the Circuit Research Department which undertakes studies of control circuits, radio connecting circuits, modulating systems, the artificial generation and analysis of

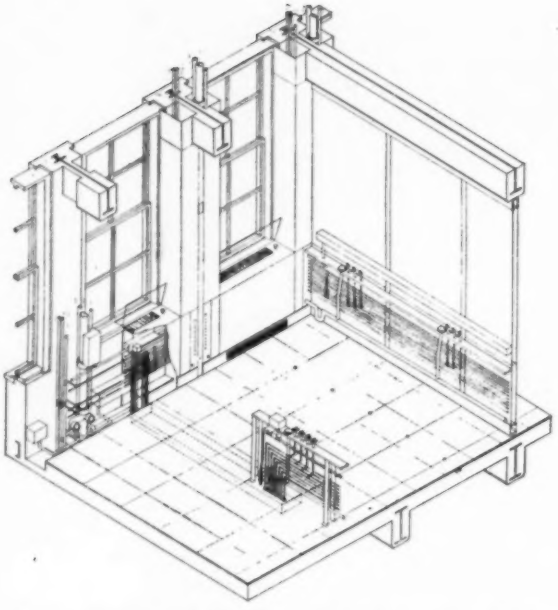

FIG. 5. Piping and electrical wiring are carried along the outside walls and into the laboratories either along the partitions or to "island" benches through a duct in the floor.

speech, as exampled by the Voder, multiplex telephone systems, and fundamental research on broad frequency band and short-wave telephone circuits.

STRUCTURAL FEATURES

The main buildings are approximately fifty-eight feet wide outside. There is a row of columns spaced twenty-four feet apart down the center of each building and a six-foot corridor along one side of them, which leaves laboratory space nineteen feet deep on one side and twenty-seven on the other. Windows are spaced on six-foot centers throughout the main buildings and on eight-foot centers in the office wings. They are all four feet wide and extend to the ceiling to admit more light.

A shallow girder is located on each side of the center columns of the building. Between them there is space extending from cellar to attic for ducts and large service risers. Floor beams run every six feet from the light columns between each pair of windows to the girders, to support the floors. This leaves the entire enclosed area, except for the center columns, clear for partitions. The partition along one side of the central corridor runs under one of the girders and a false girder is run the full length of the building on the other side to permit using partitions of the same height on both sides of the corridor. Similar false beams are installed along the corridor of the office wings. The lower faces of all of the cross beams are flush with the girders so that partitioning of standard height can be used throughout the buildings. The width of laboratory space can be any multiple of six feet which is the distance between two beams.

In designing the Murray Hill building, plans were made not only to provide laboratory and office space of any size needed, but to make quick changes and rearrangements possible. The girder and beam structure adopted made this practicable. There are no permanent partitions in the buildings except the sidewalls and those around the stair wells, toilets, and elevator shafts. All of the partitions are built of standard double steel panels ten feet eight inches high and, with a few exceptions, four feet wide (Fig. 4).

The outside surfaces of these units are sheet steel which is stiffened by transverse members welded to it inside on nine-inch centers. The steel sides are separated by a three-inch space which is packed with rock wool to prevent the transmission of sound and heat. The inside surface of the steel is coated with a deadening material. Doors and transoms are made in one unit which is also four feet wide so that it can be interchanged with a standard partition panel in any part of the building.

A support along the bottom of the panels forms a double wire-way which is used for telephone and signal services. There is also a wire-way at the top for lighting and miscellaneous wiring.

The partitions are held in place by punched steel pieces fastened to the floor between each pair of panels and by a forked sliding plate at the top of each unit, which is pushed over a flange fastened to the ceiling. Adjacent panels are held together by metal spiders which fit into a flange on their lateral edges. These spiders are spaced at two-foot intervals between the panels and turned to lock them in place. The locking units have an open center to provide a vertical wire-way. After two panels are in place, the space between them is packed with rock wool and a cover plate is snapped over their edges. Flat metal finishing

strips are clipped, without screws, along the bottom and top of the panels to fill the space up to the ceiling and down to the floor.

Along the outside wall of the rooms there is a sheet steel wainscoting under the windows and up the columns between them. This wainscoting is the same in appearance as the partition panels and like them it is also stiffened with transverse members and coated on the back side with mastic for deadening.

The wainscoting is removable without special tools to give access to the laboratory services which are located behind it. Similar wainscoting is applied around interior columns. Special panels with a removable top section are provided to let intercommunicating ducts pass from room to room or to permit installing a ventilating fan in enclosed areas, such as dark rooms or special air-conditioned laboratories. One panel with an escape door above bench height is installed in small chemical laboratories where a secondary exit is desired. This avoids sacrificing space for a standard door.

These standard panels and fittings, together with an occasional one of other widths and the standard interchangeable door and transom unit, make partition alterations a simple job with the additional advantage of great savings of time. For example, a partition unit can be exchanged for a door unit in a few minutes.

SERVICE FACILITIES

A research laboratory requires many special facilities such as compressed air, vacuum, hydrogen, oxygen, nitrogen, and illuminating gas; steam at several pressures; hot, cold, chilled, and distilled water; chemical drains, electric power at different voltages; and a quiet ground. Fifteen such services are regularly supplied and distributed to individual laboratories at Murray Hill and there are also special services. The service mains are installed either in the basement or the attic. Risers are grouped at the outside walls and pass up through vertical chases located there at six-foot intervals throughout the buildings. Each service appears once in twenty-four feet except those for heating, electric power, and telephone which are installed in alternate chases

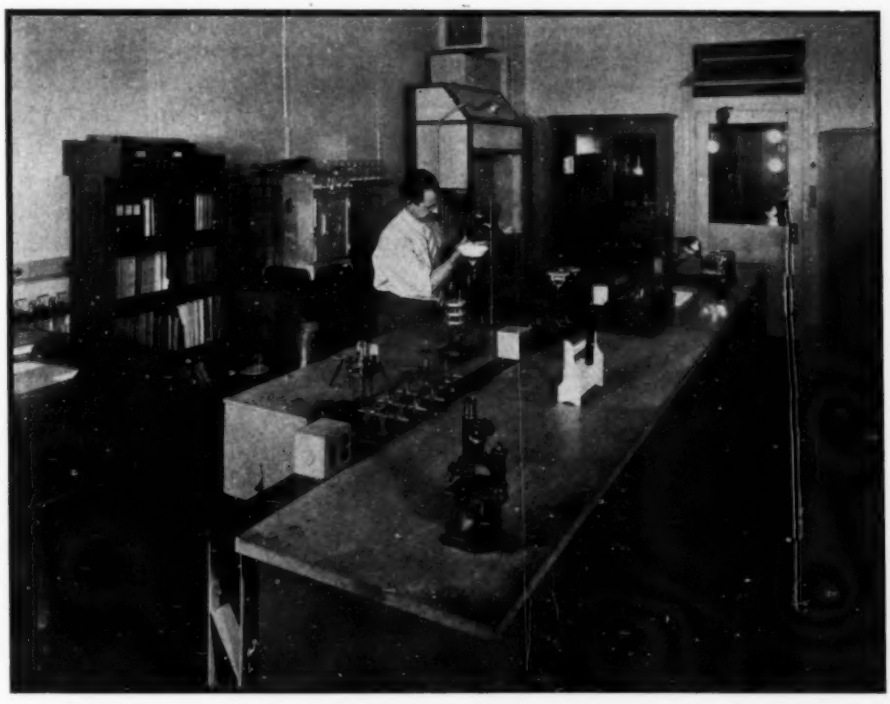

Fig. 6. Typical chemical laboratory showing "island" benches. The bench units are made of sheet steel with soapstone tops and are removable.

FIG. 7. The acoustics building is separate from the main structure. It houses besides ordinary laboratories, a dead room, two connecting live rooms, and a large listening room, which also serves as an auditorium. (Photograph by Gottscho-Schleisner.)

and for drains which are located in every chase. Horizontal runouts below the window sills pass behind the metal wainscoting and make all services available at six-foot intervals in individual laboratories.

To get these services from the risers at the side walls to laboratory benches, special supports were devised for quick attachment to the partition posts. These were also designed to be easily removed without marring the finish. The edge strips of the panels are made of heavier steel than their side walls and are slotted every six inches. A special box-shaped fitting with wings projecting from two opposite sides and keyholes in the other faces is slipped into the vertical space between two panels, turned to bring the wings into a slot in each of the panels and then driven down. This holds the fitting tightly to the panels. The keyholes in the fitting are nearly flush with the surface of the panels and provide the points of support for whatever is mounted on the partitions. Partition post coverplates with matching holes punched in them are used where keyhole fittings are installed. A variety of mounting strips, pipe clamps, angle plates, and shelf brackets are available for attachment to these keyhole fittings. This arrangement permits all necessary wiring, piping, and supports to be attached to the partitions without mutilating the panels.

Laboratory services are usually run out into the room along the partition from the outside wall of the building through a narrow slotted plate with deep sides called a "shadow box." This box hides the piping behind the wainscoting. Another method of bringing service pipes into the laboratories is through ducts in the floor fill which extend eight feet into the room from the outer wall (Fig. 5). These ducts are installed only when required for "island" benches located in the center of the room and are used principally in the chemical laboratories (Fig. 6). They have steel covers with open sections where the services turn up at the benches.

These panelling, wainscoting, and fitting arrangements permit great flexibility in changing laboratory space with very little loss of material. Panels and supports can be reused indefinitely with only an occasional painting.

GAS DISTRIBUTION SYSTEM

Hydrogen, oxygen, and nitrogen, as well as illuminating gas, are distributed to individual laboratories at Murray Hill by pipes from a central supply. The hydrogen is stored in pressure tanks in one room and the oxygen and nitrogen in

another, to avoid fire hazard. Pressures are reduced in two stages from 2000 to 50 and then to 10 pounds per square inch. Four cylinders are at present connected to the system at a time and four are held in reserve but there is room for additional tanks as needed. A rate of flow gauge in the hydrogen lines keeps the amount used in any room below that which could form an explosive mixture. All of these gases are distributed from the attic, to the limited number of laboratories requiring this service, by mains which are installed there under the roof.

ACOUSTIC BUILDING

The acoustic laboratories are housed in a separate building to avoid noise and vibration from other activities (Fig. 7). Besides regular laboratory space, this includes a large dead room for response measurements of microphones and loudspeakers, two live rooms, or reverberation chambers, for transmission and absorption measurements, and a listening room which also serves as an auditorium.

The dead room is a forty-foot cubical structure. It is to be lined on the inside with thirty layers of cloth separated from each other by different distances to absorb sound of different wavelengths. These cloth layers, whose installation has been delayed by the present emergency, will cover the walls, ceiling, and floor. Apparatus is to be brought into the room by a track which suspends a platform from the ceiling and to which access is had through a door which leads to the second floor of the laboratory. The entire structure is isolated from the rest of the building by double bulkhead doors and a four-inch air space. A smaller dead room with similar interior treatment serves for the present. The reverberation chambers are also isolated. There is an opening between these two live rooms in which may be placed panels of different materials to determine their absorption and transmission characteristics.

The listening room was built primarily for experiments in auditorium acoustics but its construction follows the latest practice in acoustic treatment and it also serves for staff meetings and lectures. It seats 363 persons. Back of the platform there is steel paneling similar in construction to the partitions throughout the rest of the laboratories but built of units approximately three by four feet in size. These panels are mounted on a steel framework and they separate the auditorium from the laboratory rooms. Any one or several of them can be removed to mount loud speakers for experimental installations. For decorative effect and to permit sound from the loudspeakers to pass

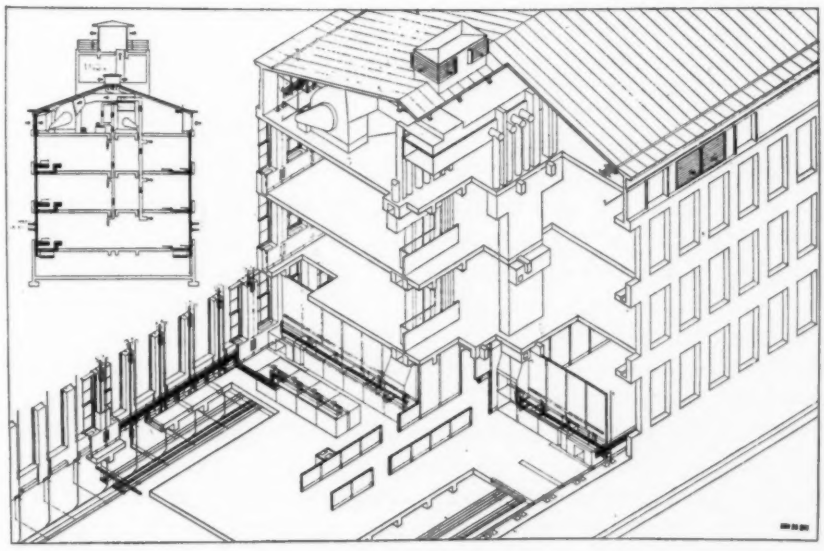

FIG. 8. Forced ventilation is provided in the chemical section of the building by blowers in the attic. They take in fresh air, filter and temper it, and force it through ducts into each laboratory. The air is exhausted through the fume hoods.

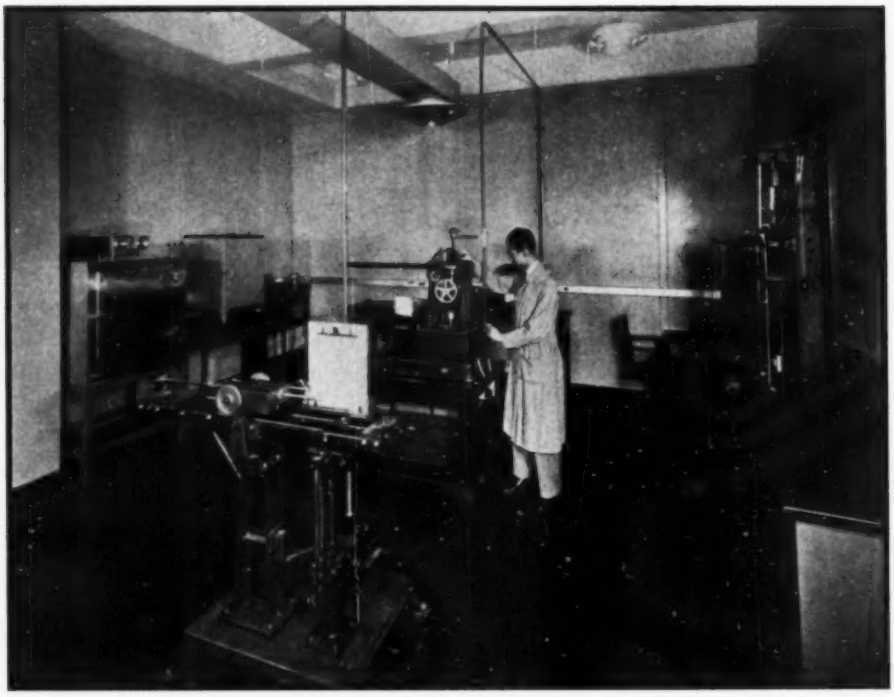

FIG. 9. Testing the physical properties of rubber at Murray Hill. Tensile, compression, and plasticity tests are conducted here on rubber compounds under controlled temperature and humidity conditions.

through, there is a cloth partition in front of the panels on the auditorium side. The side walls and ceiling of the room are panelled with mahogany. To break up reflections, the side walls are splayed and the rear wall is sloped away from the seats for the same purpose.

Paneling at the rear of the room, and that on the adjacent side walls and ceiling is perforated and backed with absorbing material to reduce reflected sound from these areas. The seats are upholstered so that each will absorb about as much sound when not occupied as a person, thus maintaining the same reverberation characteristics in the room whether it is empty or filled to capacity. For the convenience of the audience, the rows of seats are widely separated in accord with European practice. Although made quite reverberant for musical reproduction, the excellent acoustic characteristics of the listening room make it exceptionally satisfactory for speaking. There are no windows. Decorative lights are mounted on the side walls. Recessed lamps are distributed uniformly over the ceiling and spot lights illuminate the platform and speaker. These groups of lights can be used separately or in combination and most of them can also be dimmed.

LIBRARY

A technical library is an indispensable adjunct to a research laboratory and provision has been made at Murray Hill for this need by transferring about eight thousand volumes from the main library at New York. Reference books and technical periodicals make up most of the collection, since other books are always available on request from New York. The stacks are made of sheet steel with adjustable metal shelves, slotted to prevent the accumulation of dust, and the front edge of the two lowest shelves is tilted upward to aid in reading titles. Along two sides of the room, at the windows, there is a row of study carrells with chair, writing table, and shelves for the convenience of those who have long assignments and who wish to have several reference books immediately at hand. This is a valuable feature because it provides privacy and avoids the confusion and disturbance of a common study table.

ELECTRIC POWER SUPPLY

Electrical power is received from the local power company over two 13,200-volt feeders which supply a substation located near the boiler house. The voltage is reduced there by transformers to 4156 volts and then carried underground to the cellars of the main buildings by two separate feeders in non-metallic conduit encased in concrete. These feeders are connected to three loops which are buried under the cellar floors in steel conduit. Each loop is supplied by three transformers which reduce the voltage to 120 volts single phase and 208 volts three phase for distribution to the laboratories. There are transfer switches to connect each feeder to any one or to all three of the transformer groups. Each group of three transformers supplies power to one of the three distributing loops located under the cellar floors. Power to each laboratory room is supplied by connections to these loops through distributing boxes which are mounted on the building columns in the cellar. Electric power for lighting and other laboratory uses is obtained from these boxes. For lighting there is a riser at each column to serve a twenty-four foot length of the building. Electric power for the laboratories is carried from every other basement column to the outside wall and then along it to cover a forty-eight-foot section. At twelve-foot intervals there are risers which extend to the attic and power is taken from them for the laboratories through a fifty-ampere circuit breaker on each floor.

In the laboratory rooms electric power is distributed along each wall in a metal trough with removable cover plates which face out so that wiring can be readily changed. These plates are interchangeable and may be either plain or equipped with outlet and protective devices.

VENTILATING SYSTEM

Forced ventilation is provided for the chemical laboratories by blower units which take in fresh air, filter and temper it, and force it through ducts into each laboratory room (Fig. 8). The air is exhausted through the fume hoods by another set of fans. All of the ventilating equipment is located in the attic of the chemistry section of the building. Supply and exhaust ducts extend vertically from the center of this building down to each laboratory. Intake ducts are metal but those for the exhaust are ceramic tile pipes to prevent corrosion by chemical fumes. One exhaust flue is assigned to each laboratory room and a booster fan can be inserted in the line above the attic floor when greater air velocity is required. The exhaust fans maintain the air in the chemical laboratories at a slightly lower pressure than in the rest of the buildings to prevent fumes from spreading.

There is no centralized air-conditioning system in the Murray Hill buildings but a number of small conditioning units have been installed where special laboratory work requires them. The auditorium also is air conditioned.

HEATING SYSTEM

The plant is heated from the central boiler house by the vapor-vacuum system with differential control for each of the ten zones into which the buildings are divided. Areas with similar exposure are put in the same zone. The radiators in any one zone are controlled by nine resistance thermostats, a window stat, and a heat balancer. Steam is supplied by two 225-horsepower boilers at 125 pounds per square inch. The mains carry this pressure to the distribution points where it is reduced in two stages to 50 and 5 pounds. Steam at the highest and lowest of these three pressures is also available for laboratory use. A radiator is located under each window.

Completion of the Murray Hill Laboratories fortunately came just prior to our entrance into the war. The additional facilities provided there are in great demand in the present emergency and are contributing effectively toward the solution of many problems posed by the conflict (Fig. 9). The flexible building arrangements have made it possible to meet quickly all new requirements without the usual time-consuming alterations. Practically the entire staff is now engaged in war work.

Frictional Phenomena. XIV

BY ANDREW GEMANT
The Detroit Edison Company, Detroit, Michigan

Chapter XIV. Technical Applications of the Internal Friction of Solids

Abstract

IN this chapter technical applications of the solid friction concept in four different fields are discussed. These are: (1) mechanical engineering, (a) damping of unwanted vibrations in machinery—for instance, crank-shaft vibrations, (b) vibrations excited by internal friction—for instance, whirl of rotating shafts; (2) metallurgy in which damping measurement promises to be a useful new tool; (3) rubber technology, as applied to automobile tires with regard to the heat generated therein; and (4) electrical engineering, specifically dielectric losses in electrical insulating materials.

52. Damping of Crank-Shaft Vibrations

As an illustration of the technical significance of internal friction, a few selected subjects will be dealt with in this chapter. First, two instances from the field of mechanical engineering in which the damping of materials is essential will be dealt with, to be followed by a brief discussion of certain points in metallurgy in which determinations of δ seem to be of promising significance. Next comes rubber technology, in which measurements of δ are of increasing importance, and, finally, an application of solid damping to electrical engineering, namely, dielectric losses in solid insulators, will be discussed. This last mentioned section can be considered as the analogue to Section 48, in which the d.c. conductivity of solids was explained on the basis of the plastic properties of the solid.

Concerning the first of these items, namely, *vibration in machinery*, it is interesting to note that internal friction leads, according to circumstances, both to damping and to excitation of mechanical vibrations. We consider first the damping effect. This in principle is quite an obvious effect and follows from the contents of the previous chapter.

Every engine contains parts that can vibrate at certain natural frequencies, the vibrations being flexural, torsional, etc., as the case may be. In rotating engines oscillatory forces and torques are often built up, acting upon the parts mentioned, the frequencies of which are the various harmonics of the frequency of rotation as the fundamental. If one of these harmonics coincides with any of the natural frequencies of the parts, vibrations of appreciable amplitudes are sometimes built up. Such vibrations, if extended over a long period, may lead to fatigue and even ultimate fracture of the parts in question and, therefore, are most undesirable. Only low orders of harmonics—both of the exciting and natural frequencies—are dangerous, since the amplitudes of higher orders are too small. The rotation speeds at which these dangerous coincidences occur are called the critical speeds.

There are several methods of combating such resonance. One utilizes a type of dynamic compensation—for instance, the so-called inertia balance, which aims at reducing the exciting forces themselves. Another is to change the elastic constants of the affected parts in order to remove critical speeds from the range of actual running speeds. For engines that cover a wide range of running speeds (locomotives, ship drives) such procedure is not feasible, and in such cases one has to revert to damping mechanisms.

All damping processes limit the vibration amplitude by consuming the energy of vibration. Figure 124 shows this diagrammatically. The input energy (work done by the engine on the vibrating parts) is usually a linear function of the vibration amplitude of the part. The energy dissipated by damping processes is usually a second or higher power function of the amplitude. The amplitude obtained will obviously be given by the crossing point of the two curves. It will be understood that the more intensive the damping mechanism (the steeper the dissipation curve), the lower the final amplitude.

There are several ways of damping. Some are natural, such as dissipation in bearings or the viscous damping of water acting on the propeller of a ship drive. This latter type acts, however, only on certain modes (harmonics) of vibration, involving an antinode in the propeller itself. If the mode is such that there is a node in the propeller, such natural damping remains inactive. For such cases artificial dampers, operating on the dry friction basis (see Chapter XVI) are used.

There is, however, a third damping mechanism, and with this we are concerned here. It is the internal friction of the vibrating parts which, as mentioned above, helps to damp the vibrations and thus to reduce the amplitudes. The practical significance of this mechanism is, generally speaking, limited for the reason that natural damping in bearings dissipates a much larger part of the energy than internal friction. The amount dissipated through solid friction is generally not more than 10 to 15 percent of the total. Still, the fundamental fact remains that solid friction is one of the various mechanisms that keep the amplitude at a low level, and besides, there is the possibility—as suggested by Allen[1] and Kroon[2] in connection with turbine blade vibrations—of increasing artificially the solid friction of vibrating parts for the purpose of achieving a more efficient reduction of amplitudes. The present author will elaborate on this possibility in a separate paper.

Here it should suffice to illustrate this process by means of a special case, the torsional vibrations of crank shafts in reciprocating engines, for instance, Diesel ship drives.[3,4] The gas pressure torque, owing to the processes in the combustion chamber, has an irregular time curve, which shows a positive maximum at the firing period, a small negative value at the compression period and a zero value at the exhaust and intake periods. From this non-uniformity of the pressure-time curve it follows that there must exist sinusoidal torques in addition to the average unidirectional torque acting on the crankshaft. This irregular curve with a period of twice the period of rotation can be broken up by Fourier analysis into an average torque that drives the crank shaft and a number of superimposed sine curves with frequencies $\nu/2$, ν, $3\nu/2$, etc. (ν=frequency of rotation). In addition there will be sinusoidal torque components, owing to the inertia of the piston, the connecting rod, and the crank pin. While this torque will approach a pure sine curve of frequency 2ν in case of very long connecting rods, there will appear harmonics of frequency ν, 3ν . . . for connecting rods of usual length. These components have to be correctly compounded with the previous ones in order to obtain the resultant torque components.

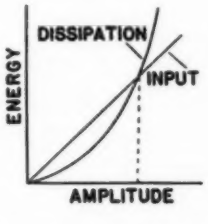

FIG. 124. Diagram of energy balance for the damping of resonance vibrations.

As to the natural frequencies of the crank shaft, stepwise numerical computations have to be carried out according to a method suggested by Holzer. In applying this method, DenHartog[3] considers a particular six-cylinder Diesel ship drive with assumed numerical data, and deduces for the first mode of torsional vibration of the crank shaft (one node between fly wheel and propeller) a frequency of 4.25 c.p.s. The second mode (two nodes) has a frequency of 21.3 c.p.s.

The next step is the computation of the work input (see above) in the case of resonance. Since the cylinders have different phases, this work will have different signs for the various cylinders, so that they partly compensate each other and the total input will be generally very small. An analysis shows that only for the third, sixth . . . orders of harmonics (with frequencies 3ν, 6ν, etc.) will the phase relations of the cylinders be such as not to compensate each other. Hence, continuing the example of DenHartog, with a critical speed of 85 r.p.m., the third harmonic ($(85/60)\times 3$) will be in resonance with the first mode (4.25 c.p.s.). The energy input as the product of torque times amplitude is proportional to the first power of the amplitude, and is given for the particular resonance just mentioned by

$$53{,}000\beta \text{ ft. lb./cycle}$$

if β, the amplitude of the propeller, is measured in radians.

Because of the antinode at the propeller,

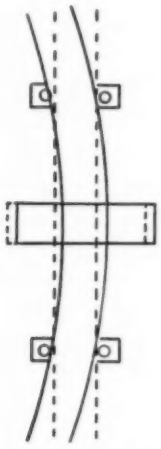

FIG. 125. Deflection of a rotating shaft in whirl.

viscous damping will be the chief factor; the energy dissipated per cycle is computed by Den Hartog as

$$2{,}150{,}000\beta^2 \text{ ft. lb./cycle.}$$

From these two expressions

$$\beta = 0.025 \text{ radian} = 1.4 \text{ deg.}$$

is obtained.

Internal friction (plus bearing losses) will determine the amplitude in cases where the second mode with a node at the propeller is excited, or when the engine does not drive a propeller but, say, an electric generator. The losses due to solid friction can be computed, but the bearing losses cannot. It is customary to multiply the former by an empirical factor so as to obtain the total loss.

In the previous chapter it was shown that the loss per cycle is given by the product logarithmic decrement $\times$ vibrational energy. The former is independent of the amplitude for small amplitudes, but increases with the amplitude for larger values of the latter. The elastic energy of a vibrating shaft is proportional to $\beta^2 D^4/l$ (D = diameter, l = length). Since β is different for the various sections of the shaft, the loss for each section has to be computed and the total loss obtained by addition. The empirical factor for steel as used in practice for this case is 635,000, giving the loss in in. lb. if D and l are measured in inches. The logarithmic decrement is taken empirically as proportional to $\beta^{0.3}$ and the dimensionally correct empirical formula for the losses then reads:

$$635{,}000\frac{D^{4.3}\beta^{2.3}}{l^{1.3}} \text{ in. lb./cycle.}$$

In cases with no external damping the latter formula may be used for computing the amplitude.

Let us estimate the amount of energy dissipated in the shaft as compared with the total loss of 1300 ft. lb./cycle as given by Den Hartog for a propeller amplitude of 1.4 deg. The only section to be considered is that between fly wheel and propeller, since the amplitude in the sections between cylinders is much too small. The elastic constant k of this section was computed by Den Hartog to be 13.5×10^6 in. lb./rad. The amplitude of this section is 1.26 times that of the propeller. Thus the total energy is known from the formula $(1.26^2/2)k\beta^2$. This has to be multiplied by the logarithmic decrement for relatively large amplitudes of strain. Taking the value of 0.09 as determined by Föppl[5] for torsional vibrations of steel at 5 c.p.s. and a strain around 10^{-3}, the loss per cycle due to damping is 50 ft. lb., i.e., about 4 percent of the total.

For speeds higher than the one considered here, say, around 200 r.p.m., the sixth harmonic will be in resonance with the second mode of vibration (21.3 c.p.s.), and corresponding computations will show that internal friction will have a much greater influence upon the amplitude than for the first mode of vibration.

53. Whirl of Rotating Shafts

As a counterpart to damping of mechanical vibrations by internal friction, instances in which vibrations are excited by internal friction will now be discussed.

A few words should be added here regarding the general principle of self-excited vibrations. While maintained vibrations are caused by external forces, in the case of self-excited vibrations there is an internal force active, and it can be shown that this internal force acts in phase with the rate of displacement. The general differential

equation has the form:

$$-m(d^2x/dt^2)+R(dx/dt)-kx+F=0. \quad (159)$$

It will be remembered that in the usual differential equation of this type [see Eq. (140) for instance], the factor proportional to dx/dt is negative, indicating a damping force. In the present case the term $R(dx/dt)$ is of the nature of a driving force. The solution of Eq. (159) is then a sinusoidal vibration with an exponentially increasing amplitude. Thus, a vibration will build up. In practice this increase will continue, until other, typical damping forces will absorb the work done by the driving force $R(dx/dt)$.

There are a large number of instances in which vibrations of this type occur, not only in mechanical but also in electrical engineering. Some of these will be dealt with in Chapter XVI, in connection with external friction of solids. In particular, it will be shown that a driving force decreasing with increasing velocity (so-called negative characteristic) is often encountered in cases of self-excitation.

In the present connection the so-called whirl of rotating shafts will be discussed, since the driving force in this case is the internal friction of the shaft material. It will be recalled (Section 50) that Kimball utilized this effect for the determination of δ in various materials.

Figure 125 shows a rotating vertical shaft between two bearings with a fly wheel in the center. The normal position of the shaft is shown by the dotted line. The shaft may perform flexural vibrations that, if performed in two perpendicular directions, correspond to a whirling motion, the position of the shaft being that shown by the full line. Whirl will take place with the natural frequency ν_w of flexural vibrations, given in terms of the constants of Eq. (159) as

$$2\pi\nu_w=(k/m)^{\frac{1}{2}}.$$

Apart from this whirling motion the shaft will perform the machine rotations of frequency ν_r. It will now be shown that for $\nu_r>\nu_w$ internal friction in the shaft gives rise to a driving force that builds up a whirling motion originating from the slightest disturbance.

Figure 126 shows the cross section of the shaft (large circle) at the location of the fly wheel. Anticlockwise rotation is assumed. Independently there is a whirling motion owing to which the shaft center A is driven around the point B (center of shaft at rest). The whirl should have the same direction as the rotation. It is now assumed that $\nu_r>\nu_w$, and for the sake of simplicity (this is not necessary) let us add that the difference is large; thus, while one cycle of rotation is performed the position of the shaft remains practically the same as shown in the figure.

It will be noted from the figure that the left half of the shaft is under compression, the right half under tension, the middle plane (CD) being the neutral plane in which the strain is zero. Because of the rotation, individual fibers will perform cyclic changes of strain: the fiber at E, for instance, is in tension; after $\frac{1}{4}$ of a cycle it arrives at C and has no strain, and so on. The frequency of this cyclic process is obviously $\nu_r-\nu_w$.

It now should be recalled that, in cases where the material has an internal damping, strain and stress are not exactly in phase. This is brought out clearly in Fig. 121 of Chapter XIII to which the reader is referred. When the fiber at E (Fig. 126) rotates toward and passes the point C, the corresponding curve in Fig. 121 will be the curve DEF of the loop. From this latter curve it can be seen that the point of zero stress E does not coincide with the point of zero strain, but is a little in advance. Reverting to our present Fig. 126, this means that the point of zero stress will not coincide with the point C, but will be a little in advance, say, at F. Extending this reasoning to the lower half of the circle, it will be seen that the neutral plane of stress (FG) is

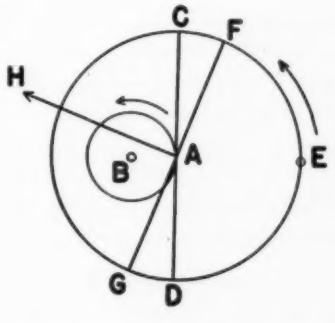

FIG. 126. Cross section of a rotating shaft in whirl.

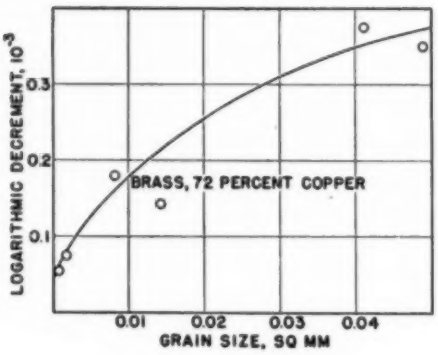

FIG. 127. Damping of brass *vs.* grain size (Förster and Köster).

tilted by a little angle (exaggerated in the figure) toward the plane *CD*.

If, now, the neutral stress plane is shown by the line *FG*, then the plane of maximum stress is that shown by the line *AH*. The stress in this direction can be resolved into two components. The larger one acts in the direction *AB*, and corresponds to the elastic force opposing the bending of the shaft. A smaller component acts in the direction *AC* and drives the shaft center along the path of whirl. This component is thus in the direction of the whirl velocity and will help in building up the whirl in a direction equal to that of the rotation.

It can be shown by similar reasoning that the component in the *CD* direction will oppose the motion, acting as a damping force, if the rotational frequency is less than the resonance frequency ν_w. Only if the rotational frequency becomes larger than ν_w will a whirl develop, the amplitude of the whirl increasing with increasing internal friction. In cases like this high internal friction is unwanted, since excessive whirl might lead to fatigue.

In the light of this explanation the method used by Kimball (compare Fig. 109) for the measurement of internal friction, and discussed in Section 50, will now be completely understandable with regard to its physical basis.

54. *Metallurgical Applications of Damping Measurements*

The measurement of internal damping promises to be a very useful tool in metallurgy. These studies are in preliminary stages yet, chiefly because the decrement is affected by various properties of the metals; thus it is generally not easy to draw definite conclusions from the former to the latter. In all those cases, however, in which one particular property is varied, the influence upon δ is clear and instructive.

The chief advantage of the method is that it is non-destructive, and does not even change the shape of the specimen. Besides, it is comparatively simple and can be carried out quickly. For series measurements, the purpose of which is to follow up the changes with time that occur during certain treatments of the specimens, the method appears to be of particular value.

The great variety of properties that have an influence upon δ can best be discussed under three different groups, as follows:

(*a*) *Characteristic Properties of Metals*

In the previous chapter we mentioned that δ generally increases with increasing *temperature*, but there are occasional maxima observable, for instance, with glasses. With metals, such maxima are observed in temperature ranges at which the metal undergoes a transition from one crystallographic structure to another, so-called polymorphic transitions. Such a maximum occurs with cobalt near 400°C when a transition takes place from the hexagonal ϵ to the cubic γ-state. This transition, as well as the maximum in the δ-temperature curve is reversible. Nickel-steel, taken at decreasing temperatures, shows a maximum near 100°C where a transition from the γ- to the α-state takes place. These data, as well as most of the others in this section, are taken from an extensive research of Förster and Köster.[6,7] It is known that metals in the state of transition

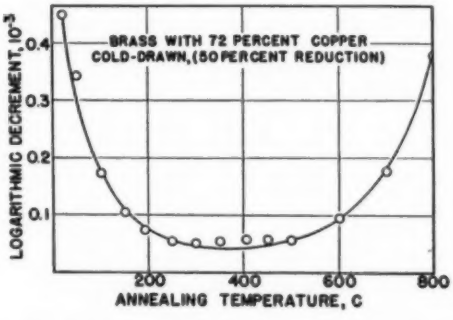

FIG. 128. Damping of brass *vs.* annealing temperature (Förster and Köster).

show an increased plasticity; high values of δ are explainable on this basis [Eq. (157)].

The *grain size* has a pronounced effect upon δ, as was discussed theoretically in the previous chapter [see Eq. (153)]. For a given frequency δ should then go through a maximum if plotted against the grain dimension. Figure 127 shows δ of brass (72 percent copper) *vs.* grain dimension (after Förster). It seems that the maximum corresponds to somewhat larger grains than those investigated. Recalling Fig. 120, it may be seen that with frequencies around 10^4 the maximum lies around 10^{-1} mm grain size. Orders of 1-mm grain size will produce a maximum around frequencies of 10^2.

The influence of *annealing* upon δ is usually complex, since various single effects might overlap. An example is given in Fig. 128, showing δ *vs.* annealing temperature in the case of brass. Below the range of recrystallization (300°C) the decrement drops rapidly owing to relief of internal stresses (see below). With increasing grain size due to recrystallization, δ later increases considerably. The hardness slightly increases up to 300°C, then falls off considerably.

In the case of alloys, δ is usually a function of the *composition*. This can be shown for brass, the decrement decreasing considerably with increasing percentage of zinc, the reason being the increase of plastic resistance. The decrement of steels also decreases if the carbon content is increased.

(*b*) *Faults in Metals*

One of the features to be discussed here is the presence of *residual stresses* in metals due to the previous heat treatment. Figure 129 shows this effect clearly on steel (0.9 percent of carbon) that had been quenched from 900°C, and on a sample of cold-drawn brass. With shelf-aging [see Subsection (*c*) below] the residual stresses caused by quenching and drawing are released, and the damping decreases with time in both samples. The same effect is noticeable in Fig. 128 at temperatures below 300°C, as already mentioned.

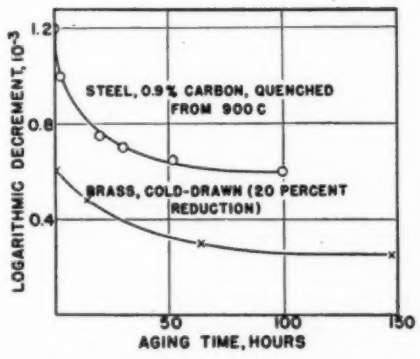

FIG. 129. Relief of internal stresses during aging of steel and brass, as measured by damping (Förster and Köster).

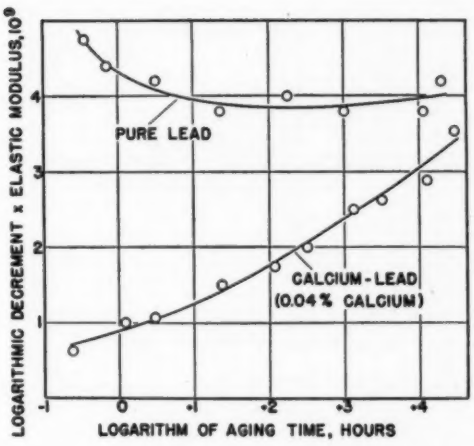

FIG. 130. Damping of pure lead and calcium-lead *vs.* aging time (Wegel and Walther).

Tarnopol and Morgan[9] noticed a drop in δ of machined steel after being aged for several weeks and subsequently annealed at 400°F. The original values were 0.01 at 6000 lb. per sq. in. maximum stress and up to 0.09 for 24,000 lb. per sq. in. whereas the final values were 0.005 and 0.02, respectively.

The theory of this effect in the light of Zener's mechanism has been discussed in Section 51, these practical applications being a qualitative check of the theory.

Another instance of faulty, unwanted properties in metals, detectable by measurements of δ, is the presence of internal cracks, or generally *flaws* of any kind. If, for instance, steel is quenched from 1100°C, damping increases considerably with time, owing to the formation of microscopic cracks.

The damping method also enables one to determine the orientation of a flaw in a metal specimen. If a circular specimen is excited to vibrations starting from different points along its circumference, a polar diagram showing δ in all radial directions is obtained. If the curve

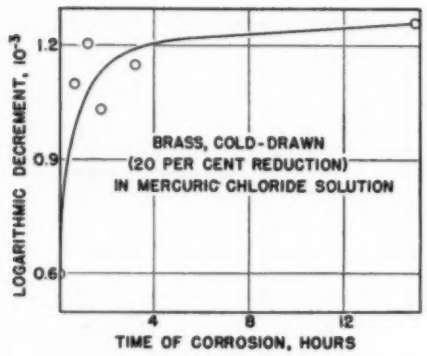

FIG. 131. Damping of brass *vs.* time of corrosion (Förster and Köster).

deviates from a circle, showing peaks in a particular radial direction, it can be concluded that the flaw is oriented perpendicularly to that direction.

(*c*) *Processes in Metals*

This third group is particularly important from a technical standpoint. One of the processes of interest is *aging*. This was previously mentioned under (*b*) in connection with residual stresses. Aging in general might cause either a decrease or an increase of δ, depending upon the particular effect in question. We show here two interesting curves (Fig. 130) of δ *vs.* time on pure lead and calcium-lead, as obtained by Wegel and Walther.[5] The tests were extended over a period of three years. The damping is shown here as the so-called hysteresis constant, $E\delta$ (see Table XVII, Section 50); since E varies little, if at all, with aging, the quantity is a direct measure of the decrement. The data show that the damping of pure lead is 2 to 5 times larger than that of calcium-lead, in agreement with similar differences noted in their plastic resistance (see Fig. 100). Besides, pure lead shows a decrease of δ with time, probably owing to relief of residual stresses, as in the cases shown in Fig. 129. The other sample indicates an increase of the damping, probably owing to a slow formation of condensation nuclei of a compound Pb_3Ca, which act as grains of increasing size. Thus, measurement of δ is a suitable means for following up the aging of metals.

Another process of technical importance in this group is intercrystalline *corrosion*. This process leads to a loosening of neighboring grains, hence to a large number of minute cracks that will increase the damping considerably. The mechanism of increased loss in these cases may be due partly to a decreased flow resistance of the material at the location of flaws (see Section 43), partly also to local external frictional processes between opposite walls of a microscopic crack.

Figure 131 shows the increase in damping of a cold-drawn brass specimen under the corrosive action of a one percent mercuric chloride solution (Förster).

The method is very suitable for this particular purpose, since it is non-destructive and can be carried out on a single sample. The latter is removed from the bath for each measurement, after which it is reimmersed and the corrosion process allowed to continue.

55. *Damping in Rubber—Automobile Tires*

While measurements of internal friction in metallurgy are made chiefly for the purpose of determining other properties and the nature of the pre-treatment of the specimen, in rubber technology internal friction is used in its primary meaning, namely, as a measure of heat losses from vibrations. A brief explanation of this field, in particular reference to automobile tires, now follows.

The chief purpose of tires is to provide an adequate damping of such vibrations as may be caused by the unevenness of the road surface. Figure 132 is a schematic presentation of an automobile, A representing the mass of the body, B the spring suspensions, C the mass of the axles, and D the tires in contact with the road surface. The role of the two elastic elements B and D in series is to minimize the vibrational amplitudes of the body x_b as compared with the forced vibrations of the tires due to bumps in the

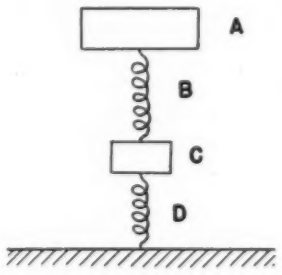

FIG. 132. Schematic model of a vertically vibrating automobile.

road surface x_r. This ratio is called transmissibility and is given by

$$x_b/x_r = \nu_1^2\nu_2^2/(\nu^2-\nu_1^2)(\nu^2-\nu_2^2), \qquad (160)$$

where ν_1 and ν_2 are the two natural frequencies of the system, and ν is the impressed frequency. It can be seen that sufficiently small values of the ratio are obtained only if ν is larger than either of the natural frequencies. This is equivalent to saying that the natural frequencies have to be kept sufficiently low, i.e., the two springs sufficiently soft.

We are not concerned here with the steel spring design, only that of the tires. The tires then should be sufficiently soft to fulfill the above-mentioned frequency condition. The softness of the tires depends partly upon the elastic modulus of the tire material, partly upon the tire pressure. It is only the former factor with which we are concerned in this connection, and our present requirement then means that the modulus of the tire material should not exceed a certain upper limit.

There are, however, other considerations that will affect the choice of material. The tire material must have good abrasion resistance and high mechanical strength. This consideration excludes the use of soft rubber mix, although it has a very low modulus. It has been found that it is possible to improve the mechanical properties of the rubber, without increasing the modulus beyond the above-mentioned limit. This aim is achieved by adding to the mix so-called reinforcing fillers of which finely divided carbon black is the most important. Carbon black acts similarly to a vulcanizer in that chemical bonds between the carbon particles and the rubber molecules play an essential role, an effect by which the reinforcing mechanism is explainable.

These considerations show that a certain medium range of modulus for rubber is required which is obtainable by the addition in various amounts of various fillers. The question as to the best filler and its optimum concentration in the mix can be answered, however, only by taking into account a third essential factor, and this is the heat generation in the tires.

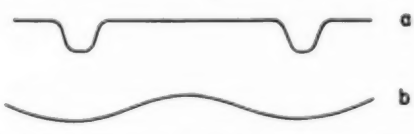

FIG. 133. (a) Cyclic deformation of an automobile tire *vs.* time. (b) Fundamental of the deformation. (Both schematic.)

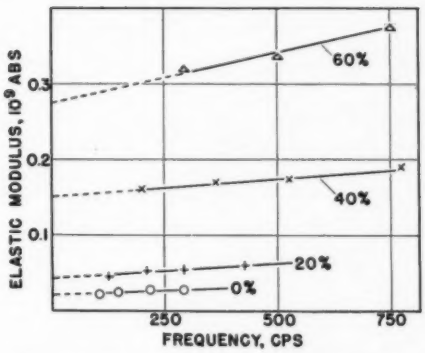

FIG. 134. Elastic modulus *vs.* frequency for rubber stock and tread containing various loadings of gas black (Naunton and Waring).

As the wheel rotates, each part of the circumference is compressed when it touches the ground, the length of the section compressed at a given moment decreasing with increasing tire pressure. The deformation *vs.* time curve of each element will look somewhat as shown in the schematic Fig. 133a, a curve that—analyzed after Fourier—will have a fundamental as shown in Fig. 133b and a number of harmonics. The fundamental has the frequency of the rotation of the wheel, which is about 11 c.p.s. for 60 m.p.h., the various harmonics (of which only the lower orders have relatively large amplitudes) being the multiples of this figure, the tenth, for instance, having a frequency of 110 c.p.s.

This alternating deformation develops heat according to the principles detailed in Chapter XIII and causes the temperature of the tire to rise. External frictional processes also contribute to the heat produced, but internal friction is the chief source. Since rubber deteriorates at a rate that increases rapidly with temperature, it is essential to keep the amount of heat generated in the time unit low.

This amount can be calculated by using Eq. (143) in which δ is related to ΔW, the heat produced per cycle. The heat generated per second, H, is then, with ν = frequency

$$H = 2\nu\delta W.$$

W can be expressed in the terms of Eq. (140) as

$$W = F^2/2k,$$

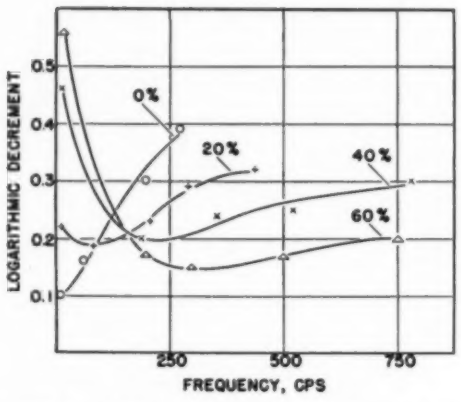

FIG. 135. Logarithmic decrement *vs.* frequency for rubber stock and tread containing various loadings of gas black (Naunton and Waring).

where F = external force, giving

$$H = F^2\nu\delta/k. \tag{161}$$

By means of Eq. (145) δ can be replaced by the equivalent viscosity, a quantity proportional to b of Eq. (140), if wanted.

In our particular case, the external force F, that compresses the rubber is the weight of the car, thus a constant for a given car (this is only approximately true). In order to evaluate the amount of heat generated it is essential to have the damping and the modulus measured as a function of frequency for various mixes. The equation shows the loss to increase with increasing decrement and with decreasing modulus. A high modulus within the range allowed—as specified above—is, therefore, desirable. The reason is that higher modulus causes smaller deformation, hence produces less heat, for a given external force.

Extensive research was carried out along these lines by Naunton and Waring[10,11] and also by S. D. Gehman[12,13] *et al.* Some of their experimental data will be given in order to illustrate the considerations above.

Of the several possible reinforcing fillers, carbon black is most frequently used. Figures 134 and 135 show—after data of Naunton and Waring—elastic modulus and logarithmic decrement for gum stock and for tread containing 20, 40, and 60 percent gas black (Kosmos *T*). The frequency was varied from low values to around 1000 c.p.s. Losses were obtained in terms of what rubber technologists call "percentage resiliance," a quantity given by $100e^{-\delta}$, from which the data in Fig. 135 were plotted.

The modulus increases somewhat with the frequency, and quite considerably with the volume loading. The function δ *vs.* frequency goes through a minimum with frequency. For the low frequency range, up to about 150 c.p.s., δ increases with the volume loading; for higher frequencies the situation is reversed. As explained above, the range below 150 cycles is of chief interest. It will be seen, if values for, say, 40 percent gas black and gum stock are compared in the low frequency range, that the increase in modulus exceeds the increase in decrement. According to Eq. (161) this means that the heat generated must be smaller for the mix than for the gum stock.

This conclusion is brought out clearly in Fig. 136 (after S. D. Gehman *et al.*) which gives relative dissipation values, obtained at a frequency of 60 c.p.s., as a function of volume loading for three different fillers. The superiority of carbon black as compared with zinc oxide is evident for concentrations above 20 percent. From combined mechanical and thermal considerations it follows that carbon black in a concentration of around 40 percent will yield the technically best product.

Synthetic materials can be compared with rubber, using the same method. This was done for Neoprene (polymer of chloroprene, $H_2C : CCl \cdot\cdot CH : CH_2$), as shown in Fig. 137. Equivalent viscosity, η' and modulus E are plotted *vs.* frequency. The heat generated is proportional to η'/E^2. In the low frequency range E of Neoprene is about 40 percent higher than that of rubber,

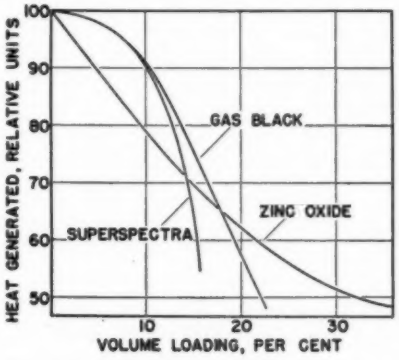

FIG. 136. Heat generated *vs.* volume loading for three rubber mixes at a frequency of 60 c.p.s. (S. D. Gehman *et al.*).

while the viscosity is about doubled. Thus the heat generated is about the same in both materials, showing that Neoprene—from this standpoint, at least—is equivalent to rubber. It should be added, however, that heat losses in other types of synthetic rubber (styrene copolymers, for instance) are higher than in natural rubber.

The logarithmic decrement of natural and synthetic rubber is often found to decrease with increasing temperature. According to the plastic mechanism the decrement obviously increases with increasing temperature [compare Eq. (154) or (157), also Figs. 112 and 115]. Hence the loss over the temperature range in question must be due to the thermal mechanism.

It is also possible to follow the process of vulcanization by means of this method. The modulus increases and the decrement drops considerably during the first hour of vulcanization at 140°C, after which both change only slightly.

56. Dielectric Losses in Solid Insulating Materials

In concluding this chapter, some remarks will be made on the correlation between internal friction and dielectric losses in insulating materials. This section is to be considered as a logical extension of Sections 38 and 48. The former explained ionic and dipolar mobility in liquids in terms of liquid viscosity, the second dealt with the possibility of explaining ionic mobility in solids in terms of the plastic resistance. In this section it will be shown that, in keeping with our general idea, mobility of dipoles in solids might be explained in terms of the internal friction.

In homogeneous liquids the viscosity constant describes both steady and alternating processes. Thus the same value of η—as obtained by mechanical measurements—was used in Stokes' equation, describing ionic mobility, Eq. (105), and in Debye's equation [Eq. (107)], characterizing the frequency peak for dipole rotations.

In solids the situation is somewhat different. While steady state processes are controlled by the plastic resistance η, vibrations are controlled by internal friction, corresponding to an equivalent viscosity η', which is numerically much smaller than η. Hence the latter, and not η, must be used, if dipole rotation in solids is described.

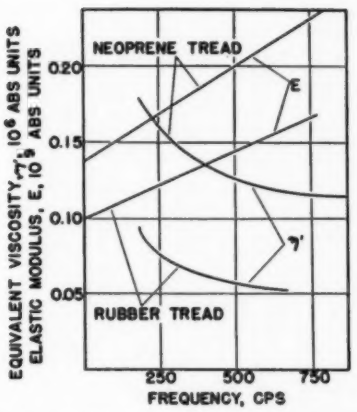

FIG. 137. Equivalent viscosity and modulus *vs.* frequency for Neoprene and rubber treads (Naunton and Waring).

Of course, first the general question must be answered—whether it is at all correct to describe the motion of these small electrically charged particles in terms of resistance obtained by mechanical deformation of the body. This question was discussed in Section 48 and answered (with certain restrictions) in the affirmative. When dealing with rotation of dipoles—responsible for dielectric losses in a large number of cases—the same doubt might arise. In vibrating a body as a whole, all particles shift against each other while, in the vibration of a dipole molecule, this dipole molecule will shift against its immediate neighborhood. This obviously means that the resistances in both cases are not identical. However, a close relation between the two certainly exists, as was shown in Section 48 for the ionic mobility in glass.

In a solid material that is inhomogeneous—for instance, a plasticized polymer—the two resistances might be quite different, because the dipoles probably move in the internal liquid phase; whereas in mechanical deformations the solid frame itself will be deformed and shifted against the liquid phase. The more a solid approaches homogeneity, the closer the relation between the two resistances in question.

In attempting to give an explanation of dipolar mobility in terms of solid friction, it will be useful first to give a few examples of experimental material in this field.

Data on various insulators exist in great number. The results can be summarized roughly by saying that the dielectric power factor shows

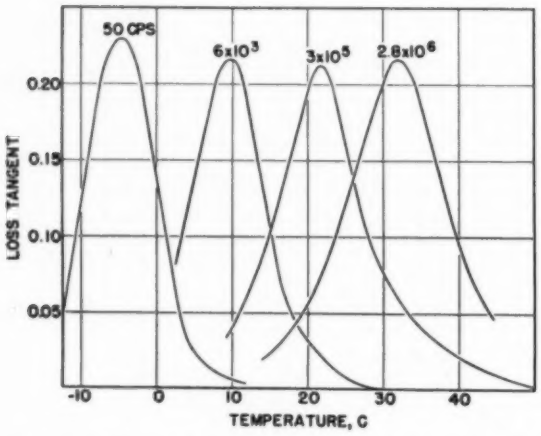

FIG. 138. Dielectric loss tangent of chlorinated diphenyl as a function of temperature, at various frequencies, as shown (after W. Jackson).

an irregular variation with frequency and temperature. Generally, however, the power factor varies only little with frequency, showing rather flat maxima in certain regions; it generally increases with increasing temperature, again interspersed with regions of maxima.

While the interpretation of data on technical insulators is difficult, the picture becomes much clearer on homogeneous substances that are chemically better defined. Figure 138 gives the loss tangent of chlorinated diphenyl as a function of temperature for frequencies varying from 50 to 2.8×10^6 c.p.s. These data are from the Oxford Engineering Laboratory, obtained by W. Jackson.[14] Extensive research along similar lines using dipole materials of homologous series in paraffin wax was carried out by Sillars[15] and Pelmore,[16] both at Oxford. Fuoss *et al.*[17,18] and Garton,[19] on the other hand, carried out a similar research on polymer materials that are chemically well defined. Figure 139 gives the loss tangent of polyvinyl chloroacetate as a function of frequency from 60 to 10^4 c.p.s. for different temperatures after Fuoss. Both sets of curves shown in Figs. 138 and 139 show pronounced maxima.

Maxima of this type in the presence of dipolar molecules indicate clearly that the loss is due to the rotation of the dipoles in the alternating field. The maximum loss occurs when the frequency coincides with the reciprocal of the relaxation time τ_d of the dipoles, as given by

$$\tau_d = 4\pi\eta' r^3/kT, \qquad (162)$$

with r = radius of rotating molecule (or radical if only part of a complex molecule rotates). The loss tangent itself, according to Debye's theory, is given approximately by

$$[(\epsilon_0-\epsilon_\infty)\omega\tau_d]/[\epsilon_0+\epsilon_\infty(\omega\tau_d)^2], \qquad (163)$$

where ϵ_0 and ϵ_∞ = dielectric constants at frequencies zero and infinite, and $\omega = 2\pi\nu$. The difference $(\epsilon_0-\epsilon_\infty)$ is a measure of the concentration of dipoles and their dipole moment. We are not concerned here with a derivation of these equations. Although valid only for liquids, the equations may be used as an extrapolation for solids as well; for certain crystalline materials in which several distinct orientations of the molecules are possible, quantum relations will enter into the process.

In contradistinction to these pronounced peaks, Fig. 140 gives the loss tangent of polyvinyl acetate at 33°C as a function of frequency from 10^3 to 10^7 c.p.s. (after Mead and Fuoss). The loss tangent varies here only little with the frequency. This type of behavior has its basis often in a superposition of several time constants (several peaks), but might be explained also by the characteristic of internal friction, as will be shown below.

In interpreting dipole losses in solids, the use of the steady state plastic resistance in Eq. (162), as already stated, is not correct. It will hold for the liquid state, up to viscosities of 10^3 poises or so, but not beyond. This can be shown clearly through an analysis of Jackson's data as given in Fig. 138. He computed relative viscosities for chlorinated diphenyl, using Eq. (162), in a temperature range from -5 to $+40$°C. Viscosities of the compound were then measured in a temperature range from 15° to 55°C by means of the Gemant-Southwell oscillation viscometer (see Section 25). The computed relative set was made to coincide with the measured set at a viscosity of 100, and the two sets were plotted (Fig. 141). The agreement is, indeed, very good, as far as the direct viscosity determinations were feasible. Beyond this range, however, the values for η certainly rise very rapidly, much more so than the calculated curve, since the material at -10°C is a glassy solid, with η of the order 10^{14} to 10^{16}, while the calculated curve approaches 10^8 for that temperature.

The plastic resistance of solids (see Chapter XII) is of the order of 10^{16} and higher. The order of r is 5×10^{-8} cm, so that in the neighborhood of room temperature we have from Eq. (162) approximately

$$\tau_d = 3\times10^{-8}\eta'. \qquad (164)$$

With a viscosity value of $\sim10^{16}$, the order of τ_d becomes 10^8, in obvious disagreement with experimental results that show that τ_d is around $10^{-2}-10^{-4}$ (corresponding to frequencies at the peak of 10^2-10^4 c.p.s.).

The use of such high viscosities would mean, in other words, that with the usual frequencies the dipoles are unable to move at all. This conclusion would be wrong, however, since the finite elasticity E, which is in series with η (see Fig. 122a) will permit a certain motion, however high the viscosity. The motion of the dipole is then described by an equation of the type Eq. (140), and the viscosity to be used is the equivalent viscosity η' (see Fig. 122b).

The value of η' can be deduced on a physical basis, making use of the simple model (Fig. 122a). This model shows a reversible elastic component, the deformation of which occurs with finite rate because of the parallel frictional element; the model was set up to comply with observations of the plastic flow in solids. It was shown in Section 51 that numerical values assigned to the elements in the case of lead, which values were derived from experimental data on the plastic flow of this material, allow values for the decrement δ to be deduced, again in agreement with experimental data on vibrating lead samples.

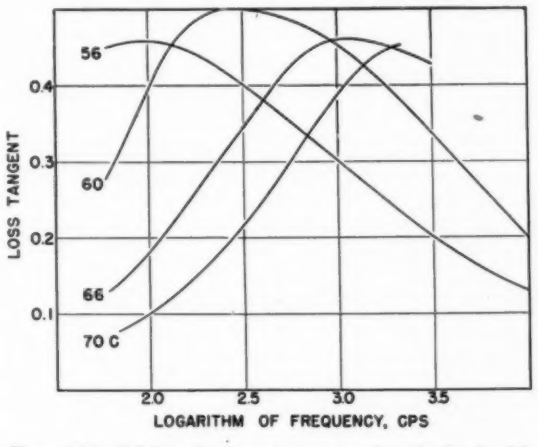

FIG. 139. Dielectric loss tangent of polyvinyl chloroacetate as a function of frequency, at various temperatures, as shown (after Mead and Fuoss).

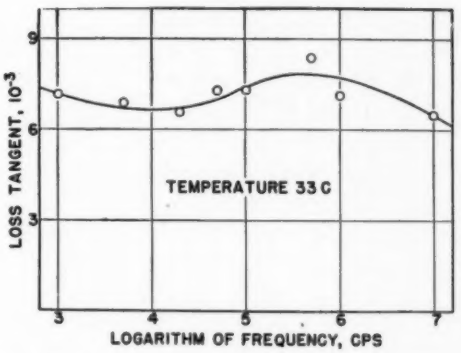

FIG. 140. Dielectric loss tangent of polyvinyl acetate *vs.* frequency (Mead and Fuoss).

While the author does not know of the existence of any quantitative experimental data on insulating materials comparable to those of Lyons on lead, it will be perfectly allowable to use the same concept for the plastic properties of both. This is the more justifiable as tests on creep (see Chapter XI) indicate a general similarity between processes in metals and dielectrics. Hence the use of η' in Eq. (162), as derived from internal friction data by means of Eq. (145), is also justified.

Decrement data on solids are available in the low frequency range and, in order to check orders of magnitude, a value of 3×10^{-2} should be taken (see Table XV). The elastic modulus ranges around 10^{11} abs. units. With these values and $\nu\sim10^2$ to 10^4, the order of the equivalent viscosity η' in the low frequency range becomes around 10^5 abs. From Eq. (164), τ_d then becomes 3×10^{-3}, corresponding to a frequency at the peak of 300. In other words, our theory yields for the equivalent viscosity of a solid dielectric an order that points to dipole loss maxima near room temperature occurring in the low frequency range. This is exactly what happens, as can be seen from Figs. 138 and 139.

There are two possibilities as to the behavior of η' with varying frequency. One is that in a certain frequency range η' varies only slightly with the frequency. In this case a typical maximum in the power factor curve will develop. Apart from the examples shown above, rubber seems to belong in this group too.

Rubber was dealt with in Section 55 in which

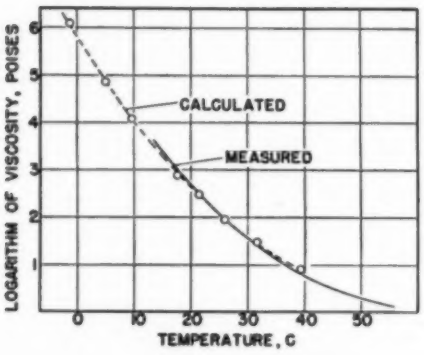

FIG. 141. Viscosity *vs.* temperature for chlorinated diphenyl. ○ = calculated points (made to coincide with measured curve at ordinate = 2), after W. Jackson.

Fig. 137 indicates that η' for frequencies above 500 does not change much. Similarly data of S. D. Gehman[12] show the value of η' for gum stock containing 3 percent sulfur to be fairly constant (3×10^3) between 50 and 100 c.p.s. With this value τ_d becomes 10^{-4}, i.e., the frequency at maximum is 10 kc. This might be compared with data of Scott *et al.*[20] on a rubber sample containing 4 percent sulfur. The peak at 5°C occurs with a frequency of 100 kc, which is in fair agreement with the computed order [a slight change in r, see Eq. (162), has a great effect on τ_d].

The other possibility is that, in a certain frequency range, η' decreases with the frequency, and it is the decrement δ that varies only slightly. In the previous chapter this occurrence was shown to be quite frequent. From Eq. (145), which may be written as

$$\omega\eta' = E\delta/\pi, \tag{165}$$

it can be seen that $\omega\eta'$ is then approximately constant and, combining this with Eq. (164), $\omega\tau_d$ will be constant, too. From expression (163) it can be seen that in such a case the loss tangent must be a constant in the particular frequency range, an occurrence that, as pointed out before, often happens (see Fig. 140).

With $\delta\sim0.03$ and $E\sim10^{11}$, $\omega\eta'$ becomes 10^9—compare with Eq. (149)—and $\omega\tau_d$ about 30. Equation (163) then shows the power factor level to be of the order of 0.03 which again is the correct order of magnitude.

In spite of the fact that the numerical calculations given above are very crude, it can be seen that the theory, as developed by the author,[21,22] gives a fairly unified and quantitatively acceptable explanation of losses in solids. It reduces an electrically measurable quantity to mechanically measurable data—and the quantitative connection of widely differing fields is the chief purpose of any theory.

It should be mentioned that there are several other viewpoints from which to consider dipolar losses in solids. One, suggested by K. S. Cole,[23] does excellent services in analyzing power factor data obtained on solids, and has been utilized successfully by Mead and Fuoss,[17] and by Field.[24] This analysis can be used whatever the physical nature of the loss mechanism. Among other viewpoints, that based on a superposition of several time constants is the most popular. This idea, originally developed by K. W. Wagner, has recently been applied to dipolar losses successfully by Garton[19] and Kirkwood and Fuoss;[25] there is no contradiction between this idea and those developed in this section.

BIBLIOGRAPHY TO CHAPTER XIV

1. R. C. Allen, Trans. A. S. M. E. **62**, 689 (1940).
2. R. P. Kroon, Trans. A. S. M. E. **62**, A161 (1940).
3. J. P. Den Hartog, *Mechanical Vibrations* (McGraw-Hill, New York, 1940), p. 226.
4. Ralph Poole, Proc. Inst. Mech. Eng. **146**, 167 (1942).
5. O. Föppl *et al.*, *Die Dauerprüfung der Werkstoffe* (Springer, Berlin, 1929).
6. F. Förster and W. Köster, Zeits. f. Metallk. **29**, 116 (1937).
7. F. Förster and W. Köster, The Engineer **166**, 626 (1938).
8. R. L. Wegel and H. Walther, Physics **6**, 141 (1935).
9. L. Tarnopol and J. R. Morgan, J. App. Phys. **13**, 343 (1942).
10. W. J. S. Naunton and J. R. S. Waring, Proc. Rubber Tech. Conf. (1938), p. 805.
11. W. J. S. Naunton and J. R. S. Waring, Trans. Inst. Rubber Ind. **14**, 340 (1939).
12. S. D. Gehman, D. E. Woodford, R. B. Stambaugh, Ind. Eng. Chem. **33**, 1032 (1941).
13. S. D. Gehman, J. App. Phys. **13**, 402 (1942).
14. W. Jackson, Proc. Roy. Soc. **A153**, 158 (1935).
15. R. W. Sillars, Proc. Roy. Soc. **A169**, 66 (1938).
16. D. R. Pelmore, Proc. Roy. Soc. **A172**, 502 (1939).
17. D. J. Mead and R. M. Fuoss, J. Am. Chem. Soc. **63**, 2832 (1941).
18. D. J. Mead, R. L. Tichenor, and R. M. Fuoss, J. Am. Chem. Soc. **64**, 283 (1942).
19. C. G. Garton, J. Inst. Elec. Eng. **85**, 625 (1939).
20. A. H. Scott, A. T. McPherson, and H. L. Curtis, Bur. Stand. J. Research **11**, 173 (1933).
21. Andrew Gemant, Trans. Faraday Soc. **34**, 269 (1938).
22. Andrew Gemant, J. App. Phys. **9**, 730 (1938).
23. K. S. Cole and R. H. Cole, J. Chem. Phys. **9**, 341 (1941).
24. R. F. Field, Trans. A. I. E. E. **60**, 890 (1941).
25. J. G. Kirkwood and R. M. Fuoss, J. Chem. Phys. **9**, 329 (1941).

Résumés of Recent Research

High Centrifugal Fields and Radioactive Decay From the discovery of natural radioactivity and extending over a period of more than twenty-five years, many attempts of very diverse character were made to influence radioactive decay and all failed. The discovery of artificial radioactivity, of new types of disintegration and of the new basic particles raised the question whether the new radioactive decay processes might be affected by forces which may be brought to bear upon them. Scattering experiments of neutrons by protons and of protons by protons had brought about the recognition of obscure non-electromagnetic forces as operating within the nucleus. Also the importance of the theory of relativity in nuclear phenomena is still not clear.

Because of the equivalence of gravitational and centrifugal fields according to relativity, and because the latter were available at high intensity, S. Freed, A. H. Jaffey, and M. L. Schultz[1] examined whether centrifugal fields from 500,000 to 1,000,000g had any effect on the intensities and rates of decay of every type of disintegration process now known except fission. Rutherford and Compton[2] had found no change in the intensity of emission of gamma-rays in natural radioactivity within 0.1 percent when centrifugal fields of 20,000g were used.

In the recent experiments, air driven and supported rotors were employed. Some of the experiments were performed with toroidal tube counters (see Fig. 1) surrounding the spinning rotors whose outer cylindrical surfaces had been activated. Other measurements were made with an ionization chamber. The latter furnished an accuracy of several tenths of a percent, the former of several percent. No definite effect was established. However, in Br^{80} where a transition occurs between isomers by emission of gamma-rays rather than the usual emission from the nucleus of charged particles and, hence, where the centrifugal field might not meet such excessively strong competition from electrical forces, there was some sign of systematic deviation from the accepted half-lives in a centrifugal field of 632,000g but the deviation may have been within the total error

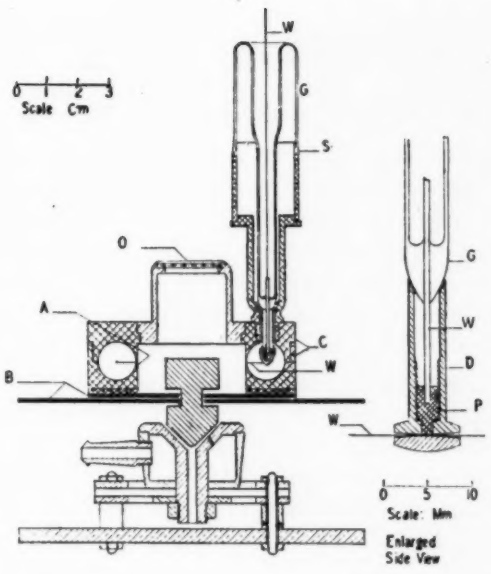

FIG. 1. Toroidal counter with rotor on stator. *W*—tungsten wire; *A*—copper foil window; *B*—baffles; *C*—copper case; *D*—Lavite insulator; *G*—glass; *O*—glass window for observing rotation with stroboscope; *P*—copper plug; *S*—glass-copper seal.

[1] S. Freed, A. H. Jaffey, and M. L. Schultz, Phys. Rev. **63**, 12 (1943).
[2] E. Rutherford and A. H. Compton, Nature **104**, 412 (1919); A. H. Compton, Phil. Mag. **39**, 659 (1920).

Electron Polarization Since 1928, when Cox, McIlwraith, and Kurrelmeyer[1] first attempted to detect polarization in a beam of fast electrons by a double-scattering experiment, a number of such experiments have been performed with contradictory results. Recent experiments, including that of Dymond,[2] have been designed to test the theory of Mott[3] based on the Dirac electron, or some modification of Mott's theory.

In an effort to clarify the situation, Chase and Cox,[4] in 1940, studied the single scattering of 50-kev electrons under such conditions that electrons losing appreciable energy in the scattering process would not be counted. They found that under these conditions the experimental results were in agreement with Mott's theory for

single scattering, upon which the double-scattering theory was based. It was further observed that electrons were more copiously scattered from the side of the foil upon which the electrons were incident, than from the other side. This observation suggested that possibly the negative experimental results of Dymond and others might in part be due to the fact that electrons had been detected, after scattering, on the same side of the foil as the incident beam. This question has been considered by Goertzel and Cox,[5] who reach the conclusion that the possibility of two 45° scatterings in the foil will cause more electrons to be "reflected" than transmitted at 90° from the incident beam, requiring an altered concept of the conditions for single scattering from foils inclined to the incident beam. The bearing of this fact on the polarization experiment is discussed.

Recently Shull, Chase, and Myers[6] have repeated the double-scattering experiment using 400-kev electrons and Geiger-Müller counters (Fig. 1). Using gold foils, a polarization effect was found which became more pronounced when only "transmitted" electrons were studied. Electrons scattered by aluminum foils showed no polarization. A repetition of the experiment by Trounson and Simpson,[7] using counters in coincidence circuits instead of single counters, new foils, and somewhat altered geometry, verified the positive polarization effect mentioned above (see Fig. 2).

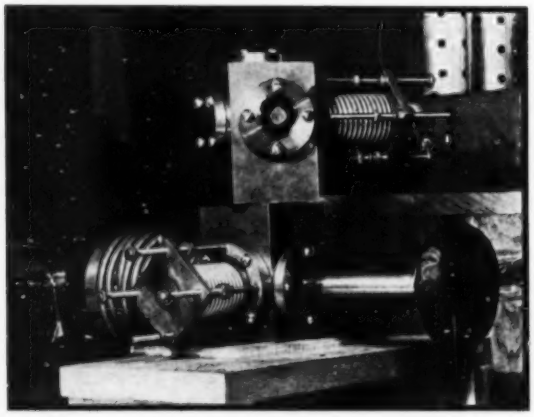

FIG. 1. Scattering chamber used in polarization experiment. The electron beam enters the chamber from the lower left. The two scattering foils are located inside the two chamber blocks. One of the small exit windows, through which electrons pass to the Geiger-Müller counters (not shown), can be seen in the upper center.

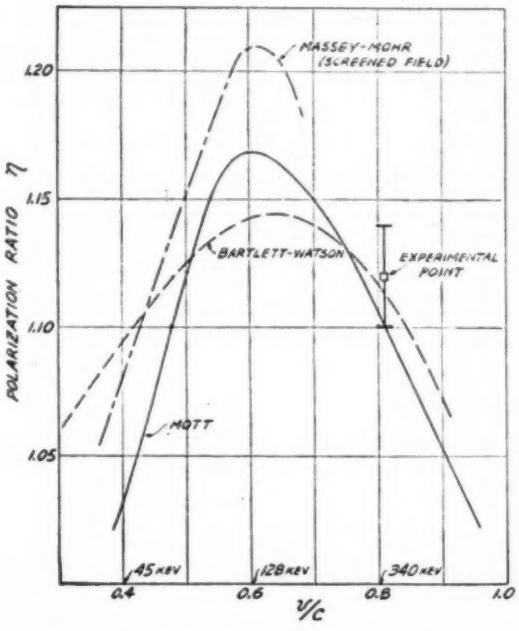

FIG. 2. Theoretical values for the polarization ratio as a function of the velocity v of the scattered electrons ($c=3\times10^{10}$ cm/sec.).

[1] R. T. Cox, C. G. McIlwraith, and B. Kurrelmeyer, Proc. Nat. Acad. Sci. **14**, 544 (1928).
[2] E. G. Dymond, Proc. Roy. Soc. **A145**, 657 (1934).
[3] N. F. Mott, Proc. Roy. Soc. **135**, 429 (1932).
[4] C. T. Chase and R. T. Cox, Phys. Rev. **58**, 243 (1940).
[5] G. Goertzel and R. T. Cox, Phys. Rev. **63**, 37 (1943).
[6] C. G. Shull, C. T. Chase, and F. E. Myers, Phys. Rev. **63**, 29 (1943).
[7] E. Trounson and J. A. Simpson, Phys. Rev. **63**, 55 (1943).

Contributed Original Research

On Torsion Combined with Compression

P. W. Bridgman
Harvard University, Cambridge, Massachusetts
(Received March 4, 1943)

If a rod is twisted while subjected to longitudinal compression it will support without fracture angles of twist many-fold greater and maximum torques somewhat greater than is possible in the absence of load. Under compressional load the curve of shearing stress against shearing strain rises to a maximum and then sinks with a long drawn out tail to an approximate asymptote. Fracture is never complete, but some coherence always remains, probably due to cold welding. The maximum torque is not marked by any visible beginning of fracturing or other discontinuity. The strain hardening curve in torsion, therefore, under proper circumstances passes through a maximum. The whole mechanism of strain hardening appears to be different in torsion and in tension, and reasons are given for anticipating such a difference because of the difference of the atomic kinetics in torsion and tension. It is shown in particular that the method of correlating tension and torsion through the "octahedral" coordinates which is applicable for small strains is not applicable to the large strains which are the subject of the present discussion. It is shown that the equations of conventional plasticity theory correctly reproduce certain qualitative aspects of the secondary longitudinal and radial flow which accompany twisting, but it is possible to establish large failures of isotropy not covered by the elementary theory. With regard to fracture, it is necessary to distinguish sharply between fracture in tension and in shear. The latter is not clean cut and it is probably possible to realize a continuous gradation of atomic disorganizations, culminating under proper conditions in complete shearing fracture.

INTRODUCTION

IF a bar is twisted while a longitudinal compressive load is simultaneously applied it is possible to twist the bar through much greater angles without fracture than is possible without the compressive load. At the same time the magnitude of the torque which the bar can support without fracture is increased. There are also other related phenomena, such as an alteration during twisting in the radial and longitudinal flow which would normally be produced by a pure longitudinal compression. In this paper some of these phenomena are examined.

EXPERIMENTAL METHOD

The torsion specimen is shown in Figs. 1 and 2. The central part is separated from the ends by two deep and narrow notches; the two ends are held from rotating and the center is twisted between the ends. The requisite torques are applied with the help of keyways milled in the three segments, not shown in the figure. A longitudinal compressive load may be applied at the same time as the twist. The compressive load is applied with a small hydraulic ram in such a way that longitudinal extension or shortening is free to occur. The measurements consist of the torque of the twisting force against the angle of twist. There are various advantages in giving the specimen the shape shown. One of the most important is that no end thrust bearings are needed and there is no frictional resistance to twist. Furthermore, there are two regions of twist, so that essentially two experiments are performed simultaneously, and the result, being an average of two, is correspondingly more accurate. By confining the twisted region to a narrow isthmus longitudinal stability is ensured under the joint action of twist and compression. By making the specimen hollow instead of solid and making the

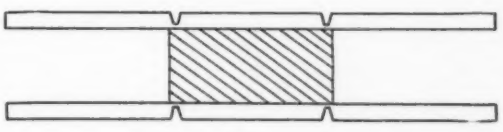

FIG. 1. Section of the torsion specimen with central pin for stability.

wall thickness at the notch small, approximate uniformity of stress distribution is attained and

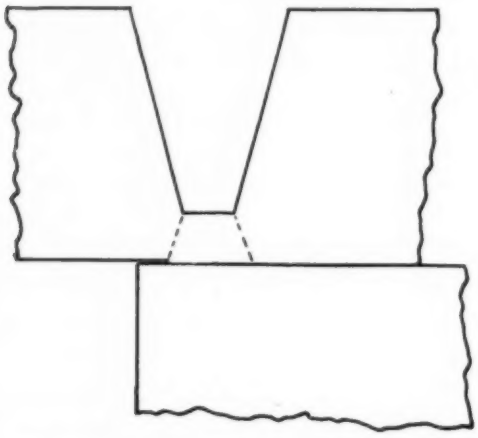

FIG. 2. Enlarged detail of the notch of the torsion specimen with part of the central pin.

the problem becomes approximately a two dimensional one. With the hollow specimens geometrical stability up to complete fracture was secured by inserting a hardened guiding pin in the central hole. Control experiments show that no appreciable error from friction is introduced by the pin.

The central part was attached to a pulley of diameter 75 times greater than the notch diameter, and rotation of the central part against the ends was produced by a flexible wire cable which was wound off the pulley onto a drum actuated by a motor through variable gears so as to give a wide range of speed. The arrangement was essentially one, therefore, in which the *velocity* of twist was impressed—the requisite torque automatically adjusted itself. The effect of speed was studied in the range from 0.006 to 40.0 degrees per second. In this range there is an increase of torque with increasing speed of the order of five percent. This effect is so small that it was neglected in the following; the measurements of this paper were carried out with a speed of rotation of approximately 0.15° per second.

Much preliminary work was done in selecting the best dimensions, starting with solid specimens $\frac{1}{4}''$ diameter, then increasing to $\frac{5}{16}''$ and finally to $\frac{3}{8}''$, and with several sizes for the hole, starting with $\frac{1}{8}''$ up to 0.290″, which proved too large, settling back on 0.277″. The final outside diameter at the bottom of the notch was 0.297″. Different notch widths were also tried; that finally adopted was 0.010″ at the bottom. The sides of the notch are inclined at 30° to each other. The early notches were made with rounded corners to avoid danger of fractures starting at sharp edges. The uncertainty in the effective width of the zone of flow introduced by the rounding was so great, however, that finally notches with sharp corners were tried, although with much misgiving. It was a surprise to find that there is no tendency for the fracture to start at the corner, but the crack still usually appears in the central portion. It is evident that the effect of stress concentrations at corners is quite different under these conditions than in ordinary tension tests.

The results were recorded photographically. The twisting force deflects a stiff spring which carries at the end of a long arm a source of light and a lens system by which a spot of light is thrown onto a revolving drum with photographic paper geared to rotate with the central part of the specimen. The apparatus is not sensitive in the elastic range. Arrangements are made for recording on the paper fiducial marks from which the absolute values of force and angle of twist may be obtained.

In Figs. 3 and 4 are shown typical photographic records of twisting force against angle of twist with and without compressional load for two grades of steel. The great effect of compressional load is apparent. The records read from right to left. The long horizontal dimension is proportional to the angle of twist, the vertical one to twisting force. The initial part of the curve, corresponding to the elastic range, is straight. The elastic deflection is too small to show on the scale of the reproduction. The rectilinear part corresponding to elastic deflection is not at right angles to the horizontal line because of stretch in the twisting cable and lack of complete rigidity in other parts. The photographic record therefore gives stress against strain in oblique coordinates. On the record the second horizontal line is a fiducial line for a known force, made at the conclusion of the twisting experiment. The interruptions in the trace are fiducial marks for angle.

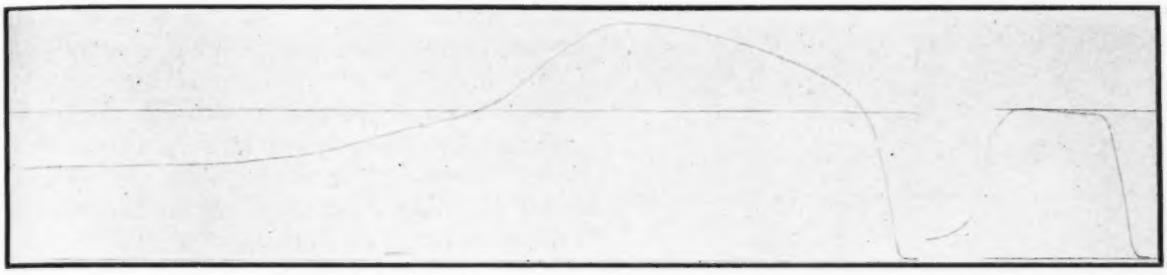

FIG. 3. Cold rolled steel—photographic record of angle of twist (abscissa, reading from right to left) against torque. The short graph on the right was obtained with zero compressional load, the long graph on the left under an average compressional load at the isthmus of 5700 kg/cm². The total angular displacement of the long graph is 85°.

METHODS OF CALCULATION

In order to reduce the records to characteristic properties of the material, the shearing stress and the shearing strain in the material corresponding to any point on the record should be determined. The mean shearing stress can be found at once from the torque and the dimensions. If it is assumed that the shearing stress, S, is constant across the section, which must be very approximately true under the conditions, the following equation holds:

$$\text{Torque} = 2S\int_{r_i}^{r_0} 2\pi r^2 dr,$$

or

$$S = \frac{3}{4\pi}\frac{\text{Torque}}{r_0^3 - r_i^3},$$

where r_i and r_0 are the internal and external radii of the notch. The factor 2 before the integral arises from the two sections of twisting.

The mean shearing strain demands a knowledge of the angular displacement and the width of the zone of plastic flow. This width is far from constant, but the zone spreads out from the bottom of the notch to the inner surface in a manner indicated qualitatively in Fig. 2. One can see that the spreading must be an accompaniment of the strain hardening. At the surface of separation of the elastic from the plastic zone the flow stress is at its minimum, corresponding to zero plastic distortion and zero strain hardening. In the interior of the flow zone stress is greater because of strain hardening. Equilibrium demands that the area of action of the minimum flow stress be greater than the area of action of the greater flow stress. Spreading of the flow zone and extension of the plastic-elastic boundary provides this greater area of action for the smaller stress. There seems to be no method by which one can calculate with confidence the amount of spreading to be expected. One might perhaps hope to get it experimentally by polishing and etching a section of the twisted specimen, but an attempt to do this did not yield definite results. It turns out that the spreading can be obtained by scratching

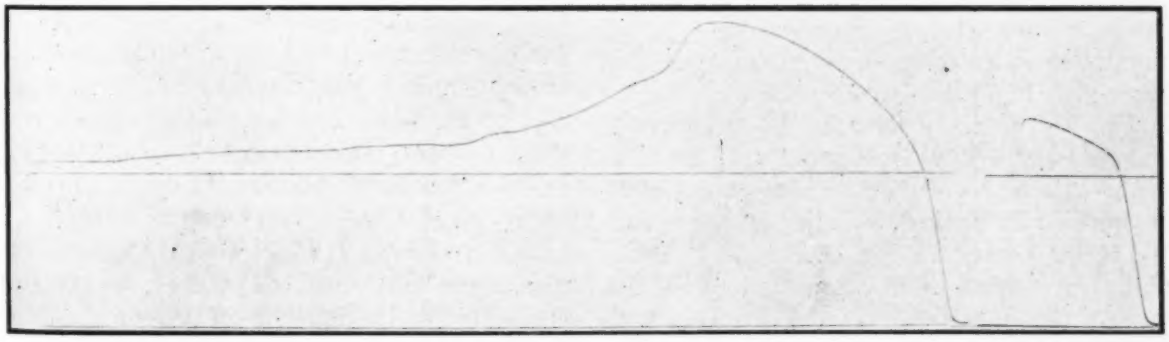

FIG. 4. Drill rod—procedure and significance as in Fig. 3.

FIG. 5. Enlarged view of an interior longitudinal scratch, displaced by the rotation of the central part against the ends.

the surface of the untwisted specimen with suitable straight lines and measuring the displacement of these scratches after twisting. By running a fine scratch down the sides of the notch and across its bottom it was possible to establish in the first place that at the corner of the notch the zone of flow does not extend perceptibly out of the notch into the surrounding material. After twisting the scratch continues to run straight down the sides of the notch, with no deviation as it approaches the corners. At the cylindrical surface of the notch the scratch takes a sharp break in direction and runs diagonally across the cylindrical face of the notch, still in a straight line, indicating uniform shearing strain across the width at the outside of the flow zone.

The inside surface was marked with six longitudinal scratches engraved with a special broach pushed through the hole. After the conclusion of the experiment the specimen was split in two lengthwise with a thin milling cutter; the general appearance of the displaced scratches is indicated in Fig. 5. The circumferential displacement, a, and the angle, φ, were measured. Unlike the outer surface, the edges of the flow zone at the inside are not sharply marked, as shown by the rounding of the corners in Fig. 5. However, in the central two thirds or three quarters of the distance a the scratches remained straight, indicating constant shearing strain in this part of the flow zone. The effective width, w_i, of the flow zone at the inside was taken to be $w_i = a \tan \varphi$. For one series on a 1045 steel w_i was found to vary from 48 to 77 percent greater than the initial width of the notch bottom at the outside surface. The lower figure, 48, is for twist with no longitudinal load, and the larger, 77, for twist with the highest load and an angular displacement three times as great. Because of longitudinal flow the notch itself decreases in width under twist with compression, the decrease being greatest for the greatest loads. The resultant of the increase in width at the inside and the decrease at the outside is a mean width that is approximately independent of the compressional load within limits of error and is about 20 percent greater than the initial notch width. The dimensions of the specimen were such that the mean width is roughly equal to the mean breadth as determined by the difference between inside and outside radius at the notch. The decrease of width of the bottom of the notch under the action of compressional load may be determined from measurements before and after twisting. The corners of the notch remain sharp, and precise settings are possible both before and after. In the case of the 1045 steel mentioned above the notch under the greatest compressional load flowed down to 67 percent of its initial width.

The mean shearing strain was taken as the mean circumferential displacement divided by the mean width of the flow zone.

In addition to the longitudinal flow under combined twist and compression, decreasing the notch width, there is radial flow, increasing the diameter at the bottom of the notch. This radial flow is nearly uniform across the entire notch width, any tendency to assume a barrel shape being slight. There is a tendency to radial flow in both directions, out at the outer surface, and in at the inner surface, but the inner guide pin prevents the inward flow. The increase of outer notch diameter was measured at the conclusion of twisting, before slitting. For the steel mentioned above the increase of notch diameter under the largest compressional load was 2.2 percent. The diameter enters the formula for the mean shearing stress through the difference of two cubes, so that the effect of a change of diameter is much magnified in the final result. Thus above, the effect of

a 2.2 percent increase in notch diameter is a 32 percent correction on the shearing stress.

In reducing the observed torques and twists to mean shearing stress and strain at intermediate points below the maximum it was assumed that the over-all longitudinal and radial flow were distributed in proportion to the angle of twist. This is not quite correct, as will appear later, but the error so introduced is negligible.

The various measurements just outlined cannot be made unless the specimen hangs together during the splitting subsequent to twisting. Since the specimen becomes increasingly fragile with increasing twist, in most cases twisting was stopped shortly after the torque had passed its maximum. Under these conditions the specimen retained sufficient strength, even when twisted without load, to permit such handling as was involved in splitting it longitudinally.

EXPERIMENTAL RESULTS

Results for one series on a 1045 steel are shown in Fig. 6 and Fig. 7 gives the results for drill rod, said to be a 1.25C steel. There are marked differences between the two steels. Up to the maximum the shape of the stress-strain curve for the 1045 steel is little affected by compressional load beyond a low initial effect. The difference in the curves is mostly in the magnitude of the strain which can be reached at the maximum shearing stress; this is a strong function of compressional load. It is probable that below the maximum the apparent variation with compressional load is within experimental error. With the 1.25C steel on the other hand, the shape of the curve below

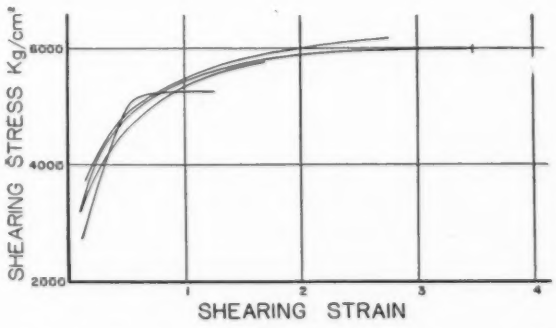

FIG. 6. Shearing stress against shearing strain (conventional) for a 1045 steel. The four curves are for compressive loads of: zero, 2300, 4400, and 5700 kg/cm² respectively in the order of length of the curves.

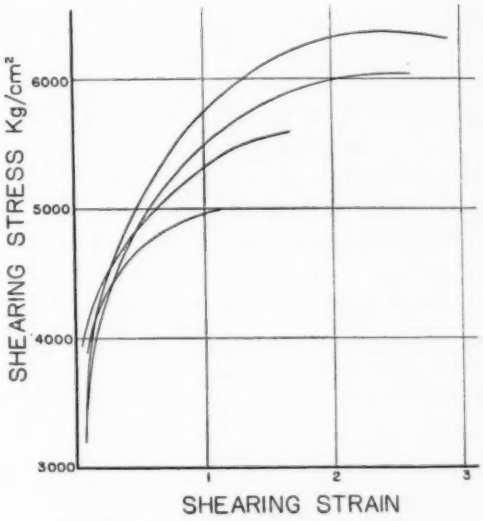

FIG. 7. Same as Fig. 6, but for drill rod.

the maximum depends markedly on the compressional load, and the shearing stress at maximum torque increases by more than 50 percent with compressional load in the range covered. If the strain at maximum torque is plotted against compressional load it will be found that the curve is concave upward for both steels, that is, the strain at maximum torque increases more rapidly than the compressional load.

It is especially to be emphasized that the maximum marks no abrupt break in any of the physical properties. It would be natural to think that the maximum marks the beginning of fracture, but examination discloses nothing that could be described as an onset of fracture on passing the maximum. An experiment that might be expected to be especially informative with regard to fracture is the following. If, after the specimen has been twisted with longitudinal load, twist is released, longitudinal load released, and then twist reapplied without load, it would be expected that fracture would occur at less than the normal torque if microscopic fractures had been initiated by the previous twisting under load. As a matter of fact, if the initial twisting has been through an angle as much as the angle at the maximum torque in the absence of compressional load, the torque which can be supported on the second application after strain hardening may be considerably more than the normal maximum torque without load. This holds whether the

twisting under load stopped short of the maximum or was carried beyond it. As twisting under load is carried to greater extents beyond the maximum there is a progressive deterioration, until finally the torque which can be supported the second time sinks below that for the virgin specimen without load. But there is no change in the trend to mark passing of the maximum.

Up to the maximum the curves have good reproducibility; beyond the maximum increasing divergences may be expected between runs on different specimens. In general, beyond the maximum the curve drags out to a long tail, approaching an asymptote. The abruptness of the drop beyond the maximum depends greatly on the grade of steel. The drop to the symptote may be punctuated by episodes in which the rate of fall is temporarily accelerated, or even sometimes by brief reversals. Even after deterioration is extreme and the specimen is full of visible wide open cracks, there is still some cohesion between the different parts of the specimen if the load is great enough. The cohesion is doubtless a cold welding as the high parts are dragged past each other under intense pressure on small local areas. It is generally recognized that cold welding of metals would be expected to occur if perfectly clean metal surfaces could be brought into contact, even without considerable normal pressure. Such welding does not occur under usual conditions because the surfaces are kept out of immediate contact by a film of absorbed air or other impurity. In these experiments some of the fractures must occur under such conditions that the surface film does not have a chance to form, so that cold welding would be expected.

In Fig. 4 the asymptotic torque corresponds to a coefficient of friction between the parts, assumed perfectly free from each other, of about 0.7.

DISCUSSION

In the light of the existence of a maximum the significance of the strain hardening curve requires consideration. It is common experience that the strain hardening curve, that is, the curve of plastic flow stress against strain, usually rises, as shown by the very use of the word "hardening." The extent to which the curve can be followed is limited by fracture of the material. Under ordinary conditions fracture intervenes at a fairly early stage in the straining process, but if fracture can be postponed, as here, the "hardening" curve can be followed much further. The fact that under such conditions the curve passes through a maximum cannot help but throw light on the mechanism of strain hardening in general. This aspect of the matter will be discussed again later.

Correlation between Tension and Shear

A question that has been much discussed is the nature of the connection between strain hardening curves for different types of deformation, and in particular the connection between plastic flow in simple tension and in simpler shear. The general impression seems to be that for small strains there is a connection, but that for larger strains the simpler correlations, at least, that have been commonly discussed may be expected to fail by progressively larger amounts. The new evidence of this paper in which the strain hardening curve in simple shear has been carried beyond a maximum pretty well throws out of court the possibility of any extensive correlation because the strain hardening curve in tension is known to rise linearly in terms of "natural" strain to magnitudes of strain much in excess of those reached for shear here. However, even below the maximum of the curve the shearing strains reached here are considerably in excess of those usually considered, so that it is perhaps of some interest to inquire into the possibility of correlating the curves for tension and shear in the region below the maximum.

One method of correlation between tension and shear which has roused recent interest is discussed by Nadai and Davis in two papers.[1] The thesis is that if the "octahedral"* shearing strains and shearing stresses are computed, either for tension or shear, it will be found, for low strains, that the strain is the same function of stress for both tension and shear. Davis, in his paper, examined this relation for copper up to a value 0.9 for the conventional shearing strain (0.7 for the octahedral shearing strain). Up to 0.2 for the octahedral strain the curves for tension and

[1] A. Nadai, J. App. Phys. **8**, 205–213 (1937); Evan A. Davis, J. App. Phys. **8**, 213–217 (1937).

* The "octahedral" strain or shearing stress is the strain or shearing stress across one of the "octahedral" planes, that is, the plane whose normal is equally inclined to the three axes of principal stress.

torsion were in good agreement, but from here they diverged progressively. At a strain of 0.6 the difference from the mean was 10 percent. The shearing strains of this paper at the maximum torque may be more than four times higher than those discussed in Davis's paper. The formulas for the conversion of ordinary shearing stress and strain into the corresponding octahedral coordinates have been given by Nadai. This conversion was made for three of the points of the run on the 1045 steel under a mean compressional load of 5700 kg/cm². The strain hardening curve of this same steel has been determined in tension; the results are to be published in another place.

It was found that the true tensile stress is a linear function of $\log_e A_0/A$, where A_0 and A are the initial and running areas at the neck of the tensile specimen. It is evident that $\log_e A_0/A$ is the so-called "natural strain" at the neck. From Nadai's paper the conversion formulas to octahedral strain and shearing stress from the corresponding values for tension may be found to be:

$$\text{Octahedral shearing strain} = \sqrt{2} \log_e A_0/A.$$

$$\text{Octahedral shearing stress} = \sqrt{2}/3 \text{ true tensile stress.}$$

Since these are both relations of simple proportionality, it follows that for tension octahedral shearing stress is a linear function of octahedral shearing strain. Two points therefore determine the line. In Fig. 8 the straight line for tension is drawn through two of the previously determined points reduced to octahedral coordinates by the above formulas. In the same figure are plotted the three points from the torsion experiments of this paper. The figure leaves no question as to the wide divergence of the curves for shear and tension. It is probably not ruled out that within experimental error the two curves may extrapolate to the same value for infinitesimal strains, but already within Davis's range the divergence of the two curves for steel is greater than Davis found for copper.

The same sort of thing is shown by some other methods of correlation which are as a rule less successful than the correlation by octahedral coordinates. The conclusion is that in general the strain hardening curve for simple shear rises much less rapidly than the curve for simple tension. In speculating as to the reason for this the

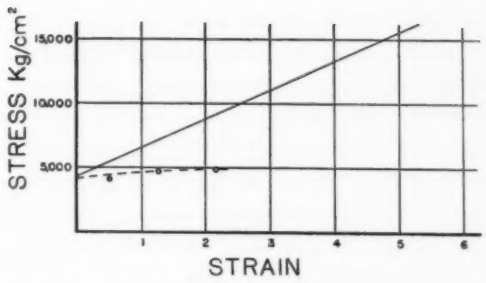

FIG. 8. "Octahedral" stress and strain for tension and shear on a 1045 steel. The upper straight line is from tension tests under hydrostatic pressure; the detailed results are to be published elsewhere. The lower dotted curve is obtained from the measurements of the longest of the four curves of Fig. 6 of this paper.

different character of distortion in tension and shear is to be kept in mind. At low strains there is an illusory similarity, but at shearing strains of the magnitude of interest here the differences are accentuated. It is instructive to consider in detail the atomic kinetics of tensile and shearing strain. In tension the principal axes are lines of fixed direction and also lines of maximum elongation and contraction. Since in the virgin material the atoms are already practically in contact, an elongation or contraction of a line of atoms can be accomplished only by pushing new atoms into line or by expelling atoms from the line—the process is not uniform or continuous as it is in the macroscopic equations. Extensions of more than twentyfold have been reached in my experiments on tension combined with hydrostatic pressure; this means that along one axis at least 19 new atoms have been forced into line for every single original atom, and along the other axis only one out of at least 20 atoms remains in place. The paths by which the atoms find their way into their new positions cannot be simple, and the entire mass of the material must be a field of great atomic disorganization. In simple shear on the other hand any plane of shear retains its direction and all the atoms in the plane retain their distances of separation. From the idealized point of view simple shear, no matter how great in amount, consists merely in the sliding of intact planes of atoms over other intact planes. It is natural to think that in the actual case the total disorganization must be less than in tension. Furthermore, from the idealized atomic point of view, after a shearing displacement of one plane

with respect to its next atomic neighbor by one atom has been reached, the initial configuration is recovered and the phenomenon repeats. That is, from the idealized point of view, any strain hardening there may be in shear should be complete for shears less than unity; beyond this the strain-hardening curve should be flat. Actually of course there is interference between slip in the different elementary domains, and the idealized state of affairs is smeared out. There should be enough residue of the idealized situation in any actual situation, however, to justify the expectation that strain hardening in shear would be less than in tension and that it would flatten off earlier. This is the state of affairs which we have found and which is indicated in Fig. 8.

Agreement with the Equations of Plasticity

We next inquire to what extent the phenomena described here conform to the conventional mathematical formulations of plasticity theory. The experiments, however, were not primarily designed for the study of flow, and results bearing on this topic were obtained only incidentally. The experiments in the literature most similar to these in their bearing on flow are probably those of Hohenemser and Prager[2] on torsion combined with tension. The details of their experiments were, however, quite different; they maintained the angle of twist constant and observed the decay of torque when the tension was manipulated.

The most generally used flow equations, written in terms of principal strains and stresses, are:

$$\left.\begin{aligned}\dot{\epsilon}_1&=\alpha[\sigma_1-\tfrac{1}{2}(\sigma_2+\sigma_3)]\\ \dot{\epsilon}_2&=\alpha[\sigma_2-\tfrac{1}{2}(\sigma_3+\sigma_1)]\\ \dot{\epsilon}_3&=\alpha[\sigma_3-\tfrac{1}{2}(\sigma_1+\sigma_2)]\end{aligned}\right\}. \qquad \text{(A)}$$

In addition to the flow equations a condition on the stress is required to ensure that the material is in the "plastic" condition. We assume the form of von Mises, namely:

$$(\sigma_1-\sigma_2)^2+(\sigma_2-\sigma_3)^2+(\sigma_3-\sigma_1)^2=k. \qquad \text{(B)}$$

The "constant" k may conceivably vary during the flow to express the progress of strain hardening.

In applying these equations to the problem above, the first step is to find the principal stresses. Conventional cylindrical coordinates will be used: r along the radius, θ circumferential, and z along the axis. Under torque with no longitudinal load the only non-vanishing stress component in the cylindrical system of coordinates is $\Theta_\theta=Z_\theta=S$, where S is the ordinary shearing stress. The directions of principal stress are the two directions inclined at 45° to the axis in the $z\theta$ plane, and the direction of the radius. Denoting the first two principal stresses by σ_1 and σ_2 and the radial component by σ_3, the numerical values of these principal stresses are:

$$\sigma_1=S; \quad \sigma_2=-S; \quad \sigma_3=0.$$

Under longitudinal compression an additional component $Z_z=-C$ is added, where C is the compressional load per unit area. What are the new principal stresses? If we seek to determine these in terms of the boundary conditions at the free faces, we find that they are under-determined. On the free faces perpendicular to the radius there is no force; on the faces perpendicular to z there is a normal component C and a shearing stress S, but the surfaces perpendicular to θ are not free because of the geometry, the hoop closing in on itself, and other considerations are necessary to fix the θ components of stress. The simplest assumption is that the Θ_θ component remains zero even after the addition of longitudinal load. In this case the two non-vanishing principal stress components are rotated in the $z-\theta$ plane, the axis of the compressional stress being rotated toward the cylinder axis. The amount of rotation and the altered values of the principal stress may be computed by elementary methods. The important feature is that in virtue of the rotation the direction of maximum shearing stress will no longer be the direction of plastic flow. Because of the geometry, the direction of plastic flow is constrained to be circumferential, and the maximum shearing stress always bisects the angle between greatest and least principal stress.

The principle of maximum shearing flow in the direction of maximum shearing stress can be maintained if one supposes that the longitudinal load generates a suitable Θ_θ component of stress. It is natural to expect the generation of a certain amount of such stress. It is a matter of observation that the compressional load produces radial

[2] K. Hohenemser und W. Prager, Zeits. f. angew. Math. u. Mech. **12**, 1–14 (1932).

flow. It would then also tend to produce circumferential flow, which would build up a Θ_θ component of stress because there is no free surface across the θ direction as there is across the radial direction. Any net Θ_θ component of stress would obviously be held in equilibrium by elastic stresses in the bulk of the material beyond the notch. If the Θ_θ component resulting from the compressional load is equal to the compressional stress, then the net result of adding the load is to add a two-dimensional hydrostatic stress to the original stress system. The direction of the principal stresses will be unaltered and therefore the direction of maximum shearing stress, so that plastic flow still has the direction of maximum shearing stress. The numerical values of the principal stresses are now: $\sigma_1 = S - C$; $\sigma_2 = -(S+C)$; $\sigma_3 = 0$.

The actual stress system is probably somewhere between the two extremes just considered. Further evidence on this point is afforded by the character of the fractures, which will be discussed later. The effect is in any event not of prime importance, for in the extreme cases in the experiments reported here the direction of flow cannot differ by more than 10° from the direction of maximum shearing stress. Let us assume for the present that flow is always along the direction of maximum shearing stress, and inquire what the equations have to say about the effect of adding longitudinal load to twisting force.

1. When twist takes place without longitudinal load we have:

$$\sigma_1 = S, \quad \sigma_2 = -S, \quad \sigma_3 = 0,$$

and the condition of von Mises, B, becomes

$$6S^2 = k.$$

2. When twist occurs with load, assuming flow in the direction of maximum shearing stress, we have for the stresses:

$$\sigma_1 = S' - C, \quad \sigma_2 = -S' - C, \quad \sigma_3 = 0.$$

The condition of von Mises now gives

$$6S'^2 + 2C^2 = k.$$

Eliminating k we have

$$S'^2 = S^2 - \tfrac{1}{3}C^2.$$

That is, less shearing stress is required to produce plastic flow in torsion when a longitudinal load acts simultaneously than when no load acts. The form of the result shows incidentally that tension as well as compression reduces the torque necessary for torsional flow.

This conclusion might at first appear to contradict the experimental findings above. The results thus far emphasized apply, however, only to large strains. At smaller angles of twist there are effects in the opposite direction. This is shown very definitely by the crossing of the curves at the low strains in Fig. 6 and careful examination of the photographic records of Figs. 2 and 3 shows the same thing. The apparatus was not sensitive enough to give good numerical values for the effects. In fact, the effect was usually noticeable only for the larger loads; this is to be expected because the effect involves the square of the load.

What about the other components of flow? In equations (A) take the direction of $\dot{\epsilon}_3$ as that of radial flow. In the first stress system above, shearing without longitudinal load, the equations make $\dot{\epsilon}_3$ zero, and there should be therefore no radial flow. But in the second stress system, twist with load, the equations give $\dot{\epsilon}_3 = \alpha C$. There should, therefore, be radial flow under any compressional load, no matter how small. The flow equations give:

$$\frac{\text{Radial Velocity}}{\text{Velocity of Shear}} = \frac{C}{3S'}.$$

Accompanying the radial flow there is an equal longitudinal flow as demanded by the condition of constancy of volume. The total radial and longitudinal flows may be measured at the termination of the experiment, or if special methods are adopted, they may be measured during the progress of the twist. The longitudinal flow may be determined either from the over-all length or from the notch width. Individual measurements of diameter or notch width after torsion are likely to be somewhat irregular, because of local irregularities in the flow, particularly after the first beginnings of rupture. The over-all length, however, smooths out the local irregularities and may be taken as the best measure of the secondary flow.

The longitudinal flow satisfies the same equation as the radial flow, that is:

$$\frac{\text{Velocity of Longitudinal Flow}}{\text{Velocity of Shear}} = \frac{C}{3S'}.$$

The experimental set-up was such that C remains constant but S' increases during progress of twisting because of strain hardening. Hence the total longitudinal shortening, plotted against the total angle of twist, would be expected at first to increase more rapidly, and then more slowly.

The longitudinal flow was studied with six series of specimens, 16 specimens altogether, and with three grades of steel: a commercial cold rolled, an annealed drill rod (carbon tool steel, about 1.25C), and the heat treated 1045 steel already referred to. At constant compressional load the change of length for the cold rolled steel was found to be roughly proportional to the angle of twist, but with a tendency to become less proportionally at the greater angles. The strain hardening of cold rolled in torsion is comparatively slight. Six measurements on one sample of drill rod gave a markedly greater falling off from linearity at the larger angles, corresponding to greater strain hardening. Measurements with different compressive loads up to 5800 kg/cm² gave for the shortening per degree of twist at the point of maximum torque a perfect straight line through the origin when plotted against load for the drill rod. For the 1045 steel on the other hand there was appreciable departure from linearity, the value at half final load being 58 percent of the final value. These results are qualitatively in accord with the flow equations and are therefore not inconsistent with an approximate isotropy of flow and strain hardening under the conditions.

Isotropy after Plastic Flow

Bearing more immediately on the question of isotropy another sort of experiment was performed. A piece of drill rod, cut to the regular dimensions of the torsion specimen, was loaded in compression without twisting. A maximum compressional stress at the isthmus of 13,700 kg/cm² was applied, and under this the total shortening was 0.0065″, or about 33 percent of the total notch width. Compressional flow was confined to the notches. It was then twisted through 15° under a compressional load of only one third as much, 4400 kg/cm², and during the twisting received an additional shortening of 0.0012″. The curve of angle of twist against torque for this specimen was indistinguishable from that of a virgin specimen. The longitudinal flow was, however, greatly affected by the previous cold working in compression. A virgin specimen twisted through the same angle under a compressional load of 4400 kg/cm² shortens 0.0044″, or 3.5 times as much as the cold-worked specimen. It would seem then that under certain conditions strain hardening and flow may be far from isotropic.

Fracture

Finally, consider the nature of the fractures, a topic on which these experiments are particularly adapted to throw light. These remarks apply primarily to the wide open fractures, after the specimen falls apart into three pieces. At zero compressional load the surface of the fracture is approximately a plane perpendicular to the axis. The surface is inclined to have a matt appearance, with little trace of burnishing. With increasing compressional load the fracture shows an increasing tendency to depart from the plane, sometimes with a distinct radial pattern like the escapement on some old fashioned clocks. The probable explanation is that slip always has a tendency to occur on the planes of maximum shearing stress, and that these are rotated from their initial location perpendicular to the axis by the compressional load. The fracture may be situated indiscriminately over the notch width; if it runs into the corner it does not run along the corner indefinitely, but snaps back after an interval, giving the escapement-like pattern. This is the reason for the suggestion above that the stress component Θ_θ is probably somewhere between the two extreme values, 0 and $-C$. Along with the increase of compressional load goes an increase in the burnished appearance of parts of the fracture, evidently due to rubbing under compression. Sometimes slivers of metal appear to get broken from the corners of the teeth of the escapement, and are rolled between the opposing surfaces. Sometimes the metal balls up in places and little nubbins of apparently

harder material plow through the mass of softer metal. Apparently fracture seldom if ever starts homogeneously, but begins in scattered localities. If twisting is not carried to separation of the segments open fractures clean through the metal in places are not uncommon, while other places remain apparently sound.

On the long tail of the torsion curves beyond the maximum when there is a heavy compressional load the metal is in a highly abnormal condition. It is still fairly strong for torsion, but for other sorts of stress it may be very weak, and it has lost nearly all capacity for further plastic flow. If a torsion specimen is removed from the apparatus after having been carried over into the long tail of the curve, it will be found still hanging together, but it may be snapped like a pipe stem in the fingers by bending.

If at any stage of the twisting process the torque is removed, keeping compressional load constant, and torque is then reapplied, twisting flow will not be resumed until the previous torque has been reached. If torque is removed, then compressional load removed, and then torque reapplied without compressional load, it is possible, if the preceding strain has not been too severe, to apply a torque greater than the maximum which can be applied to a virgin specimen free from compression. Under these conditions, however, very little further plastic flow takes place, and the specimen breaks very much more abruptly than when in the virgin condition.

Under such conditions the concept of "fracture" becomes hazy. The metal is highly disorganized from the original lattice; just how much or what kind of disorganization there must be to justify being called a fracture does not appear. In fact one would expect cold welding to occur to a certain extent, so that open fractures might under proper circumstances be partially welded together again. Many examples of such cold welding were found in my previous work on shearing under more extreme conditions of load and distortion.[3] Incidentally under these conditions strain hardening in shear reached an asymptotic limit.

In general, two types of fracture are to be distinguished, tensile and shearing fracture. Of these the tensile fracture is much more clean cut and definite, and it is no accident that by far the greater part of the speculation in the literature has been concerned with tensile fractures. The difference is primarily one of geometry. In tensile fracture the direction of the forces is such as to remove the fractured segments from the reach of mutual atomic attraction; when the separation is beyond the domain of atomic forces the process becomes irrevocable and catastrophic. In shear the primary process is one of tangential slip, and the direction of motion does not remove the atoms from mutual reach. Fracture is a secondary and incidental process under such conditions. Slip is accompanied by local disorderings; strain hardening is one evidence of this disordering. As disordering progresses the displaced parts can fit together less perfectly in their displaced positions, until eventually the cohesive forces between the high spots become unable to check the momentum imparted by the external forces and slip becomes catastrophic. One would expect under such conditions that fracture would not be clean cut, and one would be prepared for the large effects of normal pressure which are actually found.

If the onset of fracture in shear is gradual, there must be an interaction with the strain hardening mechanism. It is this interaction doubtless that is responsible for the maximum in the strain hardening curve. In tension, on the other hand, fracture terminates the strain hardening curve abruptly, with no warning. It is much more appropriate to speak of distinct mechanisms for strain hardening and fracture in the case of tension than in the case of shear.

[3] P. W. Bridgman, Phys. Rev. **48**, 825–847 (1935); Proc. Am. Acad. **71**, 387–459 (1937).

A Tension-Compression Device for Quantitative X-Ray Diffraction Evaluation of Strain in Metals and a Calibrated Series of Aluminum Alloys

GEORGE L. CLARK, GEORGE PISH, AND RALPH SEABURY*
University of Illinois, Urbana, Illinois

(Received February 26, 1943)

An easily constructed apparatus is described for applying tension and compression stresses to metal and alloy samples while being subjected to x-ray diffraction analysis. The back reflection technique is employed in which diffraction patterns can be photographed in five minutes or less. The apparatus and technique have been developed because of the increasing interest in the measurement of strain in a variety of metallurgical materials of primary war interest. A series of patterns on a familiar aluminum alloy under calibrated tension stresses is reproduced as an example by means of which evaluation of residual strains in large castings can be non-destructively evaluated.

SINCE the theory[1,2] for the measurement of stress in metals has been worked out for the x-ray diffraction method, it has found application to many practical problems. Wever[3] and Thomas[4] have employed the x-ray back reflection method for the measurement of stresses in large castings. In order to study the variations in stress for commercial type of samples it was found necessary to design and construct an x-ray tension-compression apparatus which could be used for this purpose. The existing types of equipment[5,6] in use for stress analysis in this laboratory are adapted for use only with thin samples. The apparatus described herein may be used for back reflection and transmission studies by x-rays without modifications except that in some cases a different spring must be used in the apparatus. The samples for the transmission method are much more difficult to prepare without changing some of the properties of the material examined. A great deal of cold work may be introduced when a sample is made sufficiently thin to give a x-ray diffraction pattern. Since much of the recent work now done is by back reflection, this method will be considered to a large extent.

CONSTRUCTION AND CALIBRATION OF THE APPARATUS

The finished tension-compression apparatus set up for the back reflection x-ray diffraction method is shown ready for use in Fig. 1. Figures 2 and 3 show the drawings for the assembly and parts. Since these parts are fully dimensioned, directions for their construction and assembly are unnecessary except in a few places. A $\frac{9}{32}$-inch diameter hole should be drilled (not shown in drawing) with its center $\frac{3}{8}$ inch from the turned end of part (7) in Fig. 3 for a steel dowel pin. The micrometer barrel is calibrated to read in thousandths of an inch but may be converted easily to read in terms of metric units by cutting a metric thread. For this particular instrument a one-ton spring has been adapted, but a lighter one may be substituted provided the over-all dimensions

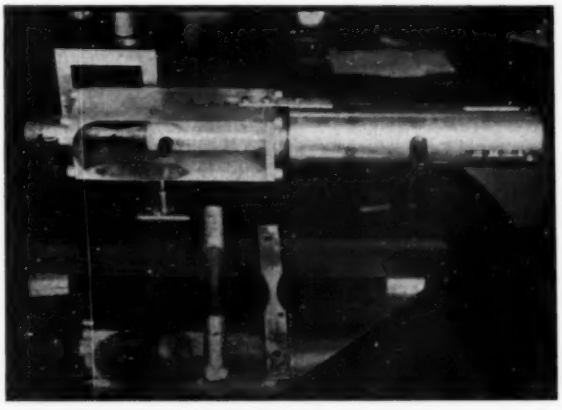

FIG. 1. X-ray tension-compression apparatus set up for the back reflection focusing method.

* Director of Research, Delco-Remy Division, General Motors Corporation, Anderson, Indiana.

[1] R. Glocker and E. Osswald, Zeits. f. tech. Physik **16**, 237 (1935).

[2] C. S. Barrett and H. Gensamer, J. App. Phys. **7**, 1 (1936).

[3] F. Wever, Ergeb. d. Tech. Röntgenk. **6**, 19 (1938).

[4] D. E. Thomas, J. Sci. Inst. **18**, 135 (1941).

[5] G. L. Clark and M. M. Beckwith, Trans. Am. Soc. Metals **25**, 1207 (1937).

[6] G. L. Clark and C. G. Dunn, Phys. Rev. **52**, 1170 (1937).

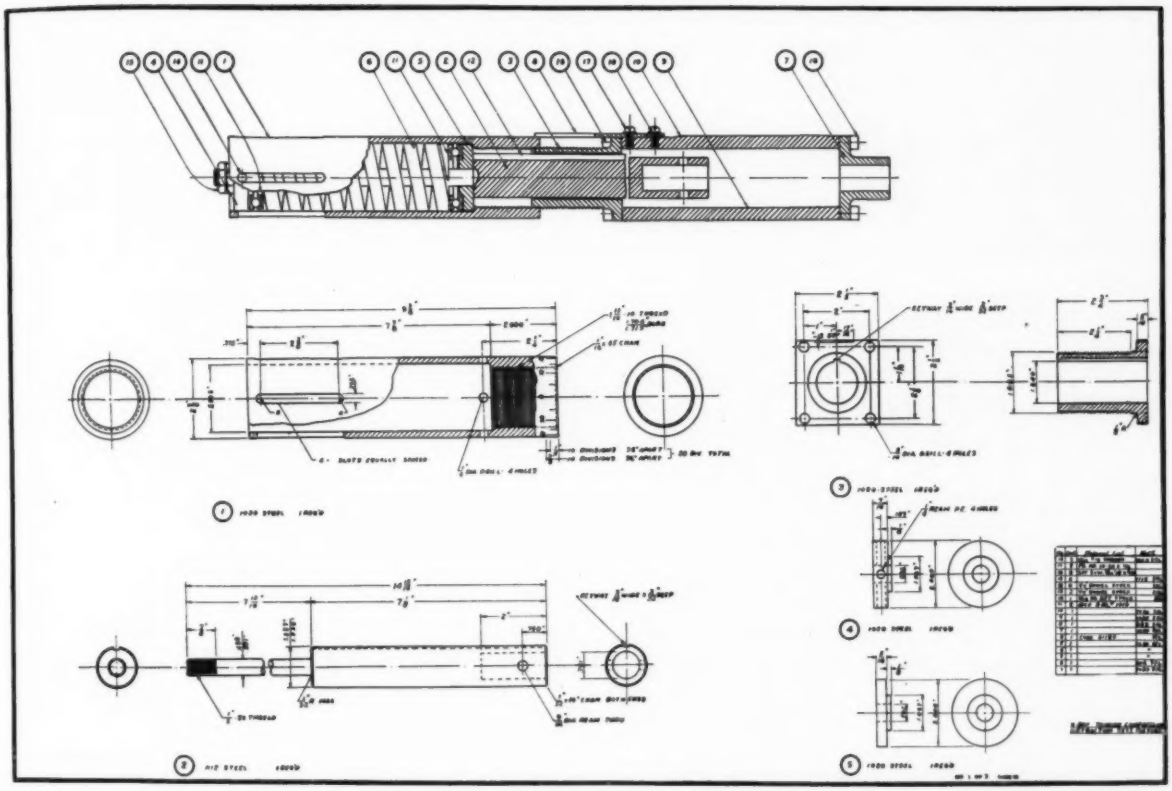

FIG. 2.

remain the same. Since the instrument was designed for use with the accessories in this laboratory, it is capable of giving a minimum sample—film distance of about 3 cm. In order to prevent part of the diffracted x-ray cone from being cut off by the instrument, parts (9) and (10) in Fig. 2 have milled tapers in the sides as indicated and should be assembled so that the milled sides face inward. The holes just behind the micrometer calibration on the barrel of the instrument are for a spanner wrench which is needed to rotate the barrel when tensile stresses are applied or relieved.

By the use of a small previously calibrated Olsen test machine it was possible to calibrate the apparatus easily to within the accuracy necessary for stress analysis. A one-foot steel rod $\frac{5}{8}$ inch in diameter drilled to receive a pin at one end was fixed into position of part (2). The entire apparatus was securely clamped to the upper bed of the Olsen tester and the extending rod to the lower bed. After the Olsen tester was adjusted to zero, the micrometer screw of the tension-compression apparatus was rotated through a definite interval. Then the Olsen tester was adjusted until equilibrium conditions were again established and the total pressure recorded from the dial for this displacement. The procedure was repeated for various displacements. For both tension and compression three complete trials were taken, and the results were plotted as total pressure (in pounds) *versus* displacement of the micrometer barrel (in inches). It may be seen from the curve in Fig. 4 that excellent agreement was obtained until a pressure greater than 1600 lb. was exceeded. As the spring was further subjected to tensile stresses, distortion occurred giving poor results beyond this point. Therefore, when the x-ray tension-compression device is used, the sample should be so prepared that the cross-sectional area at the thinnest part will have a limiting total pressure somewhere below the 1600 lb. limit.

USE OF THE INSTRUMENT

When the apparatus is used for x-ray tension studies, the test piece is set into the apparatus so

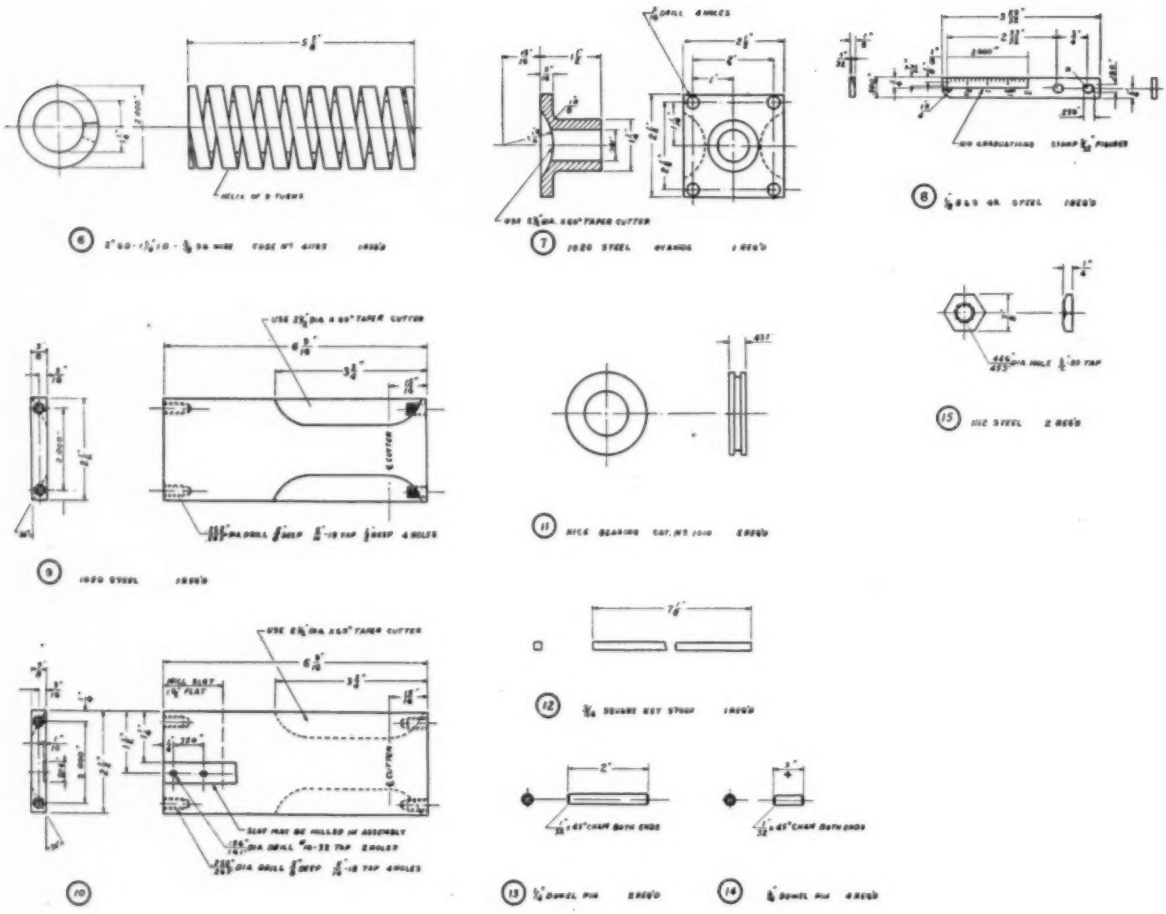

FIG. 3.

that the pins fit loosely. The slack is taken up carefully by turning the barrel outward until no play is found in the pins. The micrometer reading at this point is taken as the zero point. Then the barrel is rotated to whatever displacement is wanted. Similarly for compression experiments the barrel is first turned outward to zero on the micrometer scale; the sample is set into the apparatus so that the pins fit loosely. Now the barrel is carefully screwed inward until no play is found in the pins, and the micrometer reading taken as the zero point. For any desired displacement the barrel must now be screwed inward.

The assembled apparatus is set into a cradle (Fig. 1) which can be constructed easily. This cradle is provided with a vertical elevating screw containing a lock nut and is very useful in adjusting the tilt of the device during experiments. It eliminates constant readjustment when a number of consecutive x-ray patterns are taken from the same sample under different tensile stresses.

When everything is in readiness for x-ray diffraction studies, one of two methods may be used, the back reflection or the transmission method. Figure 5 shows the schematic set-up used in the conventional back reflection method. The x-ray pattern illustrated in Fig. 5 is of a strain free piece of sheet aluminum. The radiation from a cobalt target Machlett tube operated at 38 kv and 10 ma was used. The use of a 0.025-inch diameter defining pinhole required an exposure of one hour. In contrast to this a modified technique[4] for rapid exposures is now in constant use in this laboratory. This modified method makes use of a large pinhole system and is shown in Fig. 6. The x-ray pattern is of the same sample as that in Fig. 5. With the exception of the defining pinhole,

which in this case was 0.063 inch in diameter, the operating technique was the same, but the time for the fully exposed x-ray diffraction pattern was reduced to 5 minutes. By using higher tube ratings or somewhat larger defining pinhole either separately or together with the "focusing" method one can decrease still further the exposure time. By comparing the x-ray patterns in Figs. 5 and 6 it may be seen that the rapid method suffers slightly in resolution qualities of the $K\alpha_1\alpha_2$ doublet, but it was found that the measurements of the ring diameters can be taken with the same degree of accuracy as that by the method in Fig. 5. Thomas[4] has been able to obtain measurements of high precision in stress analysis of large castings using a similar method. In using the rapid "focusing" method the collimating defining pinhole system should approach the sample as closely as possible for best results, but care should be exercised so it does not get too close to the sample or the blind spot formed on the film by the extended portion of the system will become large enough to cut off the interference which is to be recorded. The distance will vary for the type of material and the kind of radiation used.

It has been shown that the Bragg angle θ is most sensitive to changes in interplanar spacings (d) when θ approaches 90°. Therefore, if the proper wave-length is used to give a diffracted ray having θ nearly equal to 90°, d can be calculated with a high degree of accuracy from the measurements.[4]

Examples of patterns taken by the rapid back reflection method are shown in Figs. 6 and 7.

The rapid method using large pinholes may be used for studies by transmission of x-rays through thin samples. Naturally the x-ray patterns show greater loss in resolution than those obtained using the small pinhole systems, but since the exposure time is greatly reduced, the large pinhole method may be preferred in studies where rapid routine work of a qualitative nature is to be carried out. Examples of patterns taken by this method using the apparatus described are shown in Fig. 8.

DISCUSSION

By removing one of the pins [part (14) Fig. 2] and replacing it with a longer one, a micrometer dial may be fitted to the apparatus in such a way that the displacement of the shaft (2) can be measured. Then one can measure for an applied tensile stress on a plastic sample the displacement of this shaft along with that of the barrel. These measurements along with the patterns provide sufficient data for the measurement of stress, strain, and the percent of elongation for the sample under consideration.

The apparatus is so built that each successive x-ray pattern can be obtained from the same spot on the sample for different tensile stresses. Therefore, a more representative set of patterns is obtained giving a truer history of the manner in which the specimen behaves under tension. The result of the "focusing" effect with large pinholes in the rapid method is that a more divergent beam can be used, thereby decreasing the exposure greatly. Also, when the specimen is made up of large crystals, more of them can be included in the beam thus giving a better average representation of the test sample.

The only disadvantage in using the rapid "focusing" technique in back reflection studies is the slight loss in resolution of the $K\alpha_1\alpha_2$ doublet, but as noted previously, this does not impair the accuracy of the results.

When the large pinholes are used in the collimating systems, two simultaneous x-ray patterns may be obtained rapidly and easily if

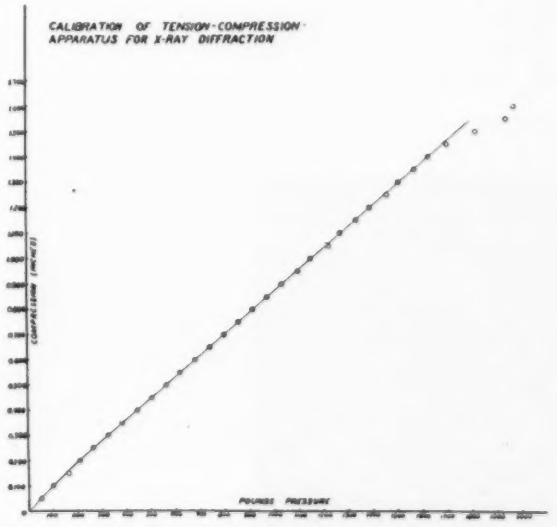

FIG. 4. Calibration curve for the x-ray tension-compression apparatus.

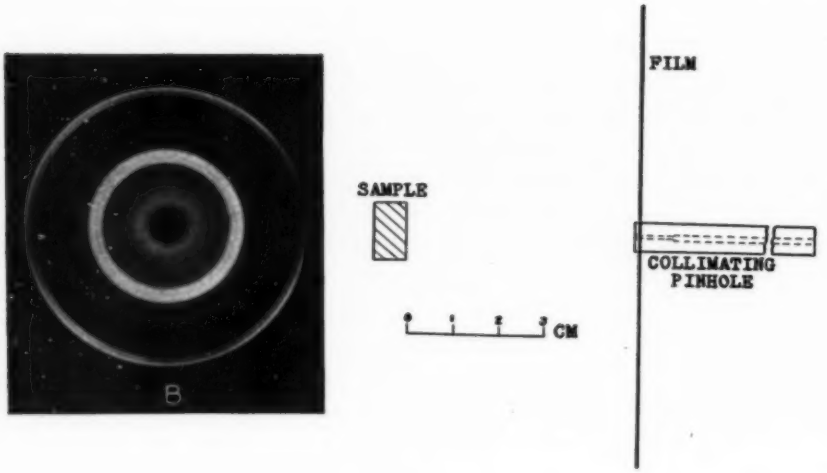

FIG. 5. Conventional set-up for back reflection x-ray diffraction method. Diffraction pattern of strain free Al. Sample-film dist., 5 cm. Defining pinhole, 0.025 inch dia. General Co radiation (Machlett tube—38 kv and 10 ma). Exposure, 1 hr.

the thin samples are used. One of these patterns is obtained by back reflection and the other by transmission.

By means of this tension-compression device a series of standard diffraction patterns is thus set up for any given material, each pattern corresponding to a quantitatively applied stress. Diffraction ring displacement, streaking, distortion and diffusing of spots for large grains and other changes indicate strain. With these patterns may be compared those of any casting or fabricated piece of the particular metal or alloy made by the same back reflection technique. The initial condition as well as effects of heat treatment, aging, etc., are then evaluated quantitatively by a strictly non-destructive method of testing.

Figure 9 presents a series of patterns made with the tension compression device on a test bar of one of the most commonly used aluminum alloys. The following table lists the values of the applied tension, the true or corrected tension and the percentage elongation corresponding to each applied stress. The original structure of the test bar is by no means perfect in the sense of

TABLE I.

Pattern	Applied tension lb./sq. in.	True tension lb./sq. in.	Percent elongation*
1	0	0	0
2	5,000	4,700	4
3	10,000	9,500	5.6
4	15,000	14,400	7.2
5	20,000	19,150	10.8
6	22,500	21,600	12.0
7	25,000	24,000	13.6
F	(fractured)	24,900	

* Calculated from lengths between two gage marks on constricted portion of specimen spaced 0.250 inch apart at 0 tension.

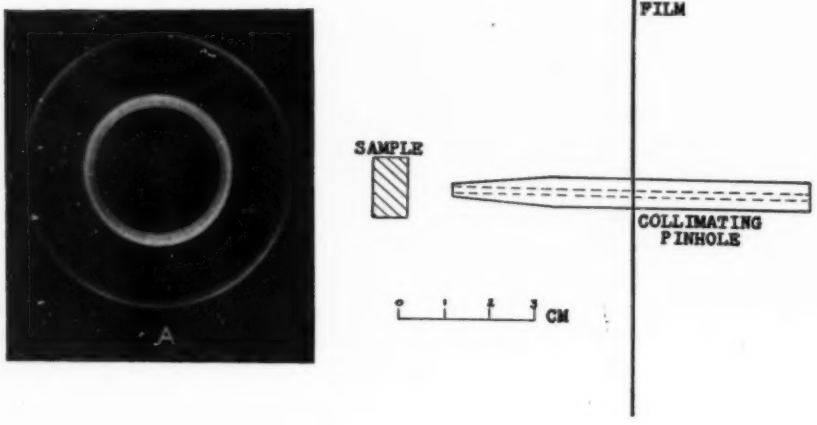

FIG. 6. Set-up for back reflection "focusing" x-ray diffraction method. Diffraction pattern of Al (same as Fig. 5). Sample-film dist., 5 cm. Defining pinhole, 0.063 inch dia. General Co radiation (Machlett tube—38 kv and 10 ma). Exposure, 5 min.

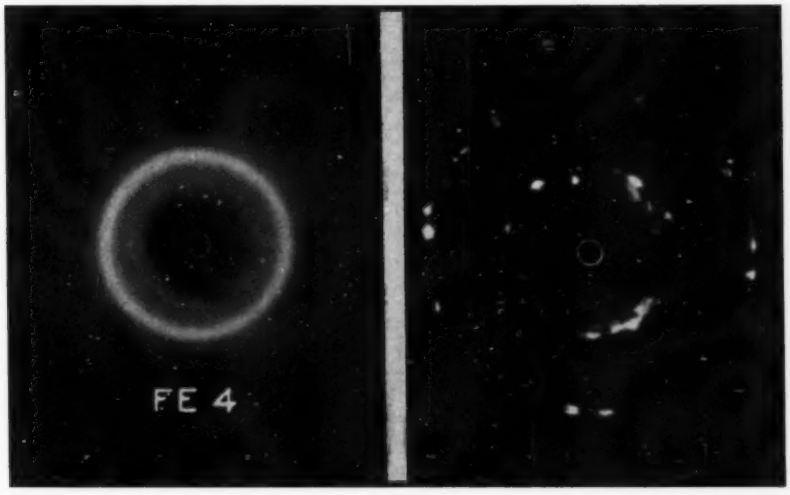

(a) (b)

FIG. 7. Back reflection x-ray patterns. (a) Carbon machine steel. Tensile stress, 45,000 lb./in.^{2}. (b) Cast Al alloy. Tensile stress 16,000 lb./in.^{2}. Technique same as in Fig. 6.

homogeneous grain size and complete freedom from inherent strain. However, it will be observed that the outer ring in the pattern for the unstressed specimen is partially resolved into the $K\alpha$ doublet. With increasing tension, there is an increasing diffuseness of the rings together with evidence of rotation of some of the larger grains as shown by the position and nature of the larger spots. The doublet resolution is lost between patterns 4 and 5, or in other words, between 15,000 and 20,000 lb. per sq. in. applied stress. The heavy spots tend to disappear thereafter by fragmentation and rotation up to the point of fracture for which the pattern is a series of diffuse, nearly uniform rings. By comparison with this series, therefore, an estimate can be made of the inherent strain in a whole casting of comparable grain texture. (See Table I.)

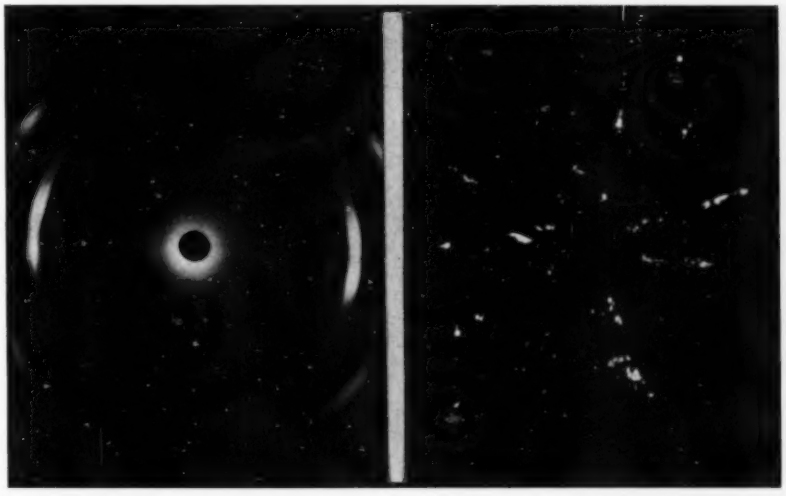

(a) (b)

FIG. 8. Transmission x-ray patterns. (a) Thin cold rolled Al. (b) Cast Al alloy. Defining pinhole, 0.063 inch dia. Sample-film dist., 3 cm. Operation data same as in Fig. 6. Exposure, 5 min.

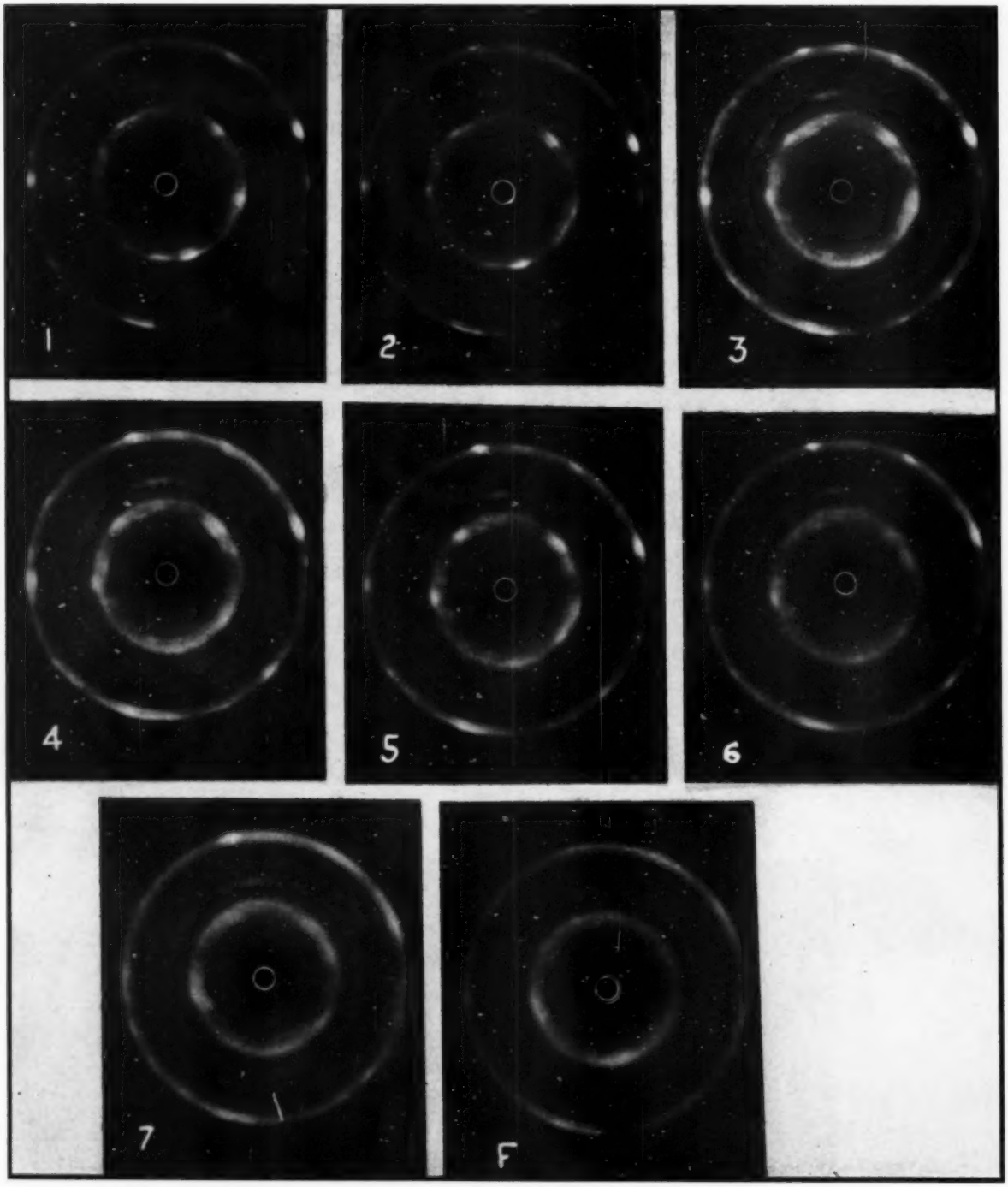

FIG. 9. Series of diffraction patterns made with tension compression device by back reflection from aluminum alloy test bar under calibrated stresses from 0 to fracture.

ACKNOWLEDGMENTS

In conclusion we would like to express our thanks to Professor F. B. Seeley of the Theoretical and Applied Mechanics Department of this University for the use of the Olsen test machine and to R. W. Eyler of this laboratory for his valuable assistance in the calibration of the instrument.

Studies on the Structure of Thin Metallic Films by Means of the Electron Microscope

ROBERT G. PICARD* AND O. S. DUFFENDACK
Harrison M. Randall Laboratory of Physics, University of Michigan, Ann Arbor, Michigan
(Received March 17, 1943)

A study was made of thin films of aluminum, cadmium, copper, gold, magnesium, and zinc using an RCA electron microscope capable of 30A resolving power. The films were formed by evaporation and condensation on collodion substrates in vacuum. An evaporating chamber was devised that permitted control of the temperature of the condensing surface. Photographs of the surfaces show that all the films are made of agglomerates of the metals separated by interstices of various widths. All evidence leads to the conclusion that the surface structure is explainable by assuming migration of the atoms over the surface. The observed structure can be used to explain the electrical conductivity, the optical reflectivity, and adsorptivity of thin films. Electron microscopic studies also provide a ready means of classifying surfaces according to the mobility of the atoms comprising them, and thus enable a rough estimate of the potential distribution over the surface to be made.

INTRODUCTION

MANY investigators have studied the properties of thin films, both metallic and nonmetallic. Special attention has been given to the optical properties, heat and electrical conductivities, oxidation, and catalytic effects of the surfaces. Electron diffraction studies of such films have indicated that they possess some crystalline properties. All lines of investigation have led to the belief that the films are not continuous, but consist of particles with spaces between them.

Recently a new instrument has been made available to the research worker and offers a new approach to the study of thin films. The electron microscope, because of its high resolving power and, hence, large useful magnification, permits direct observation of the structure of thin films to be made. With this added information it should be possible to explain some of the properties and peculiarities of such surfaces.

All of the films studied were formed by evaporation and condensation in vacuum. It was the purpose of this investigation to determine

(1) the suitability of the electron microscope for the study of thin films,
(2) the size of and interstitial distance between the particles constituting the films,
(3) the change in surface structure with film thickness, and
(4) the effect of the temperature of the condensing surface on the film structure.

Appleyard[1] in his studies with Lovell on the conductivity of thin metallic films on Pyrex glass arrived at a picture of the surface in agreement with most of the accepted speculations of previous investigators. A very thin surface (up to 100A in thickness) was considered as being made up of small agglomerates of the metal with spaces between them. Even if a continuous surface were formed by an initial layer of molecules, any imperfection in this surface due to the condition of the substrate might cause cracking. Surface tension forces would then cause the material to take the form of droplets. These forces exert very great pressures on drops a few angstrom units in diameter (the pressure is inversely proportional to the radius of the drop); thus, if the layer were broken it would go over into the stable form of small agglomerates.

Still another factor influencing the structure of thin films is the difference in thermal coefficients of expansion of the metal and the substrate. This can lead to breaking up of the metallic film if it undergoes any appreciable temperature change, and the surface tension forces will favor the formation of agglomerates.

Probably the most important factor in determining the type of surface formed is the ability of the metal atoms to migrate over the condensing surface. The theory of migration of atoms which was developed by Lennard-Jones[2] satisfactorily explains the experimental results and will be

* Now with the U. S. Rubber Company, Passaic, New Jersey.

[1] E. T. S. Appleyard, Proc. Phys. Soc. **49**, Extra Part, pp. 118–135 (1937).
[2] J. E. Lennard-Jones, Trans. Faraday Soc. **28**, 333–359 (1932).

discussed with the conclusions from this investigation.

EXPERIMENTAL PROCEDURE

The electron microscope used in this research was an RCA type B instrument. Its magnification range was from 1200 to 23,000 diameters for the 60 kv accelerating voltage used. A resolving power of about 30A was attained.

All observations were recorded photographically on Eastman medium lantern slide plates. The emulsion has a resolving power of 70 lines/mm. Development with Kodak formula DK-60a and fixing with Kodak F-5 fixing bath gave very satisfactory results. Emulsions with higher resolving power up to 500 lines/mm are available, but as they are much slower the exposures required would be correspondingly longer, and fluctuations in the instrument during the lengthened exposure time might well nullify any gain in resolving power obtained from the emulsion. Furthermore, it will be shown that extremely high resolution plates are unnecessary.

In choosing the magnification at which photographs of the specimen were to be made, it was necessary to consider the useful magnification of the microscope. By "useful magnification" is meant that magnification which will reveal all of the detail of the specimen down to the resolving power of the instrument. Any further enlargement is merely for convenience in viewing. The useful magnification is determined by the resolving power of the microscope and the resolving power of the recording medium, either the eye or a photographic plate.

As all studies with the microscope are recorded photographically the useful magnification is limited by the resolving power of the emulsion. Eastman medium lantern slide plates have a resolution of 70 lines/mm. If the microscope has a resolving power of 30A, a magnification of 4760 diameters will record this detail on the plate. Less magnification would place points separated by 30A in the specimen too close together on the plate to be recorded as separate. Higher magnification would increase the separation on the photographic plate of the images of two points 30A apart in the specimen, but could reveal no further detail as the resolving power of the microscope would then become the limiting factor.

A photograph made at a magnification of 4760 diameters thus contains all the possible detail obtainable. However, as the resolving power of the eye is 0.1 mm, this detail cannot be observed visually; so further enlargement of at least 7 times is necessary to enable the eye to appreciate all the detail in the photographic plate. Thus for the eye just to be able to see the entire observable structure of a specimen with a microscope having 30A resolution and using a photographic plate capable of resolving 70 lines/mm, an over-all magnification of at least 33,320 diameters is necessary. This is a minimum estimate as the resolving power of the eye is frequently much poorer than 0.1 mm. Many pictures will stand total enlargements as great as 150,000 diameters without serious loss of definition.

As the microscope itself is capable of magnifications from 1200 to 23,000 diameters, the useful magnification for photographic purposes falls well within its range. Considerable latitude in procedure is available for obtaining high total magnification for naked eye viewing. Pictures may be made with the microscope at 23,000 diameters and slightly enlarged optically to a convenient size for study, or they may be made as low as 5000 diameters and enlarged 10 or 15 times. Experience has shown that the latter procedure is not too satisfactory; because, in order to get a photograph capable of such enlargement, extreme care must be taken in the development and fixing of the plate to avoid excessive clumping of the silver grains and hence loss of resolution. The former procedure is also subject to objections, chiefly because the intensity in the final image is so low that accurate focusing is difficult and the exposure time becomes so long that the electrical stability of the instrument cannot be relied upon to give the ultimate resolving power.

It has been found most satisfactory to photograph at a microscope magnification of about 9000 diameters for general work, and if extremely high resolution is needed because of the detailed structure of the specimen (particularly for thin metallic films) a series of photographs made at about 17,000 diameters will give excellent results. Sharp enlargements with over-all magnification ranging from 50,000 to 150,000 diameters can regularly be made from these plates without using special fine grain development technique.

The apparatus used in evaporating metals consisted of a Cenco "Hyvac" pump acting as fore pump for a mercury diffusion pump. This in turn acted as fore pump for another high speed mercury diffusion pump with liquid air trap from which led an open tube ending in a ground joint. The evaporating chamber had its end ground to fit this tube, and the joint was made vacuum tight by sealing with Picein. This rather complicated vacuum system was used to allow gases released by the metal as it was heated to be pumped off, since the metals could not be conveniently outgassed in any other manner. A McLeod gauge was used to read pressures in the apparatus.

The evaporating chamber (Fig. 1) had two filaments, *F*, connected to the bulb through ground joints and sealed with Picein, thus permitting easy replacement. The filaments were about 3.5 mm in diameter and 4 to 5 mm long (10 turns of wire), and the metal to be evaporated was mounted inside one of them. A piece of glass tubing about 14 mm in diameter was sealed into the bulb as shown so that it could be filled with liquid air or some other substance to control its temperature. The top of the horizontal portion was ground to form a flat surface about 35 mm long. On this platform, *P*, were placed collodion covered microscope specimen screens (200 mesh) which served as the condensing surfaces. The platform had a slight downward tilt so that no air bubbles would be trapped against it when the tube was filled, thus assuring that it would quickly reach the temperature of the liquid in the tube. As the two filaments were at different distances from the platform, the angle of evaporation as viewed from the specimen could be changed by using one filament or the other.

When an evaporation was to be performed, the metal was first cleaned with distilled water and alcohol and then weighed. The amount to be used was determined by the thickness of specimen desired and which filament was used. In no case did the weight exceed a few milligrams. The metal was then placed inside the filament and up to four collodion covered wire meshes were placed on the platform. By using several specimen screens in the apparatus at once, it was possible to secure a large variation in thickness of surface deposited. The evaporating chamber was then sealed onto

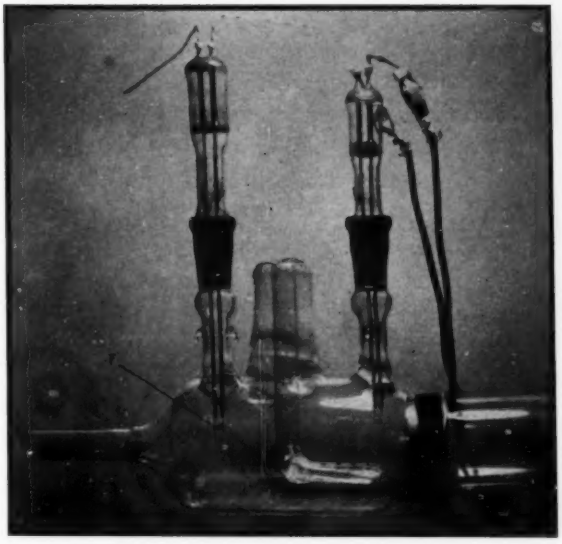

FIG. 1. Evaporating chamber. *F*, filament; *P*, platform tube; *S*, specimen screens.

the pumping system with Picein and evacuated. A sticking vacuum with the McLeod gauge was usually obtained within twenty minutes after the diffusion pump heaters were turned on.

After a high vacuum was obtained the filaments were heated, slowly at first to outgas them and the metal, and then more rapidly until the metal fused or evaporation started. As the filament started to heat, the pressure rose to about 10^{-4} mm of Hg, but the sticking vacuum was quickly recovered. The metal was not flashed, but was evaporated at a moderate rate over a period of three to four minutes. Finally, the filament temperature was raised to a higher value than that at which good evaporation of the metal occurred in order to clean the filament thoroughly.

When it was desired to have the specimen screens well below room temperature during the evaporation and condensation, the platform tube was filled with liquid air. This was not done, however, until a pressure of less than 10^{-4} mm of Hg had been established in the system, and the liquid-air trap on the diffusion pumps had been filled. In this way the possibility of water vapor or mercury vapor condensing on the cooled surfaces was eliminated. The specimen screens were carefully flattened so as to assure good contact between the cold platform and the wire mesh. The evaporation was not started until the rate of

boiling of the liquid air showed that the glass tube had reached a very low temperature.

The choice of filament from which to evaporate a given metal was made in accordance with the studies of Caldwell.[3] The metals evaporated and the corresponding filaments used are listed in Table I.

It must be emphasized that the collodion supporting film could not be outgassed due to its fragility and its inability to withstand sufficiently high temperatures, so that gaseous contamination of the substrate was a possibility for all specimens. Furthermore, the specimens had to be removed from the evaporating chamber and then placed in the microscope. As only one film could be studied at a time, the rest were exposed to the atmosphere for periods of a few hours to several days before they could be photographed, and thus some chemical reactions with the air might have taken place.

OBSERVATIONS AND RESULTS

In this investigation of the nature of metallic surfaces formed by evaporation and condensation in vacuum the first metal studied was aluminum. The surface appearance agreed with that of antimony which was studied by Marton.[4] The next metal used was zinc in order to see if the electron microscope could throw any light on the reasons why this metal forms poor surfaces on many substrates when condensed from the vapor. The surfaces were quite different from the aluminum, so cadmium was then studied, as its properties were known to be much like those of zinc. Good agreement was found between the two metals. Magnesium was studied because it has the crystal structure of zinc and cadmium (hexagonal). Copper, which has a face-centered cubic lattice as does aluminum, was used for comparison with that metal. Finally, gold surfaces were investigated, as this metal also has the aluminum crystal structure, but does not oxidize on exposure to air; hence, it served as a check on the effects of exposure of the surfaces to the atmosphere. All the metals used were of exceptional purity.

[3] W. Caldwell, J. App. Phys. **12**, 779–781 (1941).
[4] L. Marton, J. App. Phys. **12**, 763 (1941).

TABLE I. Filaments used in evaporation.

Metal	Filament	Wire size
Aluminum	Tungsten	0.015″
Cadmium	Chromel	0.015
Copper	Molybdenum	0.008 (doubled)
Gold	Tungsten	0.015
Magnesium	Tungsten	0.015
Zinc	Tungsten	0.015

In all cases during the evaporations the McLeod gauge showed a sticking vacuum, so the pressure was assumed to be 10^{-6} mm of Hg or less.

For each run usually four specimen screens were placed in the evaporating chamber at different distances from the filament, thus enabling four surfaces of different thickness to be produced at one time. Some of these screens were found to have no collodion film after the evaporation or were damaged in handling.

The only attempt at controlling the temperature of the condensing surface was made by filling the platform tube with liquid air for several runs. The condensing surface temperatures are stated in Table II as room temperature or liquid air. In the first case no cooling of the specimens was attempted and the temperature of the screens was somewhat above room temperature due to the heat given off by the filament, but the collodion films were never damaged by the heat. When liquid air was used for cooling, the glass was at −183°C and the wire mesh in contact with it must also have been at the same temperature. As the wires occupy about $\frac{1}{2}$ of the total area of the screen, it was assumed that the small areas of collodion between the wires would also come to a temperature in that neighborhood. However, again the heat from the filament raised the temperature of the collodion, but it is safe to assume that the surface temperature remained at least 100°C below room temperature.

In Table II are listed pertinent data for all runs. These data were taken to determine the change in the surface structure with the amount of material deposited and the effect of the temperature of the condensing surface on the nature of the metallic film. Unfortunately, the specimens when condensed on a cold surface had to be removed from the evaporating chamber in order to be examined with the microscope, and this necessitated

TABLE II. List of materials studied and conditions existing during the evaporation. The Roman numerals refer to the number of the evaporation.

Specimen	Mass (mg)	Condensing surface temperature	Screen number	Distance from filament
Al I	—	Room temp.	1	37 mm
			2	42
			3	50
			4	57
Al II	—	Room temp.	1	34
			2	38
			3	43
			4	51
Al III	—	Liquid air	1	30
			3	37
Al IV	9.8	Liquid air	1	38
			4	28
Al V	9.8	Room temp.	1	38
			2	34
			3	31
			4	28
Al VI	8.2	Liquid air	1	59
			2	67
			3	75
			4	82
Zn I	4.5	Room temp.	1	42
			2	35
			3	30
			4	27
Zn II	7.0	Room temp.	1	38
			2	32
			3	30
			4	27
Zn III	5.1	Liquid air	1	40
			2	35
			3	30
			4	28
Zn IV	9.5	Room temp.	1	40 mm
			2	35
			3*	30
Zn V	4.0	Liquid air	1	39–63**
	5.3**		2	34–69**
			3	30–77**
			4	28–83**
Zn VI	3.8	Room temp.	1	33***
Zn VII	9.5	Room temp.	1	50
			2	35
Cu I	8.4	Room temp.	1	39
			2	34
			3	31
Cu II	6.1	Liquid air	1	40
			2	34
			3	30
			4	28
Cd I	4.7	Room temp.	1	38
			2	34
			3	30
			4	27
Cd II	5.0	Liquid air	1	39
			3	30
			4	28
Cd III	5.8	Room temp.	1***	32
Cd IV	4.3	Room temp.	2	35–68**
	8.4**		4	28–83**
Au I	11.0	Room temp.	1	40
			3	31
			4	28
Au II	10.4	Room temp.	1	70
			2	113
Mg I	3.0	Room temp.	2	34
			3	30
Mg II	2.9	Liquid air	1	40
			2	34
			3	30

* Aluminum substrate.
** First number refers to substrate, second to coating. Zn V had an aluminum substrate; Cd IV had a copper one.
*** Copper substrate.

bringing them up to room temperature and exposing them to the air. Thus these films could never be studied exactly as they were formed. However, visual observation of the formation of the film was carried out for each evaporation, and some conclusions could be drawn from that.

(A) Aluminum

Six evaporations of the metal were made, and a total of twenty specimens were available for study. At currents of approximately 8 amperes (filament color, orange) the aluminum fused and flowed throughout the filament coil wetting it well. Good evaporation took place at currents of 13–15 amp. (white hot filament). The metal coated the specimen screens and the inside of the evaporation chamber with a highly reflecting mirror surface.

In the microscope only about a dozen openings at the center of the wire mesh could be studied, and the surfaces of all available squares of a given specimen showed remarkable uniformity. This was to be expected, as the total surface studied

was less than one square millimeter, and at distances of 30 to 80 mm from the source this should be quite uniformly covered.

In many cases dust particles and their shadows were included in the photographs as an aid to focusing. It was found necessary to take a series of photographs of each region in order to get a sharp picture.

Figures 2 through 5 show the results of a typical run (Al II) with no cooling of the screens attempted. All show a surface made up of agglomerates with channels between them, and apparently have no material in the channels, as the density of these interstices is the same as the density of the shadows cast by the dust particles. As the amount of material deposited increases, the size of the agglomerates also increases, and they appear to show more angularity. This latter effect may be due to the inability of the microscope to resolve the angles in the thinner speci-

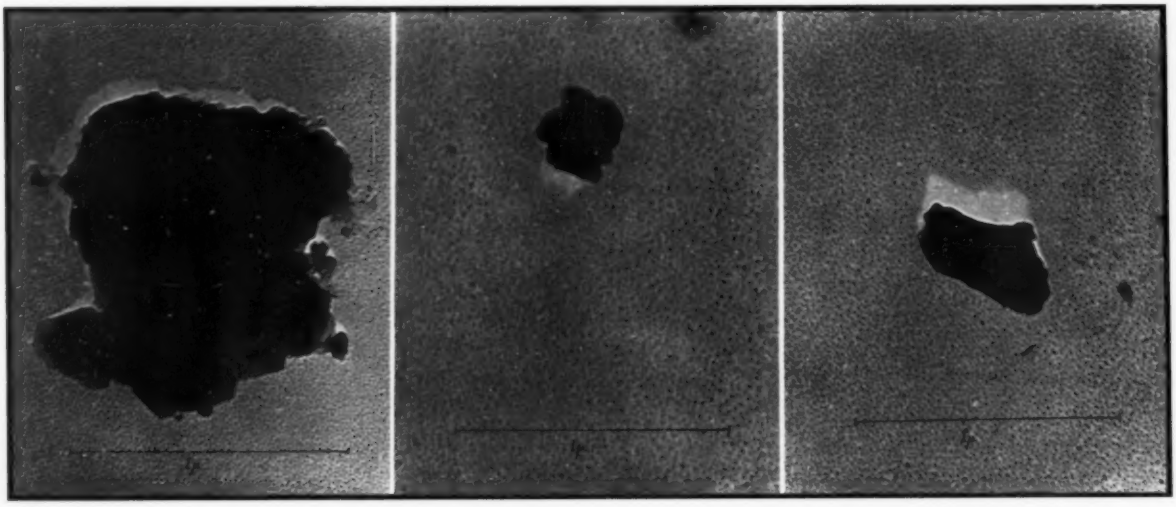

FIG. 2.

FIG. 3.

FIG. 4.

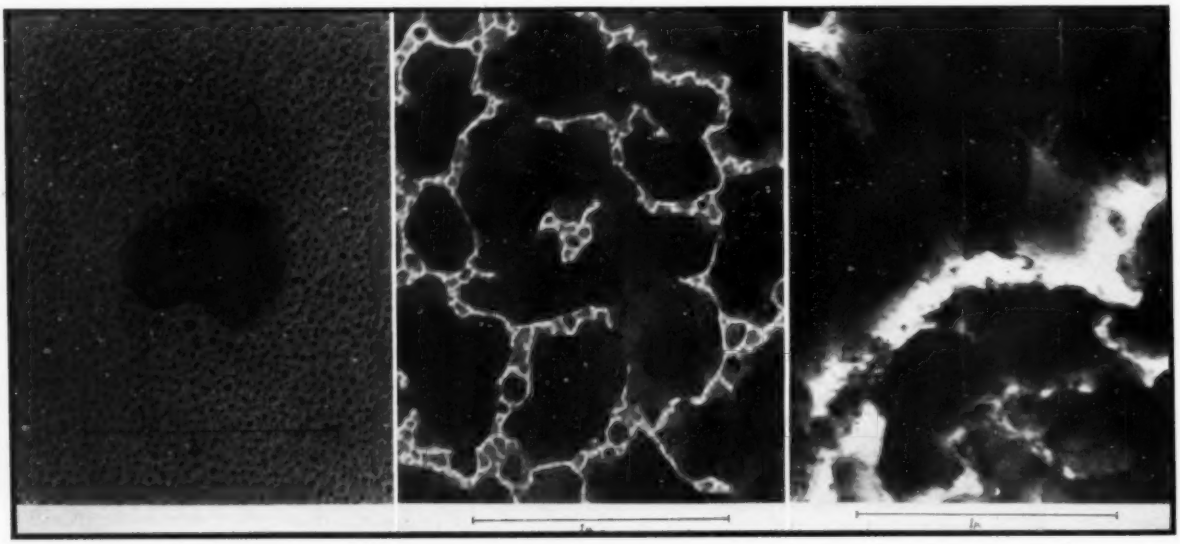

FIG. 5.

FIG. 6.

FIG. 7.

FIGS. 2–7. Aluminum on collodion. The films are successively thicker. Note the shadows cast by the dust particles in Figs. 2, 3, and 4.

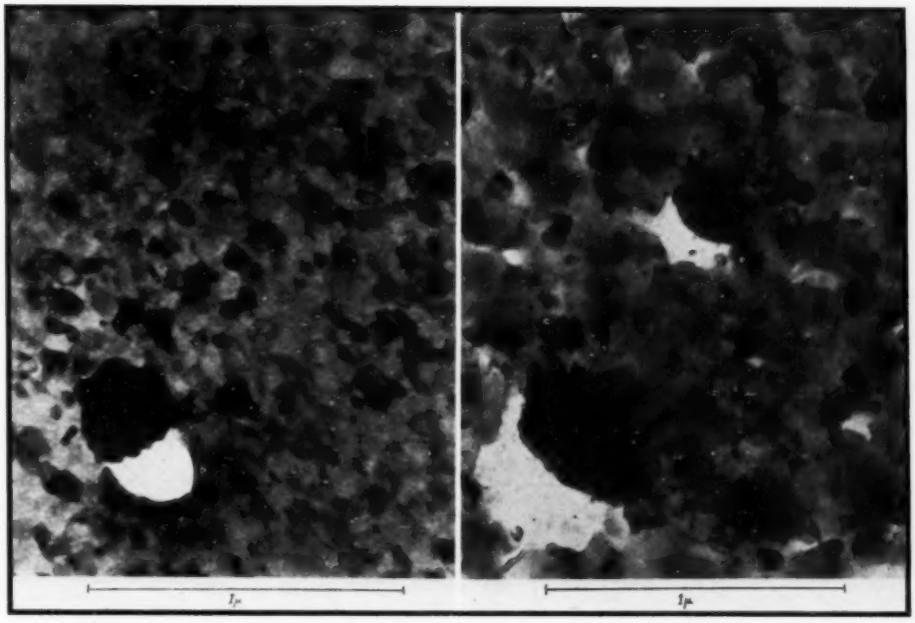

FIG. 8. FIG. 9.

FIGS. 8 and 9. Aluminum condensed on liquid-air-cooled collodion substrates. The sharp, dark lines are caused by crystalline reflections.

mens, photographs of which, however, demonstrate a resolving power of 25A. In Figs. 6 and 7 are shown much heavier deposits (Al V) prepared under the same conditions. In the former very large agglomerates have built up with smaller ones between, and the interstices are still visible. The heaviest deposit shows quite complete covering of the substrate.

Thin films of aluminum condensed on a liquid-air-cooled surface exhibit no new characteristics. Heavier films, however, cover the substrate quite completely and show many sharp, dark lines as seen in Figs. 8 and 9. According to Hillier and Baker[5] these are produced when strong reflection of the electron beam occurs at a crystal plane appropriately oriented with respect to the beam. Such a reflection prevents a portion of the beam from passing through the limiting aperture; thus no electrons from the corresponding part of the specimen will strike the photographic plate, and a black region will appear in the photographic print. Lines of this sort are evidence of the presence of well developed crystals on the surface.

Visual observation of the aluminum surface on the cooled parts of the evaporating chamber as it rose to room temperature gave no indication of any change in structure. The metal always formed a fine mirror which stuck well to the glass and the collodion.

One film was photographed six months after it was made, and showed a structure in agreement with that observed for freshly prepared specimens. From this one can conclude that if oxidation takes place it does not change the physical structure of the film, assuming that the fresh films do not react with the atmosphere completely instantly upon contact.

(B) Gold

In order to check more completely the effect of oxidation of the metals upon the surface structure, gold was used. The metal fused at a current of 15 amp. (white hot filament) and evaporated well at that current. Figure 10 shows a typical surface. Its structure is the same as that of an aluminum film. Thicker deposits showed a complete covering of the substrate and disappearance of the interstices. Extremely thin specimens (too thin to show color) showed a definite granulation of the surface with the size of the agglomerates just below the resolving power of the microscope.

[5] J. Hillier and R. F. Baker, Phys. Rev. **61**, 722–3 (1942).

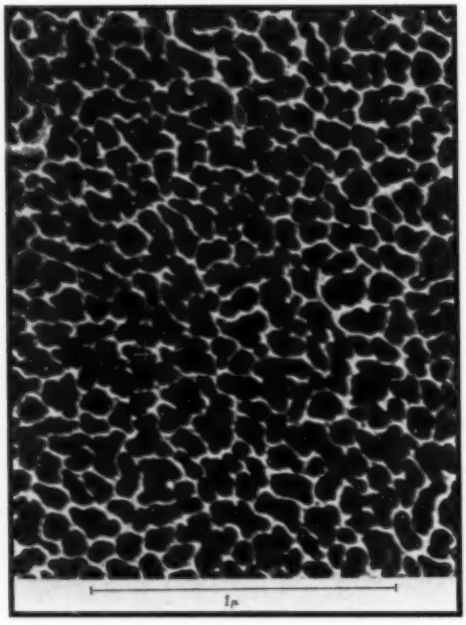

FIG. 10. Gold on collodion.

This agrees with Germer's conclusion from electron diffraction studies.[6]

(C) Zinc

Zinc was evaporated at currents of about 2 amp. (filament just starting to show color). In no case did the metal melt and wet the filament as observed by Caldwell,[3] but it seemed to sublime directly.

The zinc specimens condensed at room temperature showed large blank spaces with occasional crystals of the metal, clusters of crystals, large transparent forms, and irregular particles resembling droplets (Figs. 11 through 13).

The large, transparent structures are undoubtedly big crystals of the metal of such thickness as to be totally opaque to the electron beam. However, in this case density of the electron microscope image is not uniquely determined by the mass thickness of the specimen.[5] The observed structure is due to electrons which were reflected from the crystal but were brought back by the field of the lens and passed through the limiting aperture to give an image on the photographic plate.

The spaces between particles were considerably greater than the particle size in the few regions where any metal was present at all. The zinc formed a bluish, splotchy surface on the glass, and appeared in parts of the tube far within the shadow of obstacles. This latter effect was especially noticeable in one case when the filament temperature became too high during the evaporation, and it may readily be concluded that the zinc was reflected several times from the

[6] L. H. Germer, Phys. Rev. **56**, 58–71 (1939).

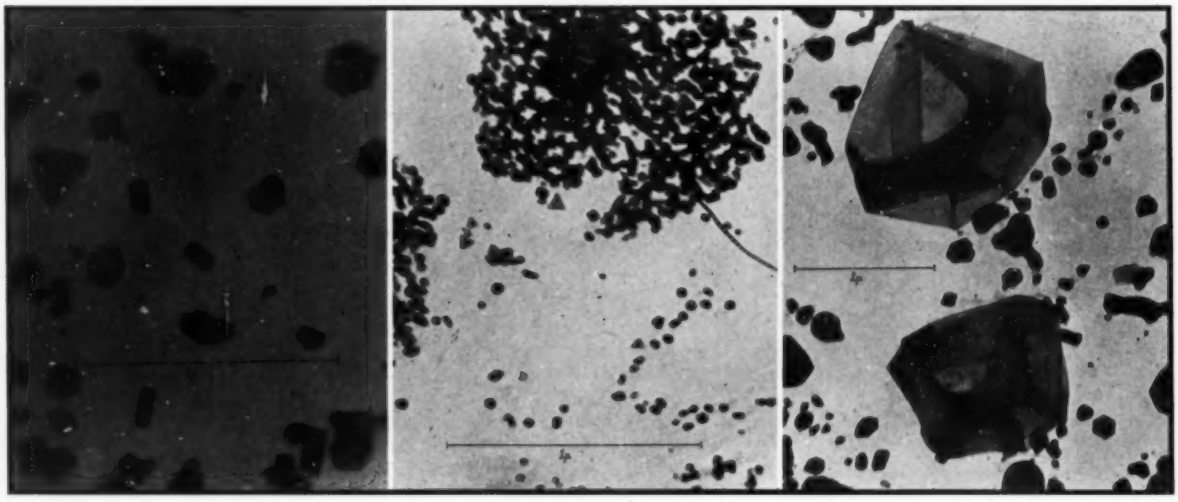

FIG. 11. FIG. 12. FIG. 13.

FIGS. 11–13. Zinc on collodion.

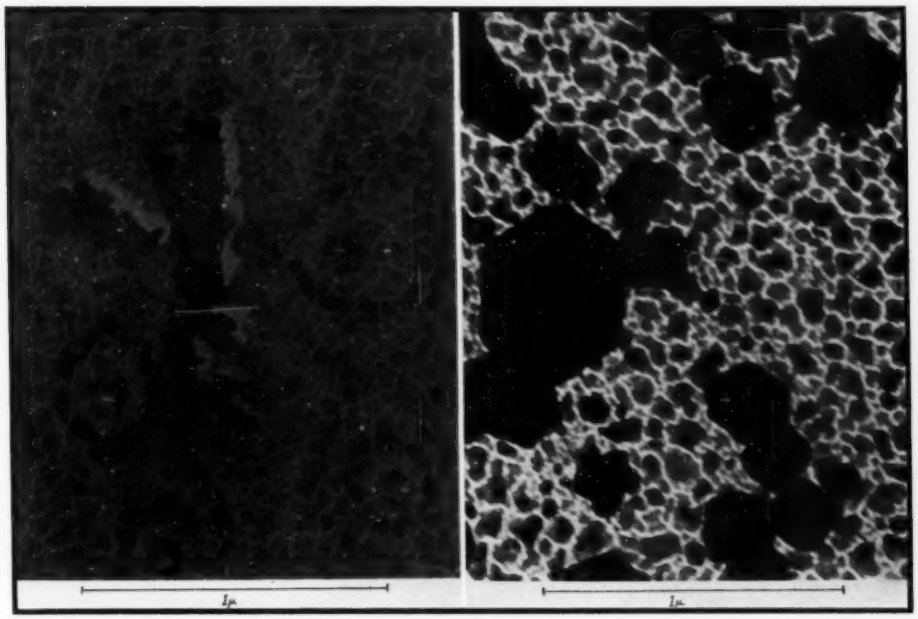

FIG. 14. FIG. 15.

FIGS. 14 and 15. Aluminum covered collodion film before and after zinc was condensed on it.

walls of the chamber before it finally stuck. The metal could easily be wiped from the glass.

When the condensing surface was cooled with liquid air the zinc formed a fine mirror surface on the cold glass but still did not coat the collodion well. On the uncooled glass surface the usual non-uniform, bluish deposit was observed. When the liquid air was removed from the platform and the glass gradually rose to room temperature, the highly reflecting mirror surface of zinc disappeared to leave ultimately a semi-transparent bluish coating as on the rest of the glass. Apparently a recrystallization of the metal had taken place below room temperature, and the zinc had gone over to the form of relatively large crystals with considerable space between them. The collodion films again showed no trace of a homogeneous surface, but only scattered crystals and droplets.

To check the effect of the substrate on the formation of zinc surfaces, the metal was next condensed at room temperature on one of the aluminum films, and two plain collodion films were included for comparison. These latter were no different in appearance from previous specimens, but the aluminum coated collodion took an excellent covering of zinc. Figures 14 and 15 show the aluminum background before and after the zinc was evaporated. The type of surface formed is shown at lower magnification in Fig. 16. Ex-

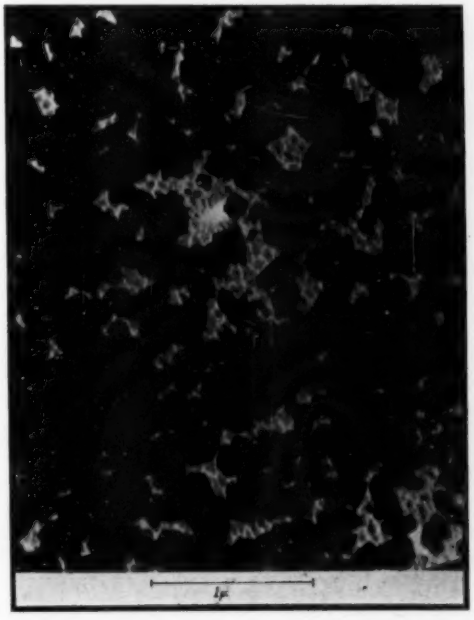

FIG. 16. Zinc on aluminum.

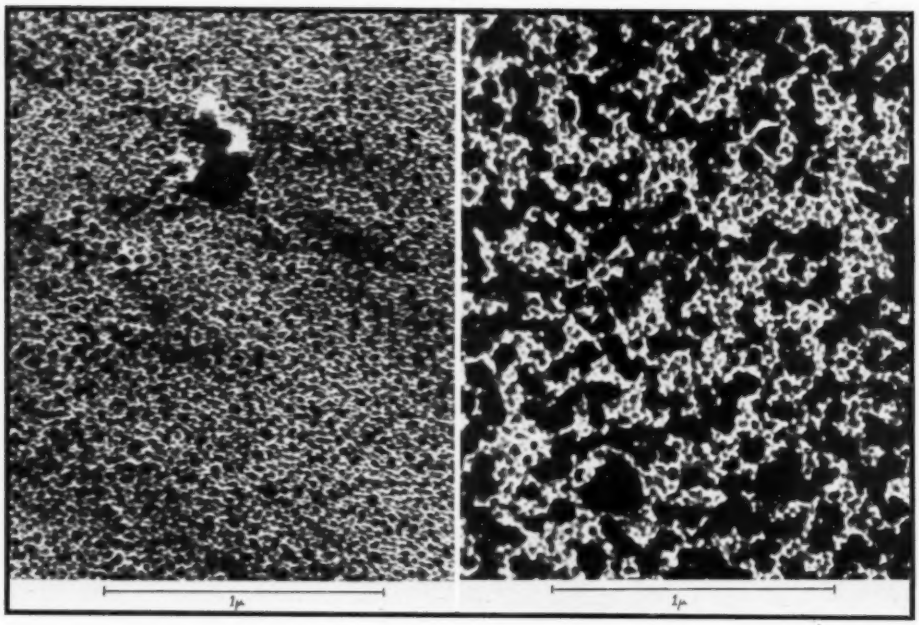

FIG. 17. FIG. 18.

FIGS. 17 and 18. Copper covered collodion film before and after zinc was condensed on it.

amination shows that the zinc never forms a film of the type observed with aluminum, but a thick network of fairly well developed crystals.

This experiment was repeated with liquid-air cooling of the films. Aluminum was evaporated from the rear filament and zinc from the front one after the aluminum evaporation was completed (Zn V). The films produced were much the same as those formed at room temperature, and, in addition, many of the large transparent forms appeared on the aluminum surface.

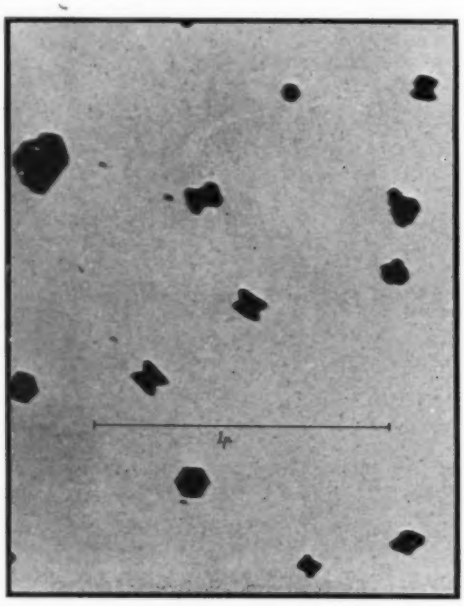

FIG. 19. Cadmium on collodion.

Finally, zinc was evaporated at room temperature onto a previously prepared copper film (Zn VI). Figures 17 and 18 show this specimen before and after the zinc was evaporated. Again the network of zinc crystals was formed.

(D) Cadmium

Cadmium was evaporated at currents of 1 amp. or less. The metal formed a bluish, non-uniform surface on the glass as zinc did, and did not coat the collodion well. Electron microscopic examination of the specimens showed irregular patches of the metal and, frequently, regions of well formed crystals, but a general coating was never obtained.

When the metal was condensed on a liquid-air-cooled surface it formed a fine mirror on the cold platform tube and the usual spotty surface on the uncooled glass. The collodion did not take a good coating. Upon being warmed to room temperature

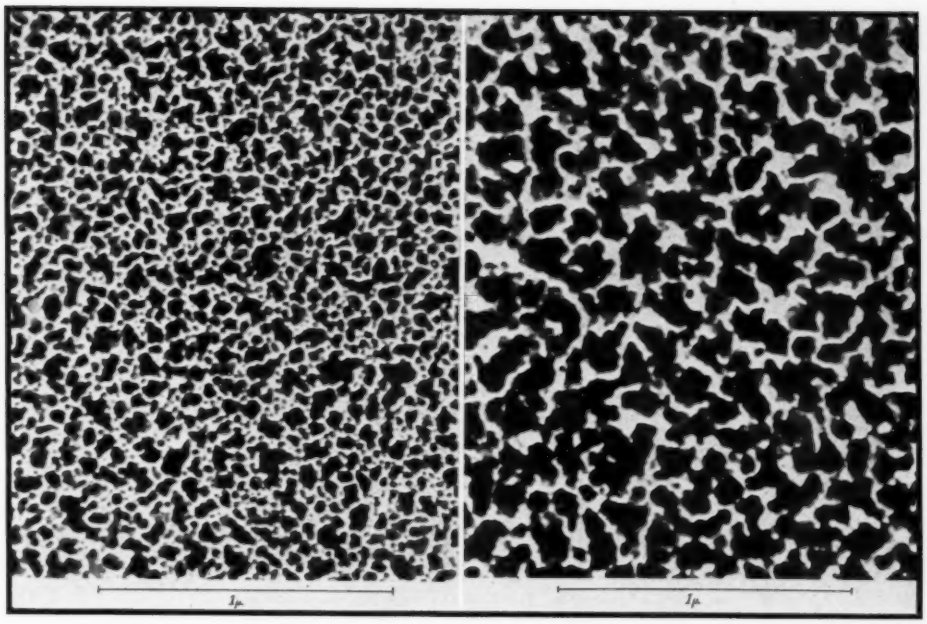

FIG. 20. FIG. 21.

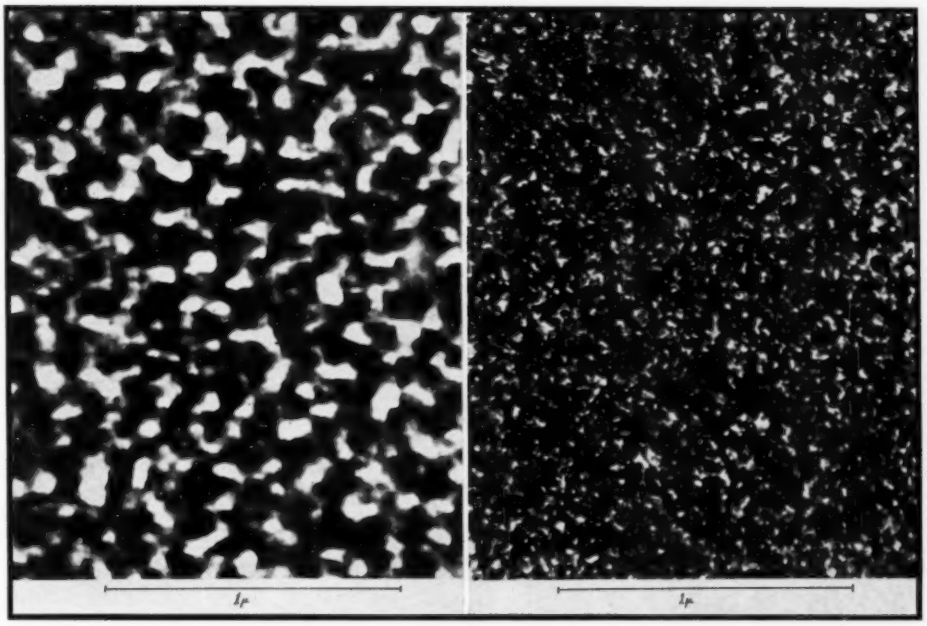

FIG. 22. FIG. 23.

FIGS. 20–23. Copper on collodion. The films are successively thicker.

after removal of the liquid air, the mirror surface did not disappear. The collodion films again showed numerous irregular patches of the metal and many well-defined crystals. Many of these crystals appear to be twinned (Fig. 19).

Finally, cadmium was condensed on a previously prepared copper surface. It coated the substrate very well, but again in the form of small crystals as the zinc had done. One specimen very heavily covered with cadmium when put in the

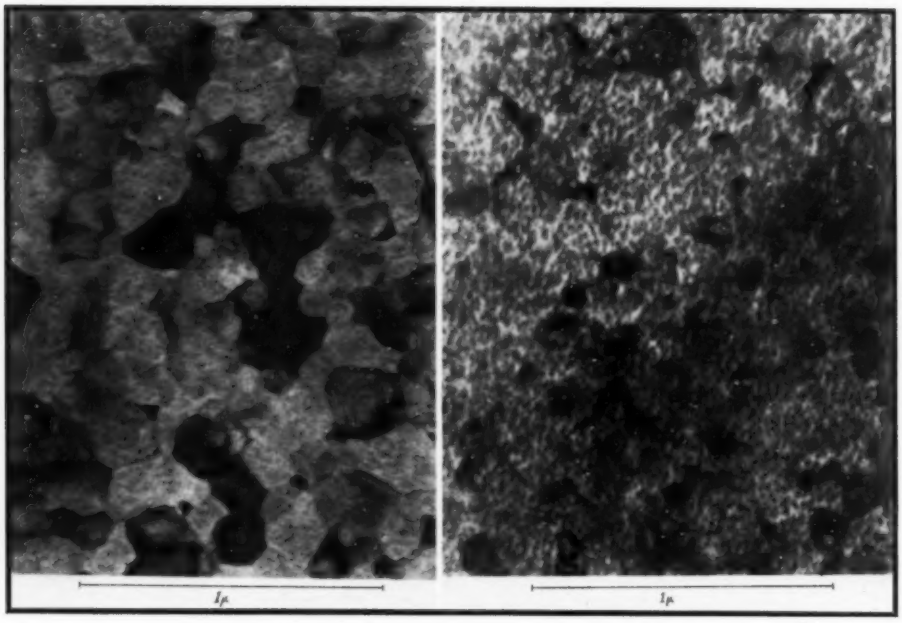

FIG. 24. FIG. 25.

FIGS. 24 and 25. Magnesium on collodion.

microscope seemed to undergo a redispersion of the cadmium, as it apparently disappeared in the beam. This was the only case for any film in which the beam was seen to affect the specimen.

(E) Copper

The metal fused and wet the filament well; good evaporation was obtained with a white hot filament. The copper coated the collodion films evenly, forming surfaces much like aluminum and producing a mirror on the glass. At liquid-air temperatures the same type surfaces were formed showing agglomerates with channels between them, and the gradual disappearance of the interstices as the deposit grew heavier. Results of a typical run (Cu II) are shown in Figs. 20 through 23.

(F) Magnesium

The metal did not wet the filament but sublimed at currents of three to five amperes (filament color, bright red), forming a mirror surface on the glass and coating the collodion films uniformly. Electron microscopic examination of films produced at room temperature showed a background of very small agglomerates overlaid with larger crystals (Figs. 24 and 25). Films condensed at liquid-air temperature showed a similar structure, with the size of the agglomerates increasing with thickness of deposit.

CONCLUSIONS

The knowledge of the structure of thin metallic films can be increased by the application to the problem of a new tool, the electron microscope. While only surfaces on substrates transparent to electrons can be studied, they show certain general features that may be easily recognized. All the surfaces studied appear to be made of aggregates of the metal separated by interstices of various widths, and the extremely high resolving power of the electron microscope enables accurate measurements of the grain and channel sizes to be made, whereas previously these could be only inferred and estimated.

For determination of the crystalline structure of those metals that form homogeneous surfaces, electron diffraction studies seem to offer more information than the electron microscope can. The pictures of the granules in many cases show only irregularly shaped aggregates which may be amorphous or crystalline, as they are large

enough to include many unit cells. Electron diffraction investigations seem to indicate that the crystalline structure is the more common form.

Electron diffraction studies also seem to offer more than the electron microscope in determining the degree of oxidation of the specimens. Microscopic observation shows no apparent change in surface structure of films known to be considerably oxidized, although it is possible that extended studies of a readily oxidizable film might show changes in grain size and channel widths as the chemical reaction proceeded.

The observed surface structure and the fact that very sharp shadows of obstacles in the evaporating chamber were formed when aluminum, magnesium, gold, and copper were evaporated can be explained on the assumption that the metals are given off from the filament in the form of molecular rays, and whatever structure is observed in the final film is due to the slight migration (not over 500A) of the atoms of these metals over the substrate after condensation. This migration of atoms over a surface has been well established by other means of investigation, and the electron microscope studies offer strong supporting evidence for it.

The non-uniform surface of zinc and cadmium on glass at room temperature and the appearance of these metals in the shadow of obstacles in the evaporating chamber show that the atoms are reflected from glass surfaces, losing some of their energy upon each impact until their energy is less than the latent heat of evaporation of the metal from glass. They then migrate over the surface until the stable crystalline forms are developed, leaving large areas of blank substrate between particles as pictured in Figs. 11 through 13. The surface structure as photographed is in excellent agreement with theories developed from such indirect methods of investigation as conductivity and optical reflectivity studies.

The electron microscope studies can be used to go a step further than the above indirect methods in explaining the formation of mirror surfaces. Measurements of the widths of the interstices between granules of such metals as aluminum, magnesium, copper, and gold, which form homogeneous surfaces, show that they are of the order of 100 to 500A, while the grains of the metal are much larger. Since the channel width is a small fraction of the wave-length of visible light, any light waves striking the metallic surface will be reflected as if the surface were continuous. On the other hand, surfaces of such metals as zinc and cadmium formed at room temperature have spaces between particles much greater than the particle size and of the order of magnitude of the wave-length of visible light, so that these surfaces will have a higher transmission coefficient for light and a lower reflection coefficient. The fine mirror surfaces observed for zinc and cadmium on glass at liquid-air temperature may be explained on the assumption that these metals at low temperatures form surfaces of much the same type as aluminum does, and as the temperature rises the kinetic energy and thus the mobility of the atoms increases until the relatively large crystals are formed with considerable space between them, resulting in the drop in the reflection coefficient. The surfaces as formed on liquid-air-cooled substrates could not be studied in the microscope prior to any crystallization occurring between -183°C and room temperature.

This explanation of the surface formation is in agreement with the theory developed by Lennard-Jones.[9] According to this theory, an atom on a surface is held there by a field of force which has a certain potential at every point. The surface has pockets of low potential separated by potential barriers, and at very low temperatures any deposited atoms will vibrate about the minima of these potential wells, as the energy of the atoms depends directly on the temperature. The latent heat of evaporation of the atom from the surface, L_s, will be the average energy required to remove an atom completely from the influence of the surface, assuming the atom is initially in its lowest vibrational level. But in order to move freely over the surface an atom needs much less kinetic energy than L_s. If the atom is given sufficient kinetic energy, A, for it to surmount the highest potential barrier along the surface, it may move freely over the entire surface as long as it retains this energy. Since A is less than L_s, free motion of the atoms on the surface is possible at temperatures below those needed to evaporate the atoms from the surface.

[9] J. E. Lennard-Jones, Trans. Faraday Soc. **28**, 333–359 (1932).

Both A and L_s depend on the nature of the surface and the atom concerned.

On the basis of the above theory Appleyard classifies metallic films into three broad classes depending on the stability of their first layers. For type I surfaces, $L_s > L_m$, where L_m is the latent heat of evaporation of the metal from itself, and the first layer is inherently stable. For type II, $L_s < L_m$, but L_s is 1 electron-volt or more, and A is a few tenths of an electron-volt. For this type fairly coherent films may be formed at temperatures below -183°C, but as the temperature rises agglomeration takes place due to the increased energy and hence increased mobility of the atoms. For type III, $L_s < L_m$, L_s is about 0.1 electron-volt, and A is only a few hundredths of an electron-volt. Such films show rapid agglomeration even at extremely low temperatures of deposition, as A (which measures the maximum height of the potential barriers) is so small.

The change in optical reflectivity and the observed physical reflection of their atoms from the substrates lead to the conclusion that the potential wells for zinc and cadmium on the substrates studied are much shallower than for aluminum, copper, gold, and magnesium, and deeper for cadmium than for zinc, as the former metal did not undergo as great a loss in reflectivity as the zinc did when the glass rose to room temperature.

The potential barrier for migration of zinc and cadmium on collodion is apparently less than for these metals on glass, as they did not form observable mirror surfaces on the collodion film even at liquid-air temperature. However, it must be remembered that the collodion films were probably not at as low a temperature as the glass when liquid air was used, even though the filament was giving off very little heat during the evaporation of these metals, and the added kinetic energy received by the metal atoms from the substrate might have been enough to allow them to surmount the potential barrier of a collodion surface even if it were as high as that for a glass surface. Furthermore, the relative cleanliness of the two substrates cannot be determined, and this is known to influence the height of the potential barrier for migration.[1]

When zinc or cadmium was evaporated onto substrates of copper or aluminum, a much more nearly complete covering of the surface was observed than in previous cases. From this it may be inferred that the adhesive forces and thus the latent heats of evaporation for these metals on copper and aluminum substrates are much greater than the forces that exist between these metals and glass or collodion. However, the formation of well-developed crystals with relatively large distances between them (Figs. 15 and 18) shows that there is considerable migration of the atoms and leads to the conclusion that the kinetic energy required for migration is still quite low. This conclusion holds for unoxidized aluminum and copper surfaces also, as in two cases the zinc and cadmium were evaporated onto freshly formed aluminum and copper substrates that had not been exposed to the air and again formed crystals of the type described.

In Table III the metals studied in this investigation are listed in accordance with Appleyard's classification as given above. None of the electron microscope studies gave evidence of the formation of an inherently stable first layer of metal giving rise to a continuous film, so none of the metals formed type I surfaces on the substrates used. The classification in this table is fundamental in that it is based on the actual distribution of potential over the surface. This is known for very few metals and substrates, but electron microscopic investigation offers a new and simple method of determining the type of surface and

TABLE III. Classification of surfaces studied according to Appleyard's scheme.

Metal	Substrate	Class
Aluminum	Collodion	II
	Glass	II
Cadmium	Collodion	III
	Glass	III
	Copper	II
Copper	Collodion	II
	Glass	II
Gold	Collodion	II
	Glass	II
Magnesium	Collodion	II
	Glass	II
Zinc	Collodion	III
	Glass	III
	Aluminum	II
	Copper	II

the order of magnitude of the potential barriers, although it does not give an absolute value for the minimum kinetic energy required for migration.

An additional classification is suggested which may prove useful in further electron microscopic investigations of thin films. This is based on the observed mobility of the atoms at various temperatures. Such a criterion is useful in that it gives an indication of the relative heights of the potential barriers and the adhesive forces between the films and substrate.

Class A—Surfaces which recrystallize with increasing temperature to form agglomerates separated by interstices which are much narrower than the diameter of the aggregates.

Class B—Surfaces which recrystallize with increasing temperature to form agglomerates separated by interstices of the same order of magnitude as the diameter of the particles.

Class C—Surfaces which recrystallize with increasing temperature to form relatively isolated crystals.

The surfaces studied are listed with their appropriate classes in Table IV.

Comparison of this classification with Appleyard's shows that both classes A and B are included in his type II group, and class C is identical with his type III. Appleyard's type I surfaces are not amenable to electron microscope investigation, as the instrument in incapable of resolving the structure of the uniform films included in this group. Electron diffraction studies should give more information regarding the structure of such films.

Electron microscope photographs of the thickest metallic films that could be penetrated (Figs. 7, 16, and 23) show that these surfaces are very porous. The interstices largely disappear under successive layers of metal, but at no time is a thoroughly uniform film formed. These pictures and those of thinner films offer new and conclusive evidence as to why surfaces deposited by condensation from the vapor have such high adsorptivity and absorptivity.

TABLE IV. Classification of surfaces studied on the basis of the electron microscopically observable particle size to interstitial distance ratio.

Metal	Substrate	Class
Aluminum	Collodion	A
	Glass	A
Cadmium	Collodion	C
	Glass	C
	Copper	B
Copper	Collodion	A
	Glass	A
Gold	Collodion	A
	Glass	A
Magnesium	Collodion	A
	Glass	A
Zinc	Collodion	C
	Glass	C
	Aluminum	B
	Copper	B

SUMMARY

In conclusion it may be said that the electron microscope studies of the structure of thin films by providing actual pictures of the surfaces give strong evidence in support of the theory of migration of atoms over substrates, provide a simple means of classifying such surfaces with respect to the surface energies of the atoms, explain the optical reflectivity and anomalous conductivity of the films, and establish their porosity, thereby doing much to explain the adsorptivity of these surfaces.

The authors wish to express their appreciation to Professor L. Thomassen of the University of Michigan for valuable advice given during the course of this investigation, and to the Rackham Fund for a grant-in-aid which made possible the carrying out of this investigation.

A Note on the Mutual Impedance of Antennas

CHARLES W. HARRISON, JR.
Cruft Laboratory, Harvard University, Cambridge, Massachusetts
(Received March 24, 1943)

An expression is derived for the mutual impedance of a symmetrical center-driven antenna in proximity to an untuned parasitic element, when the wires are parallel, and are not displaced in length. An integral, frequently occurring in antenna problems, is evaluated graphically over the range required in the present analysis.

THE question of the mutual impedance of antennas a multiple of a half-wave in length has been discussed by Carter.[1] More recently, Brown and King[2] published expressions for the mutual impedance of parallel wires of any length. These writers tacitly assumed in their formulation of the mutual impedance relations that the current distribution in the radiators is independent of the separation distance and radii of the antenna wires, and that it may be represented adequately by the relation

$$I_z=\frac{I_0}{\sin H}\sin\beta(h-|z|). \qquad (1)$$

In (1) I_z is the current amplitude at a distance z along an antenna wire from the input terminals. I_0 is the input current to the antenna. $H=\beta h$, where $\beta(=2\pi/\lambda)$ is the propagation constant, and h is the antenna half-length.

Recent research at this Laboratory demonstrates that whereas the assumption of a sinusoidal distribution of current is satisfactory for calculating the distant field of an isolated center-driven antenna of non-vanishing radius,[3] this distribution is in reality only the leading term in a complicated series involving powers of the small quantity $1/\Omega$ where Ω is defined by $2\ln 2h/a$, and a is the radius of the antenna wire.[4]

When a parasitic element is placed in proximity to a driven antenna, there is no reason to suppose that the distribution given by (1) is still the leading term in the correct current distribution along the driven antenna. Additionally, the writer can see no reason for assuming that (1) also applies to the parasitic radiator, when it is remembered that this element is immersed in a field of varying amplitude and phase over its entire length. If a rigorous solution is desired for the mutual impedance of antennas, the problem is a boundary valued one. The case of two antennas can be handled if one is willing to cope with simultaneous integral equations involving the unknown current distributions under the integral signs.

For the present purposes (assuming that a mutual impedance can be defined), the procedure is to utilize (1) as the distribution of current along the driven antenna, and the distribution

$$I_z=I_0\left\{\frac{\cos\beta z-\cos H}{1-\cos H}\right\} \qquad (2)$$

for the parasitic antenna. The latter expression is obtained as the leading term in the correct current distribution along a straight isolated wire immersed in a uniform field of constant phase.[5] It is believed that (2) is a better approximation than (1) for the case of an untuned parasitic element near a driven antenna. Having thus postulated the current distributions, one integrates the tangential electric field due to the distribution (1) over the surface of the antenna carrying distribution (2). The result should be nearer the actual mutual impedance of a driven and untuned parasitic antenna than could be obtained by predicating the current distribution given by (1) for both antennas. If the parasitic antenna is tuned to resonance by the insertion of

[1] P. S. Carter, Proc. I. R. E. **20**, 1004–1041 (1932).
[2] G. H. Brown and R. King, Proc. I. R. E. **22**, 457–480 (1934).
[3] C. W. Harrison, Jr. and R. King, "The radiation field of a symmetrical center-driven antenna of finite cross-section," accepted by the I. R. E. for publication in the Proceedings.
[4] R. King and C. W. Harrison, Jr., "The distribution of current along a symmetrical center-driven antenna," accepted by the I. R. E. for publication in the Proceedings.
[5] R. King and C. W. Harrison, Jr., "The receiving antenna," submitted to the I. R. E. for publication in the Proceedings.

a lumped reactance of appropriate magnitude and sign at its center, and additionally it is not too close to the driven antenna, a certain amount of calculation shows that the distributions of current are similar, and are given roughly by (1).[5]

The electric field in the Z direction, for a linear radiator lying parallel to the Z axis, has been calculated assuming the distribution given by (1). As given in numerous places in the literature, it is

$$E_z=\frac{j30I_0}{\sin H}\left\{2\cos H\frac{e^{-j\beta R_0}}{R_0}-\frac{e^{-j\beta R_1}}{R_1}-\frac{e^{-j\beta R_2}}{R_2}\right\}, \quad (3)$$

where

$$R_0=(z^2+r^2)^{\frac{1}{2}}; \quad R_1=[(z-h)^2+r^2]^{\frac{1}{2}};$$
$$R_2=[(z+h)^2+r^2]^{\frac{1}{2}}.$$

Integrating (3) over a parallel wire not displaced in length and carrying the current distribution (2) gives the following expression for the mutual impedance:

$$R_{12}=\frac{30}{\sin H(1-\cos H)}\Big\{\sin H(2Ci\beta r - Ci\beta(y-2h)-Ci\beta(y+2h))$$
$$+\cos H\Big(2Si\beta(x-h)-2Si\beta(x+h) - Si\beta(y-2h)+Si\beta(y+2h)$$
$$+4\cos H\int_0^h\frac{\sin\beta R_0}{R_0}dz-2\int_0^h\frac{\sin\beta R_1}{R_1}dz - 2\int_0^h\frac{\sin\beta R_2}{R_2}dz\Big)\Big\}. \quad (4a)$$

$$X_{12}=\frac{30}{\sin H(1-\cos H)}\Big\{-j\sin H(2Si\beta r - Si\beta(y-2h)-Si\beta(y+2h))$$
$$+j\cos H\Big(2Ci\beta(x-h)-2Ci\beta(x+h) - Ci\beta(y-2h)+Ci\beta(y+2h)$$
$$+4\cos H\int_0^h\frac{\cos\beta R_0}{R_0}dz-2\int_0^h\frac{\cos\beta R_1}{R_1}dz - 2\int_0^h\frac{\cos\beta R_2}{R_2}dz\Big)\Big\}. \quad (4b)$$

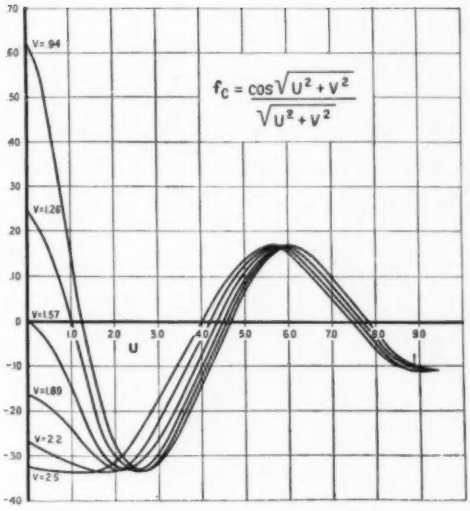

FIG. 1. f_c as a function of $U(=\beta z)$ for constant values of $V(=\beta r)$.

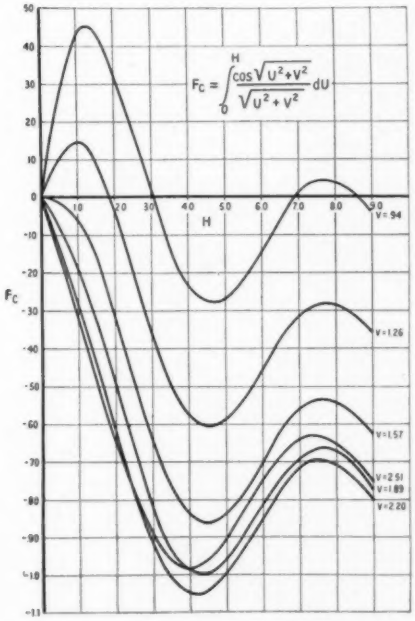

FIG. 2. F_c as a function of H for constant values of V.

In the above,

$$x=(h^2+r^2)^{\frac{1}{2}} \quad \text{and} \quad y=[(2h)^2+r^2]^{\frac{1}{2}}.$$

All of the integrals involved in (4) are solved at once by the integration of the retarded potential given by

$$\int\frac{e^{-j\beta(z^2+r^2)^{\frac{1}{2}}}}{(z^2+r^2)^{\frac{1}{2}}}dz. \quad (5)$$

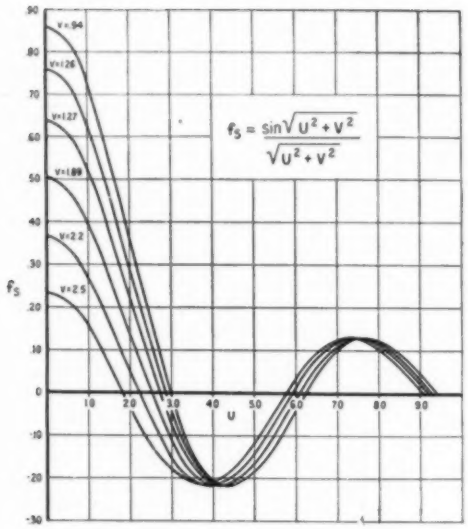

FIG. 3. f_s as a function of U for constant values of V.

Attempts to evaluate (5) analytically have failed. Accordingly, as a last resort, numerical integration was used. The results of this work are shown in Figs. 1–4 inclusive. It might be well to say at this point that this type of integral is frequently encountered in antenna problems, though apparently no work has been done on it previously.

It is to be observed that for the special case of

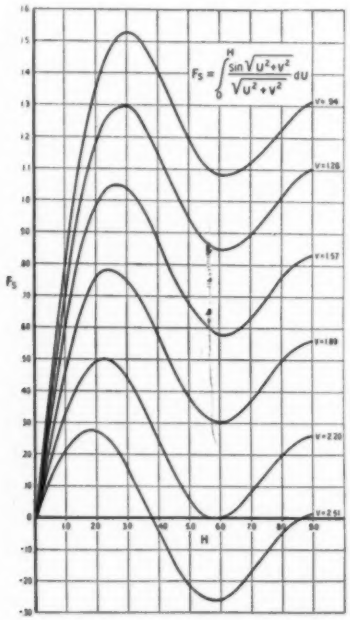

FIG. 4. F_s as a function of H for constant values of V.

$h=\lambda/4$, (1) and (2) reduce to the same form, and therefore (4) must reduce to the equation of the mutual impedance for half-wave dipoles as published in the literature. This is seen to be true. Further analysis of this special case shows that this result is uneffected by the tuning of the parasitic element. It is to be expected for these reasons that the available formula for the mutual impedance of half-wave dipoles is a moderately good approximation, but this is not true for other lengths. Equation (4) is to be preferred for the case of a single driven and untuned parasitic element antenna array to that published by Brown and King,[2] inasmuch as their equation is based on the assumption of (1) for both antennas.

In Fig. 5 are shown curves for $R_{12}\sin H$ and $X_{12}\sin H$ as a function of the spacing d/λ for several values of H computed from (4). These curves may be conveniently used in the following way: Assuming that the reciprocity theorem applies, the input impedance to the driven antenna in proximity to an untuned parasitic element is determined by Z_{11}, the self-impedance of the driven antenna (as obtainable, for example, from the curves by King and Blake[6]) Z_{12}, the mutual impedance given by (4) or Fig. 5, and the ratio of the current I_2 at the center of the parasitic antenna to the input current I_1 of the driven antenna. Thus

$$Z_{AB}=Z_{11}+Z_{12}(I_2/I_1). \tag{6}$$

If Z_{AB} is measured by the use of a suitable radio-frequency bridge, the ratio I_2/I_1 is ascertained, together with the phase angle between these currents. With these data, and using the distant fields due to (1) and (2),[7] the radiation pattern of an antenna array consisting of one driven and one parasitic element is uniquely determined. For the absolute value of the field intensity in the distant zone of the array, the amplitude of the current I_1 or I_2 must be measured.

Dr. Ronold King, Associate Professor of Physics and Communication Engineering at the Cruft Laboratory, suggested the subject of this research.

[6] R. King and F. G. Blake, Jr., Proc. I. R. E. **30**, 335–349 (1942).
[7] See Eqs. (3) and (5) of footnote 3.

APPENDIX. A METHOD OF COMPUTING THE INPUT IMPEDANCE TO A DRIVEN ANTENNA IN THE VICINITY OF A PARASITIC ELEMENT

The current at the center of an unloaded receiving antenna may be written

$$I_2 = 2h_e E/Z_{11}. \tag{7}$$

Here E is the field strength parallel to the axis of the antenna, and h_e is the effective half-length. For an indefinitely thin conducting thread

$$h_e = \frac{\lambda}{2\pi} \tan \frac{H}{2}. \tag{8}$$

Let it be supposed that (7) and (8) apply when the receiving antenna is in the immediate vicinity of a driven antenna. In this instance the electric field required in an application of (7) should be calculated from (3) by setting $z=0$.

Upon using standard circuit relations in connection with (7) and (8), the input impedance to the driven antenna may be written

$$Z_{AB} = Z_{11} + \frac{j60\lambda \tan \frac{H}{2}}{\pi Z_{11} \sin H} \times \left\{ \cos H \frac{e^{-j\beta r}}{r} - \frac{\beta \exp\{-j[H^2+(\beta r)^2]^{\frac{1}{2}}\}}{[H^2+(\beta r)^2]^{\frac{1}{2}}} \right\} Z_{12}, \tag{9}$$

where Z_{12} is given by (4).

For the specific case $h=\lambda/4$, (9) implies that

$$Z_{12} = +j120 \frac{\exp\{-j[(\pi/2)^2+(\beta r)^2]^{\frac{1}{2}}\}}{[(\pi/2)^2+(\beta r)^2]^{\frac{1}{2}}}. \tag{10}$$

On comparing (10) with (4) it is discovered that (10) is a good representation of (4) when $(r/\lambda)\,(=d/\lambda) \geqq 0.2$. It is to be borne in mind that (4) with $H=\pi/2$ is the expression published in the literature for the mutual impedance of half-wave dipoles.

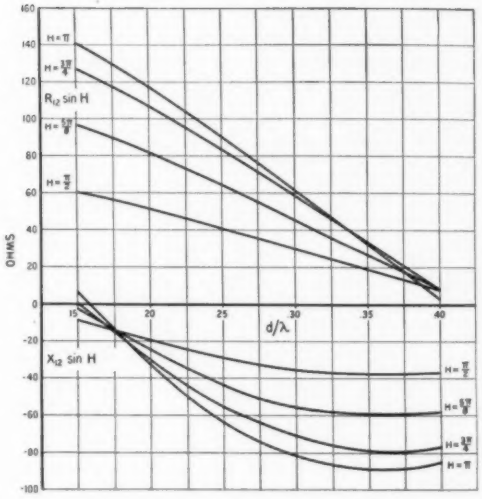

FIG. 5. The mutual impedance of a driven and untuned parasitic antenna as a function of d/λ for constant values of H.

The conclusion is that the assumption of an electric field of constant amplitude and phase over the parasitic antenna is satisfactory when the spacing is as little as 0.25λ, provided $h \leqq \lambda/4$ for each radiator. Inasmuch as the distribution of current given by (2) is derived by assuming the axis of the antenna to lie in the plane of a linearly polarized electric field, it is without question a good approximation to the correct current distribution along a parasitic element, even when relatively close to a driven antenna.

Here and There

Honors and Awards

Thomas H. Chilton, Director of the Technical Division of the Engineering Department of E. I. du Pont de Nemours & Company, has won the 1943 Egleston Medal of the Columbia University Engineering School's Alumni Association it was announced recently. Mr. Chilton received the medal because "he has made outstanding achievements in the discovery and formulation of principles underlying the unit operations of chemical engineering and in the application of these to process development, equipment design, and to chemical plant construction and operation." He has been with du Pont since 1935.

On the occasion of the annual Medal Day ceremonies at Philadelphia, April 21, the Franklin Institute announced recipients of their two highest awards—Franklin Medals—were Dr. Harold C. Urey, Professor of Chemistry at Columbia University, and Professor George W. Pierce of Cambridge, Massachusetts. Dr. Urey was cited for his discovery of an isotype of hydrogen of mass 2 which has resulted in the opening of new fields of knowledge in three of the physical sciences. Professor Pierce received the award in recognition of his inventions and contributions to the fields of electrical communications and of his influence as a teacher.

Others honored were as follows: R. H. Leach, Vice President and Manager of Research and Development of Handy & Harman, New York—The George R. Wetherill medal for his work in development of silver alloys for brazing purposes. Harry M. Pflager of Granite City, Illinois, Senior Vice President of the General Steel Castings Company—The George R. Henderson medal for his invention of the use of steel castings for large chassis frames on modern locomotives. Don Francisco Ballen of Lima, Peru—The Howard N. Potts medal in absentia, for his leadership in the scientific restoration of the guano industry in his country. Paul R. Heyl of the National Bureau of Standards, Washington, D. C.—The Howard N. Potts medal in

recognition of his contributions to physical science, in particular precise measurements in the field of gravitation. Professor Charles M. Allen of Worcester Polytechnic Institute—The Elliot Cresson medal in recognition of his contributions in the field of hydraulics. Anders H. Bull of Forest Hills, Queens, civil engineer of the Board of Transportation, New York—The Louis Elward Levy medal for the best paper published in *The Journal of the Franklin Institute* in 1942. His paper dealt with methods of determining soil pressure distribution, particularly in subway construction. Robert G. De La Mater and William Schwemlein of Parkersburg, West Virginia—The Edward Longstreth medals jointly, for invention of the hydromatic brake for the drilling of deep wells. The late Albert Kahn, Detroit industrial architect—The Frank P. Brown medal awarded posthumously, the citation saying his achievements in the development of modern industrial building construction "have been nothing short of sensational." The medal was accepted by Mr. Kahn's daughter, Mrs. Harry L. Winston. Carl S. Hornberger of the Central Scientific Company of Chicago—A certificate of merit for his development of a vacuum pump.

Dr. Karl T. Compton, President of the Massachusetts Institute of Technology, delivered the Pilgrim Trust lecture at Burlington House, London, on May 6. The Pilgrim Trust sponsors an exchange of lectures on alternate years between the National Academy of Sciences and the Royal Society.

Dr. Robert M. Burns of the Bell Telephone Laboratories, New York City, has been elected President of the Electrochemical Society for the year 1943–44.

★

Quarterly of Applied Mathematics

Physicists will be interested in the recent announcement of the establishment of the *Quarterly of Applied Mathematics* under the sponsorship of Brown University.

The new journal has been founded primarily to meet the needs of mathematicians and engineers whose interests include the application of advanced mathematical methods to the solution of physical or engineering problems. It will publish original papers of high scientific standard connected with engineering work, expository articles, short scientific notes and reports on progress made in other countries. While it is not the purpose of the quarterly to publish experimental results, mathematical contributions which have an intimate connection with application in industry or practical science will be welcomed. The editors state that "the ideal contribution to our pages would be one in which advanced and general mathematical methods lead speedily to results which are in close agreement with experiment, and which are of high importance, either in direct practical application or as an illumination of interesting phenomena hitherto unexplained."

The quarterly is edited by H. L. Dryden, T. C. Fry, Th. von Kármán, J. M. Lessells, W. Prager, I. S. Sokolnikoff, and J. L. Synge with the collaboration of H. Bateman, M. A. Biot, L. N. Brillouin, J. P. Den Hartog, K. O. Friedrichs, J. N. Goodier, F. D. Murnaghan, W. R. Sears, R. V. Southwell, G. I. Taylor, and S. P. Timoshenko. It is intended to publish four issues annually of about 80 pages each. The first issue of this publication is that of April, 1943. It includes articles relating to fluid mechanics, elasticity, and electrical engineering.

Physicists are invited to lend support to this new venture by contributing articles within its field and by subscribing to it. The subscription price for the quarterly is $6.00 per year. Subscriptions should be addressed to: *Quarterly of Applied Mathematics*, Brown University, Providence, Rhode Island.

★

Recent Appointments

Fred L. Hall, for the last six years Sales Manager of Bendix-Westinghouse Automotive Air Brake Company, has been appointed Vice President in Charge of Sales for Rogers Diesel and Aircraft Corporation. Mr. Hall will be active in plans to coordinate and expedite war contracts and also in formulating plans and charting the course for post-war sales of the organization.

The appointment of Dr. Edgar C. Bain to the newly-created post of Vice-Presidency for Technology and Research has been announced by the Carnegie-Illinois Steel Corporation. The purpose was announced as an intensification of activities relating to alloy and modern construction steels.

★

Bulletin of Mathematical Biophysics

The June, 1943 issue of *The Bulletin of Mathematical Biophysics*, edited by N. Rashevsky and published by the University of Chicago Press, will contain the following articles:

Outline of a New Mathematical Approach to General Biology: II. N. RASHEVSKY.

Note on the Hamiltonian Principle in Biology and in Physics. N. RASHEVSKY.

On the Form of Plants and Animals. N. RASHEVSKY.

A Mechanism of Division of a Cell With an Impermeable Membrane. H. D. LANDAHL.

★

Calendar of Meetings

June

14–16 American Society of Mechanical Engineers, Los Angeles, California
14–19 American Association for the Advancement of Science, Corvallis, Oregon
14–19 American Association of Physics Teachers, Corvallis, Oregon
17–19 American Physical Society, State College, Pennsylvania
18–20 American Association of Physics Teachers, Chicago, Illinois
18–20 Society for the Promotion of Engineering Education, Chicago, Illinois
21–25 American Institute of Electrical Engineers, Cleveland, Ohio
28–July 2 American Society for Testing Materials, Pittsburgh, Pennsylvania

July

10 American Physical Society, Stanford University, California

AIR SUPREMACY.. *Thanks to the* X-RAY!

Dispatches from the African Desert and other far-flung United Nations' battlefronts pay tribute constantly to the superiority of Allied aircraft. The X-Ray has played an important part in the development of the high degree of mechanical efficiency evident in design, construction, and performance of these planes. X-Ray analysis of molecular structure aids in the development of stronger alloys; X-Ray inspection of vital parts eliminates the need for excess "safety factor" to compensate for possible hidden flaws; the resultant reduction in weight means better maneuverability, superior combat performance, that have brought many a victory to our fliers at the front. The greater strength and reliability have prevented many a crack-up.

After the war, many industries will profit from these wartime lessons. Untold new fields of accomplishment will open to the design engineer who knows how to eliminate the "ignorance factor", the unnecessary extra weight, from his design considerations. The X-Ray will lead the way to more and better products of every mechanical variety.

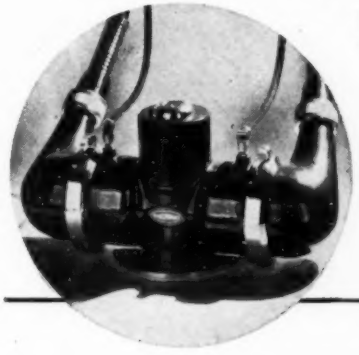

THE X-RAY TUBE IS THE HEART OF THE X-RAY MACHINE

The majority of leading makes of X-Ray apparatus are equipped with Machlett Tubes.

MACHLETT

Laboratories Inc.

SPRINGDALE CONNECTICUT

LARGEST PRODUCERS OF X-RAY TUBES

X-RAY TUBE SPECIALISTS SINCE 1898

Recent Applications of Physics

Test Chamber for Aircraft

A new altitude test chamber for aircraft radio and electronic equipment, in which engineers can now for the first time see the entire apparatus in operation under conditions duplicating the stratosphere seven and one-half miles up, has been developed by the RCA Victor Division of the Radio Corporation of America.

Built of transparent Plexiglas, a plastic developed by the Rohm and Haas Company, the chamber is actually the unfinished nose of a famous American bombing plane. The transparent construction makes possible the complete testing and inspection of any piece of radio apparatus by several engineers at one time and materially speeds test work. Defects in design, which normally would remain hidden until actual high altitude flights could be made, are now spotted at a glance.

At seven and one-half miles up, many things can happen to aircraft radio and electronic equipment, since apparatus of this type incorporates many delicate mechanisms. Low temperatures and pressures bring about changes in these delicate mechanisms which may cause current leakage, disabling electrical discharges, known among engineers as "flashover," and other failures which usually will not occur at normal altitudes.

The test chamber is cone-shaped, about four feet high and five feet in diameter at its base. Slightly less than one inch thick, the material is capable of withstanding strong shocks and pressures. An air-tight seal for the chamber is accomplished by fitting a heavy platform, arranged for mounting radio apparatus under test, with a ring of soft rubber. The test chamber cone is then lowered until its base rests on the rubber ring. As the air is withdrawn by a powerful suction pump, the atmospheric pressure on the outside of the chamber forces it down into the rubber ring and creates a perfect air seal.

Test chambers previously in use were constructed of metal with heavy glass windows serving as portholes. Lack of adequate visibility through these portholes frequently required shifting and remounting the apparatus under test to permit complete observation of results and each shift in mounting called for repeating the simulated altitude run to stratospheric pressures. Now by means of the new all-plastic chamber these tests are made in a single operation. Thus this bomber nose keeps other bombers flying with equipment that functions despite the altitude or temperature.

Glass Bearings for Combat Instruments

Tiny glass jewels, formed under heat and polished by flame, have replaced sapphires as bearings in manufacture of many combat instruments produced for the Army and Navy at the Westinghouse Meter Division at Newark, New Jersey. When the war made sapphires difficult to import from Switzerland, the American-made jewels were introduced and probably will be retained after the war for many electrical instruments. In certain instruments glass jewels produce less over-all friction than sapphires.

Million-Volt Industrial X-Rays

Operating for more than 1400 hours during two years of service is the record which has been established by the 1,000,000-volt industrial x-ray tube in use at the main works of the General Electric Company. Particularly noteworthy is the fact that in establishing this two-year record the original x-ray tube has never needed replacement. Exposures as short as one minute and some as long as 1½ hours built up a record of more than 45,000 radiographs of heavy castings and forgings, involving more than 8,000,000 pounds of metal.

In December, 1940, General Electric began industrial use of million-volt x-rays by adapting a pump-evacuated medical equipment for use in its industrial x-ray laboratory. Today more than thirty such equipments are in use in war-essential plants. Castings eight inches thick can be examined with this equipment and faults which would not be detected by the keenest of eyes are revealed, such as blow holes, tears, shrinkage cavities, inclusions, and cracks. Steels and ferrous alloys of many kinds, welded structures, and thick aluminum alloys are also inspected by this means.

New Instrument Booklets

American Instrument Company Bulletin, March, 1943, describes the Aminco heating units for industrial and laboratory heating requirements. Published by American Instrument Company, 8010–8020 Georgia Avenue, Silver Spring, Maryland (3 pages).

Nickel Steel Topics, March, 1943, Vol. 12, No. 1. The classification of steel scrap by spark testing is described in this booklet. Although this type of test cannot substitute for chemical analysis, it is stated that enough information can be obtained to classify mixed scrap according to its alloy type and its approximate carbon content. Very little equipment is needed for such tests. Other topics discussed in this issue are "The 'N.E.' steels and wartime scrap residuals" and "This is an alloy steel war," as well as "A brief history of nickel and other alloy steels." This booklet may be obtained from the International Nickel Company, Inc., 67 Wall Street, New York, New York (4 pages).

Nickelsworth, Vol. X, No. 1, published by The International Nickel Company, Inc., presents articles on "Acid baths for wartime steel" and another on a precision cleaning machine developed by the L & R Manufacturing Company of Newark, New Jersey, designed to clean instruments, gears, and bearings (8 pages).